BioMed Research International

Angiogenesis

Guest Editors: Zongjin Li, Qiang Zhao, Ian Chen, and Gang Niu

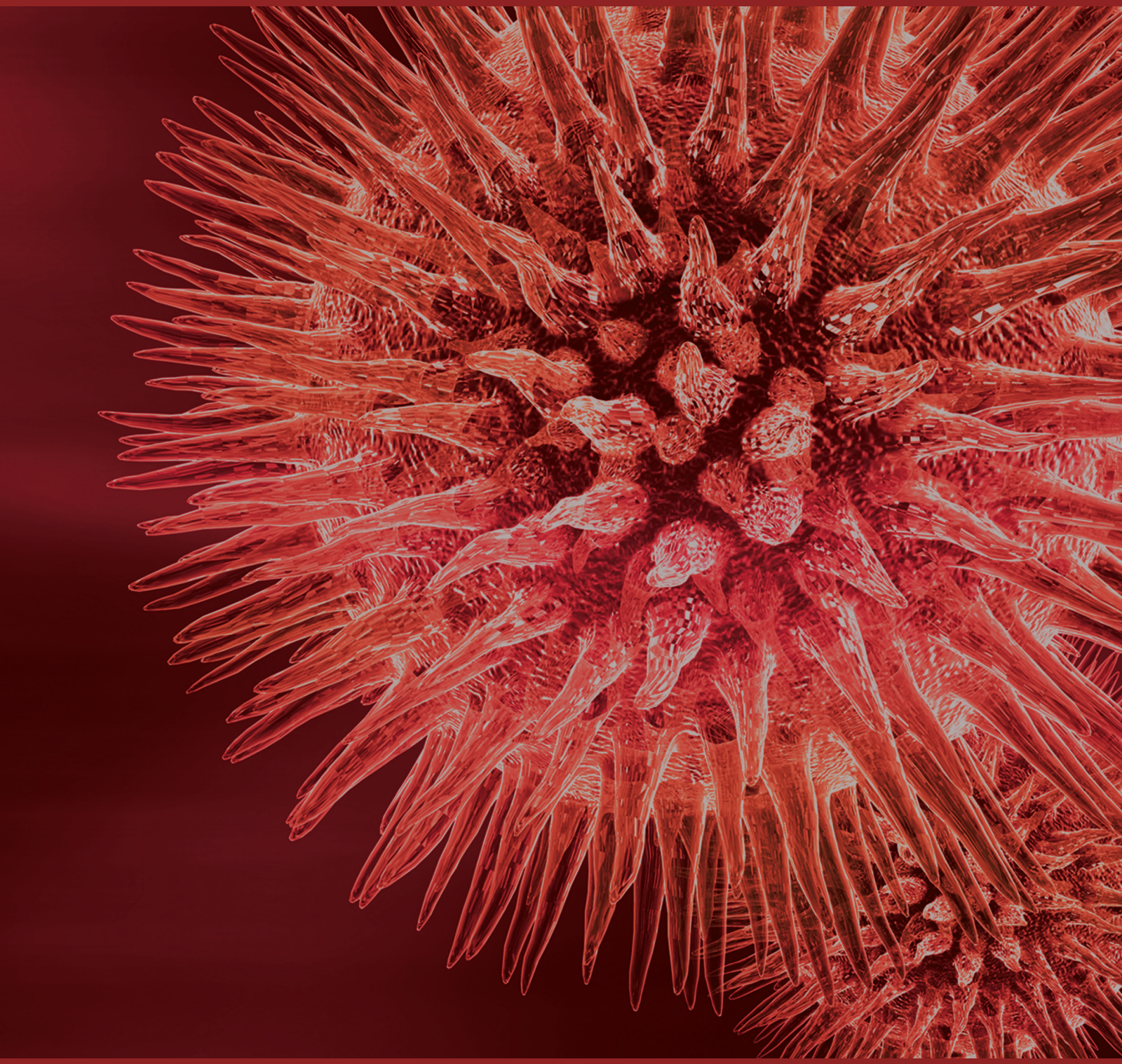

Angiogenesis

BioMed Research International

Angiogenesis

Guest Editors: Zongjin Li, Qiang Zhao, Ian Chen, and Gang Niu

Contents

Hindawi Publishing Corporation
BioMed Research International
Volume 2015, Article ID 135861, 2 pages
http://dx.doi.org/10.1155/2015/135861

Editorial
Angiogenesis

Qiang Zhao[1] and Zongjin Li[1,2]

[1]*The Key Laboratory of Bioactive Materials of Ministry of Education, College of Life Sciences, Nankai University, Tianjin 300071, China*
[2]*Tianjin Key Laboratory of Tumor Microenvironment and Neurovascular Regulation, Nankai University School of Medicine, Tianjin 300071, China*

Correspondence should be addressed to Zongjin Li; zongjinli@nankai.edu.cn

Received 11 February 2015; Accepted 11 February 2015

The development of new blood vessels, termed as angiogenesis, is essential to embryonic growth and throughout life for physiological repair processes. The field of angiogenesis research was established approximately in 1970s by the Folkman hypothesis that tumor growth is angiogenesis-dependent [1]. In addition to the tumor growth, another promising field where angiogenesis has drawn attention as a critical target is cardiovascular diseases [2]. Therefore, inhibiting angiogenesis is a promising strategy for treating diseases like cancer, while promoting angiogenesis may benefit the ischemic diseases such as myocardial infarction. Molecular insights into these processes and new therapeutic approaches are therefore particularly promising tools to understand the underlying pathologies and expand the available therapeutic options in abnormal angiogenesis. This special issue on angiogenesis highlights recent advances in our understanding of the molecular and cellular mechanisms of neovascularization. The summary of this special issue could be found in Figure 1.

With more bioassays and preclinical experiments performed, progress in understanding the relationship between tumor growth and angiogenesis has created a new perspective on therapeutic angiogenesis. Metformin is one of the most efficacious and safe front-line antidiabetics for type 2 diabetes (T2D). Gao et al. provided an overview of metformin as potential anticancer treatment by inhibiting angiogenesis. Tumor angiogenesis also influenced tumor microenvironment and C. Liu et al. described that exogenous overexpression of ATF4 (activating transcription factor 4) may facilitate the recruitment of macrophages into tumor tissues and promote tumor angiogenesis. Though atherosclerosis will trigger ischemia diseases, a clearer prescription of angiogenesis accounting for the development of the plaque of atherosclerosis is well recognized. F. Vasuri et al. evaluated the relationship between the intraplaque angiogenesis and the clinical plaque instability. Furthermore, L. Wang et al. reviewed the antiangiogenesis effects of polymethoxyflavones (PMFs), which underline the important of traditional medicine for anticancer therapy.

Ischemic cardiovascular diseases are the major cause of mortality and morbidity, which appeals for more effort on the better and more useful treatments. Therapeutic angiogenesis with stem cell and biomaterial has appeared as a powerful option. B. Chiara et al. described the angiogenic properties of mesenchymal stem cells (MSCs) and further emphasized the role of SIRT1. D. Mao et al. reported the therapeutic effects of SKP (skin-derived precursor cell) in stroke by promoting neurogenesis and angiogenesis. Furthermore, K. Wang et al. developed hybrid PCL/gelatin fibrous scaffolds with sustained release of VEGF, which could enhance vascularization *in vivo*. D. P. Zankov et al. reviewed the involvement of actin cytoskeleton-associated junctional molecules in angiogenesis and lymphangiogenesis, which may present a new approach to angiogenic therapy.

In general, this special issue on angiogenesis covered both excessive angiogenesis and insufficient angiogenesis (Figure 1). Either the reports or the reviews on angiogenesis presented in this issue will provide a further understanding

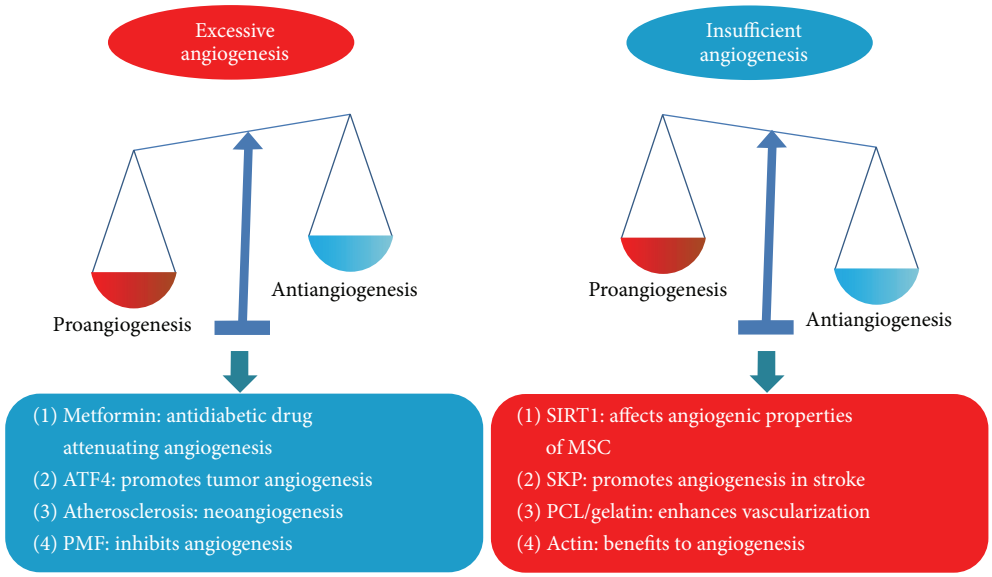

Figure 1: Summary of this special issue on angiogenesis. The impaired balance between pro and antiangiogenic factors causes pathological angiogenesis. Molecular insights described in this special issue provide new therapeutic strategies in abnormal angiogenesis management.

about the real role of angiogenesis in cardiovascular diseases or cancer.

Qiang Zhao
Zongjin Li

References

[1] J. Folkman, "Tumor angiogenesis: therapeutic implications," *The New England Journal of Medicine*, vol. 285, no. 21, pp. 1182–1186, 1971.

[2] M. Huang, W. Du, Z. X. He, and Z. Li, "Molecular imaging of angiogenesis in cardiovascular diseases," *Journal of Molecular Biology and Molecular Imaging*, vol. 1, no. 3, p. 6, 2014.

Hindawi Publishing Corporation
BioMed Research International
Volume 2015, Article ID 945846, 10 pages
http://dx.doi.org/10.1155/2015/945846

Research Article

Skin-Derived Precursor Cells Promote Angiogenesis and Stimulate Proliferation of Endogenous Neural Stem Cells after Cerebral Infarction

Duo Mao,[1] Xinpeng Yao,[1] Guowei Feng,[1,2] Xiaoqing Yang,[3] Lina Mao,[1] Xiaomin Wang,[1] Tingyu Ke,[3] Yongzhe Che,[4] and Deling Kong[1]

[1]*State Key Laboratory of Medicinal Chemical Biology, Key Laboratory of Bioactive Materials of Ministry of Education, College of Life Sciences, Nankai University, Tianjin 300071, China*
[2]*Department of Urology, Second Hospital of Tianjin Medical University, Tianjin Institute of Urology, Tianjin 300211, China*
[3]*Department of Endocrinology, Second Affiliated Hospital, Kunming Medical University, Kunming, Yunnan 650101, China*
[4]*Department of Anatomy, School of Medicine, Nankai University, Tianjin 300071, China*

Correspondence should be addressed to Tingyu Ke; ketingyu@hotmail.com and Yongzhe Che; cheli@nankai.edu.cn

Received 9 October 2014; Revised 3 January 2015; Accepted 5 January 2015

Academic Editor: Gang Niu

Stroke is one of the most common diseases that caused high mortality and has become burden to the health care systems. Stem cell transplantation has shown therapeutic effect in ameliorating ischemic damage after cerebral artery occlusion mainly due to their neurogenesis, immune regulation, or effects on the plasticity, proliferation, and survival of host cells. Recent studies demonstrated that skin-derived precursor cells (SKPs) could promote central nervous system regeneration in spinal cord injury model or the neonatal peripheral neuron. Here, we investigated the therapeutic potential of SKPs in a rat model of cerebral ischemia. SKPs were isolated, expanded, and transplanted into rat cortex and striatum after transient middle cerebral artery occlusion. Our results revealed that SKPs transplantation could improve the behavioral measures of neurological deficit. Moreover, immunohistology confirmed that SKPs could secrete basic FGF and VEGF in the ischemic region and further markedly increase the proliferation of endogenous nestin$^+$ and βIII-tubulin$^+$ neural stem cells. Furthermore, increased angiogenesis induced by SKPs was observed by vWF and α-SMA staining. These data suggest that SKPs induced endogenous neurogenesis and angiogenesis and protected neuron from hypoxic-ischemic environment. In conclusion, SKPs transplantation may be a promising approach in treatment of stroke.

1. Introduction

Stroke is a neurodegenerative disorder and a leading cause of death and disability in many countries, but only a few options support efficient recovery in stroke patients. Over the last 20 years, stem cell-based therapies were raising increasing attention on the treatment of stroke [1, 2]. Administration of stem cells resulted in beneficial effects on neuronal survival and recovery after experimental stroke [3, 4]. But limited stem cells for clinical application including ethical and safety concerns associated with the use of pluripotent stem cells have spurred great interest in the search for alternative stem cell sources for stroke treatment.

Autologous stem cells such as bone marrow mesenchymal stem cells (BM-MSCs) appeared as candidate for the regenerative therapy in the stroke treatment [3, 5, 6]. Nevertheless, BM-MSCs must be isolated by bone marrow aspiration, which is traumatic and painful. Moreover, the percentage of stem cells in bone marrow is very low and decreases with age, thus making it difficult to harvest a sufficient number of high-quality cells for clinical application. Recently, skin-derived precursor cells (SKPs) have attracted attention because they are more readily accessible from adult tissue [7] which belong to neural crest cell populations in various locations of the adult organism [8]. SKPs can proliferate and differentiate into subpopulations of cells expressing neuronal, glial, smooth

muscle, and adipocyte markers in vitro [7, 9, 10]. Moreover, SKPs show some properties like Schwann-like cells in the process of somatic nerve regeneration [11–13]. However, there has been no study on whether SKPs can effectively recover function of brain after stroke. Meanwhile, the exact effect of transplanted SKPs on damage tissue has not been clarified [14].

Most studies have shown that the underlying mechanisms of functional recovery following autologous stem cells transplantation are likely mediated by the release of growth factors, which promotes endogenous repair mechanisms, rather than stimulates neuronal differentiation or implant integration at the ischemic site [15, 16]. Moreover, neural crest-derived stem cells have been proved to secrete several active factors such as brain-derived neurotrophic factor (BDNF), basic fibroblast growth factor (bFGF), and Glial cell line-derived neurotrophic factor (GDNF) to enhance neurogenesis in brain after stroke [17, 18]. Besides, transplanted SKPs can be easily became functional vascular SMCs [19] and endothelial cells [20, 21] in the healing wound. According to these evidences, we speculated that SKPs might protect neurons, promote angiogenesis and neural regeneration, and further reduce functional deficits following transplantation into lesion areas in a rat model of transient ischemia induced by middle cerebral artery occlusion (MCAO). Our results suggested that SKPs exert multiple, independent effects on the ischemic brain that may modify outcome after stroke.

2. Materials and Methods

2.1. Isolation, Cultivation, and Characterization of SKPs. Neonatal male Sprague-Dawley rats were obtained from the Laboratory Animal Center of the Academy of Military Medical Sciences (Beijing, China). All experimental procedures were conducted in conformity with institutional guidelines for the Care and Use of Laboratory Animals in Nankai University Animal Care and Use Committee. SKPs were isolated and cultured as described previously [9]. Briefly, SKPs were prepared from infant rat skin (1–3 weeks) which was cut into 2-3 mm^2 pieces by a sterile razor blade and then transferred into a 50 mL tube containing 1 mg/mL Dispase II and 0.5 mg/mL collagenase I in DMEM/F12 medium for 30 min at 37°C, mechanically dissociated, and filtered through a 40 μm cell strainer. Cells were plated at a density of 1–2.5 × 10^4 cells/mL in proliferation medium including DMEM/F12 (Gibco) 3 : 1 containing 0.1% penicillin/streptomycin (Invitrogen), 40 ng/mL bFGF (Invitrogen), 20 ng/mL EGF(Invitrogen), and 2% B27 supplement (Invitrogen) at 37°C, 5% CO_2.

To passage SKPs, floating spheres were mechanically dissociated and reseeded in fresh medium containing B27 and growth factors at a density of 1 × 10^5 cells/mL. Cells were passaged every 7 days. To characterize the isolated SKPs, we utilized flow cytometry (FACS) method. SKPs single cell suspensions from day 14 were obtained by treatment with 0.5 mg/mL of Dispase II (Roche, Indianapolis) at 37°C for 30 min. Cells were passed through a 40 μm cell strainer and were incubated with triton X-100 for 10 min at RT and then, and cells were incubated for 30 min at 4°C with mouse anti-nestin and anti-α-SMA antibody, respectively. After being washed three times, the FITC-conjugated donkey anti-mouse secondary antibodies were added into the cell suspensions and incubated for 1 hour at 4°C. Cells were analyzed using FACScan (BD Pharmingen, San Jose, CA). To determine the differentiation potential of SKPs, myogenic, neurogenic and adipogenic differentiation was induced by medium (DMEM/F12 3 : 1 containing 0.1% penicillin/streptomycin, 2% B27 supplement). Medium changes were carried out every two days. Adipogenic differentiation was assessed by the cellular accumulation of neutral lipid vacuoles after cells were fixed with 4% formaldehyde, stained with Oil red O (Sigma-Aldrich).

To identify undifferentiated or differentiated SKPs, cells were centrifuged at low speed, dissociated, collected, and adhered to a poly-D-lysine substratum overnight. For immunocytochemistry, cells were fixed with 4% paraformaldehyde, washed with PBS, and treated with different antibodies including nestin (Abcam), fibronectin (Santa Cruz), P75 (Abcam), α-SMA (Abcam), glial fibrillary acidic protein GFAP (Santa Cruz), and β-III tubulin (Santa Cruz). After overnight incubation at 4°C with primary antibodies, cells were incubated at room temperature for 60 min with secondary antibodies. The secondary antibodies included Rhodamine-conjugated donkey anti-mouse, FITC-conjugated anti-rabbit, and anti-goat IgG (Invitrogen). After washing in PBS, samples were counterstained with a mounting medium containing DAPI (Vector Laboratories) and examined by fluorescence microscopy.

2.2. Animal Middle Cerebral Artery Occlusion Model. Transient middle cerebral artery occlusion (MCAO) was induced as previously reported [22] with a slight modification. Adult male Sprague-Dawley rats weighing 280–300 g were anesthetized with 5% isoflurane in O_2 using an induction chamber and maintained at 3% isoflurane using a face mask. Temperature was maintained at 37°C throughout the surgical procedure, using an electronic temperature controller linked to a heating pad. The right common carotid artery (CCA), external carotid artery (ECA), and internal carotid artery (ICA) were exposed through a ventral midline incision. A 4-0 monofilament nylon suture with a rounded tip was introduced into the CCA lumen and gently advanced into the ICA until it blocked the bifurcating origin of the MCA. Reperfusion was accomplished by withdrawing the suture after 60 min of ischemia.

2.3. Experimental Groups and Transplantation Procedures. The animal experiments consist of three groups: Group 1: SKPs (0.5 × 10^6) (n = 6); Group 2: Saline (n = 5); Group 3: Sham (n = 3). The injection operations were performed 24 h after MCAO. Prior to transplantation, SKPs were digested. Particularly, cell spheres were collected by centrifugation and then added 1 mg/mL dispase II enzyme to digest for about 30 min. The spheres were dissociated into single cells through mechanical approach, which were collected by centrifugation. DiI was dissolved in absolute ethanol (2.5 mg/mL) and added to the cell suspension so that the final concentration was 40 μg/mL. Cells were incubated

in the DiI-containing medium for 30 minutes at 37°C and then washed three times with PBS. Stereotaxic injections were performed using Hamilton microsyringe with a 26-gauge blunt needle. Each animal received an injection of 10 μL (at the rate of 1 μL/min, and concentration 50000 cells/μL) of DiI-SKPs into the striatum (from bregma: A + 1.0 mm, L + 2.0 mm, V 22.6 mm). The needle was left in situ for 2 min after injection before removal. At day 7 after cell transplantation, rats received injection of BrdU (Sigma, 10 mg/mL in saline) twice a day (50 mg/kg, i.p.) for 7 consecutive days. These rats were sacrificed 14 days after the cells injection [23].

2.4. Behavioral Testing. All animals were trained for 1 week after MCAO. And these behavioral measurements were performed every day since induction of MCAO until sacrifice. A modified neurological severity score (mNSS) was used in this study which includes (1) response to raising the rat-tail and placing it on the flat surface; (2) abnormal movement such as immobility, tremor, and seizures; (3) sensory deficit; (4) absent reflexes such pinna, corneal, and startle. Normal score is 0; maximal deficit score is 18 [6].

2.5. Histological and Immunohistochemical Assessment. Animals were reanaesthetized with 5% isoflurane in O_2 14 days after surgery. Rat brains were fixed by transcardial perfusion with saline, followed by perfusion and immersion in 4% paraformaldehyde, and the brain were embedded in paraffin and cut into 5 μm sections. The area of both hemispheres was measured on eight serial coronal sections per brain (200 μm apart) stained with hematoxylin and eosin, and the infarction area was averaged over these eight levels. The lesion size was estimated as a percentage of the whole brain by using the following formula: [(area of contralateral hemisphere) − (area of remaining ipsilateral hemisphere)/(area of contralateral hemisphere) × 100/2]. To identify proliferating cells, samples were incubated in 2 N HCl at 37°C for 30 minutes and then rinsed in 0.1 M boric acid with pH = 8.6. Samples were incubated with primary antibodies against BrdU at 4°C for overnight. After washing with 0.01 M PBS, samples were incubated with secondary antibodies (FITC-labeled polyclonal goat anti-mouse). For a morphological analysis of vessels, a polyclonal antibody against Von Willebrand factor (vWF; Dako) and α-SMA (Abcam) was used. The secondary antibodies were Rhodamine-conjugated donkey anti-mouse, anti-rabbit, and anti-goat IgG (Invitrogen). Slides were observed under confocal laser scanning microscopy (Leica TSC SP8, Germany). To investigate which cell-specific makers co-localized with BrdU-positive nucleus, sections were treated with different antibodies including vWF (Abcam), nestin (Abcam), and coimmunostaining with BrdU. To detect neuroblasts, a polyclonal antibody against nestin (Abcam) and β-III tubulin (Santa Cruz) were used. In order to quantify the number of immunoreactive cells, three representative sections from each animal were analyzed. The numbers of cells was blindly counted within 0.25 mm^2 of subventricular zone (SVZ), ischemic border zone (IB), and ischemic zone (IZ) using NIH image software, Image J. The immunoreactive cells were manually marked and calculated with Image J.

2.6. Statistical Analysis. All quantitative results were obtained from at least three samples for analysis. Data were expressed as the mean ± SD. An independent t-test was used for two group comparisons and one-way ANOVA for multiple-group comparison, with suitable post hoc analysis. The level of statistical significance was set at $P < 0.05$.

3. Results

3.1. Characterization and Differentiation of SKPs. As shown in bright field picture (Figure 1(a)(I)), the rat SKPs developed into sphere-like structure in suspension cultures. The SKPs specific marker nestin (Figure 1(a)(II)), fibronectin (Figure 1(a)(III)), neural crest stem cells marker P75 (Figures 1(a)(IV)–1(a)(VI)), and α-SMA negative were examined by immunocytochemistry methods and FACS (Figure 1(b)). After induction, SKP spheres began to express neuroblast marker β-III tubulin (Figure 1(c)(I)) and astrocyte marker GFAP (Figure 1(c)(II)), indicating the neural potential of SKP cells in vitro. Furthermore, some cells were positively stained for α-SMA (Figure 1(c)(III)) and Oil red O (Figure 1(c)(IV)), which revealed the mesodermal cell types differentiation capacity.

3.2. Neurobehavioral Tests and Lesion Size. To study SKPs induced neurogenesis and angiogenesis after cerebral ischemia, rats were subjected to MCAO, given SKPs on day 1 and injected cell proliferation maker BrdU on days 7–14 after ischemia injury (Figure 2(a)). Two weeks after treatment, SKPs transplantation did not result in significant reduction of lesion size compared to the control group by hematoxylin-eosin staining (Figures 2(c)(I) and 2(c)(II)) and statistical analysis (Figure 2(d)). However, the modified neurological severity score (mNSS) was significantly improved at 7 and 14 days in the SKPs treatment group (Figure 2(e)). Compared with control group, toluidine blue staining showed that more neuron exhibited relatively homogenous oval shaped nuclei in SKPs group (Figures 2(c)(III) and 2(c)(IV)). These data suggest that SKPs may contribute to neurological function improvement after stroke.

3.3. The Function of SKPs in Rat Brain. In order to clarify the therapeutic contribution of SKPs, DiI^+ SKPs were first immunostained with basic FGF and VEGF. Our results revealed that the transplanted DiI^+ cells were colocalized with trophic factors bFGF and VEGF (Figures 3(a) and 3(b)). Meanwhile, the higher blood vessel density with marker vWF (Figure 3(c)) and α-SMA (Figure 3(d)) were observed around DiI^+ cells, which indicated that secreted growth factors had angiogenic capacity in the ischemic tissue and could ameliorate the function of brain after injury.

3.4. The Neurogenesis and Angiogenesis Effect of Transplanted SKPs. To study the proliferation of endogenous stem cells in subventricular zone (SVZ) and ischemic boundary zone (IBZ), animals received BrdU injection for 7 days before sacrifice. Colocalization of BrdU-positive cells with nestin was observed in the SVZ (Figures 4(a)(I) and 4(a)(III)) and IBZ (Figures 4(b)(I) and 4(b)(III)) areas 14 days after

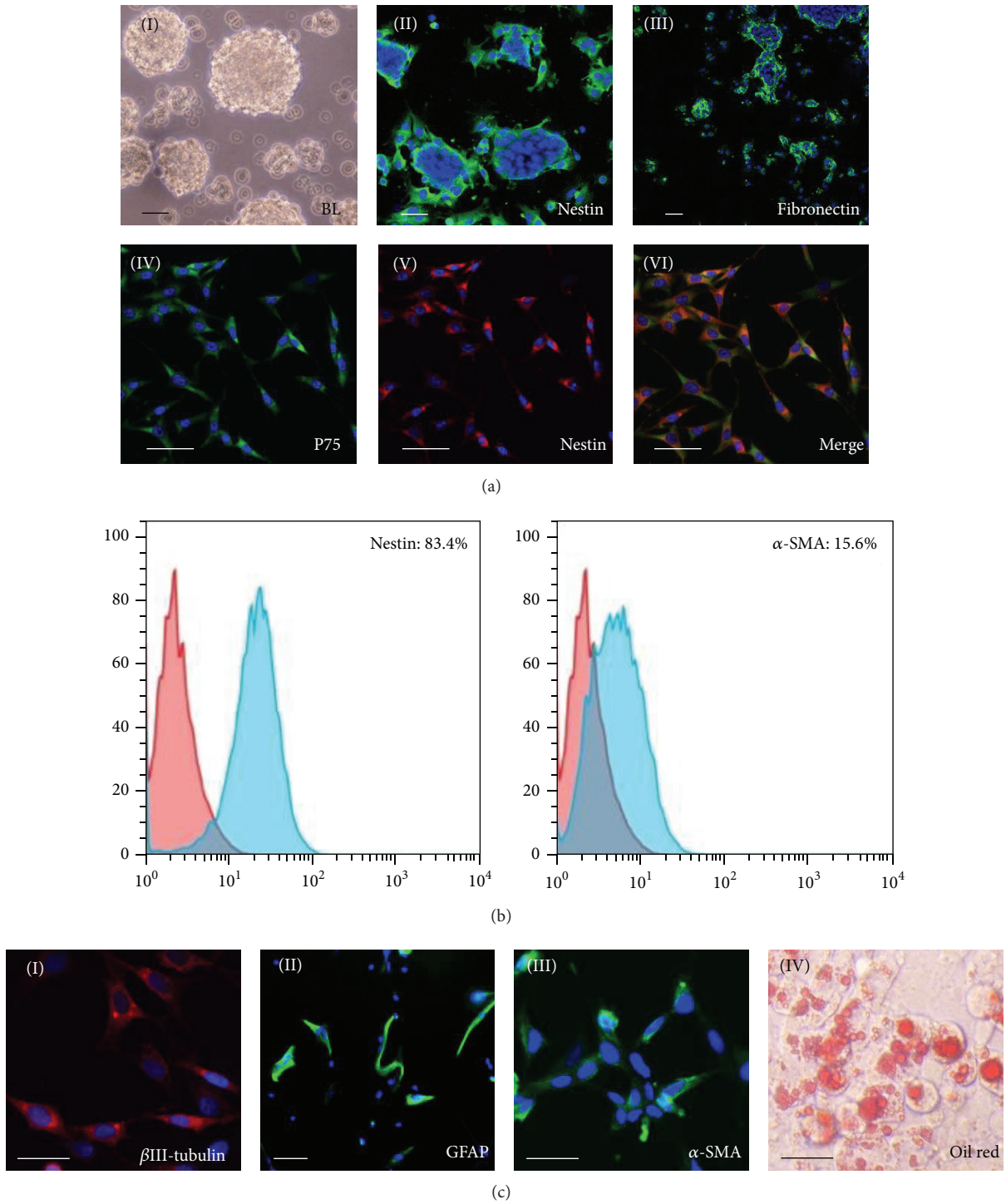

Figure 1: Phenotypic characterization and differentiation of SKPs. ((a)(I)) The appearance of SKPs by phase-contrast microscopy was neurospheres-like before passaging. ((a)(II), (a) (III)) SKPs that were adhered to a poly-d-lysine substratum overnight and then separately labeled with antibodies to nestin and fibronectin. ((a)(IV)–(VI)) Immunofluorescence colocalization analysis of SKPs showed coexpression of nestin (red) and P75 (green), and the nuclei were stained by DAPI. (b) Flow cytometric analysis of cell markers on nestin and α-SMA. Percentages indicate the fraction of cells that stained positive. (c) Differentiation of expanded SKPs into neural and mesodermal lineage cells in vitro. SKPs induced method was described in the "Section 2." ((c)(I)–(III)) Immunostaining for SKPs, βIII-tubulin (red), the astrocyte marker GFAP (green), and smooth-muscle actin (α-SMA; red). ((c)(IV)) Adipogenesis was visualized by staining Oil red O. Scale bars, 10 μm.

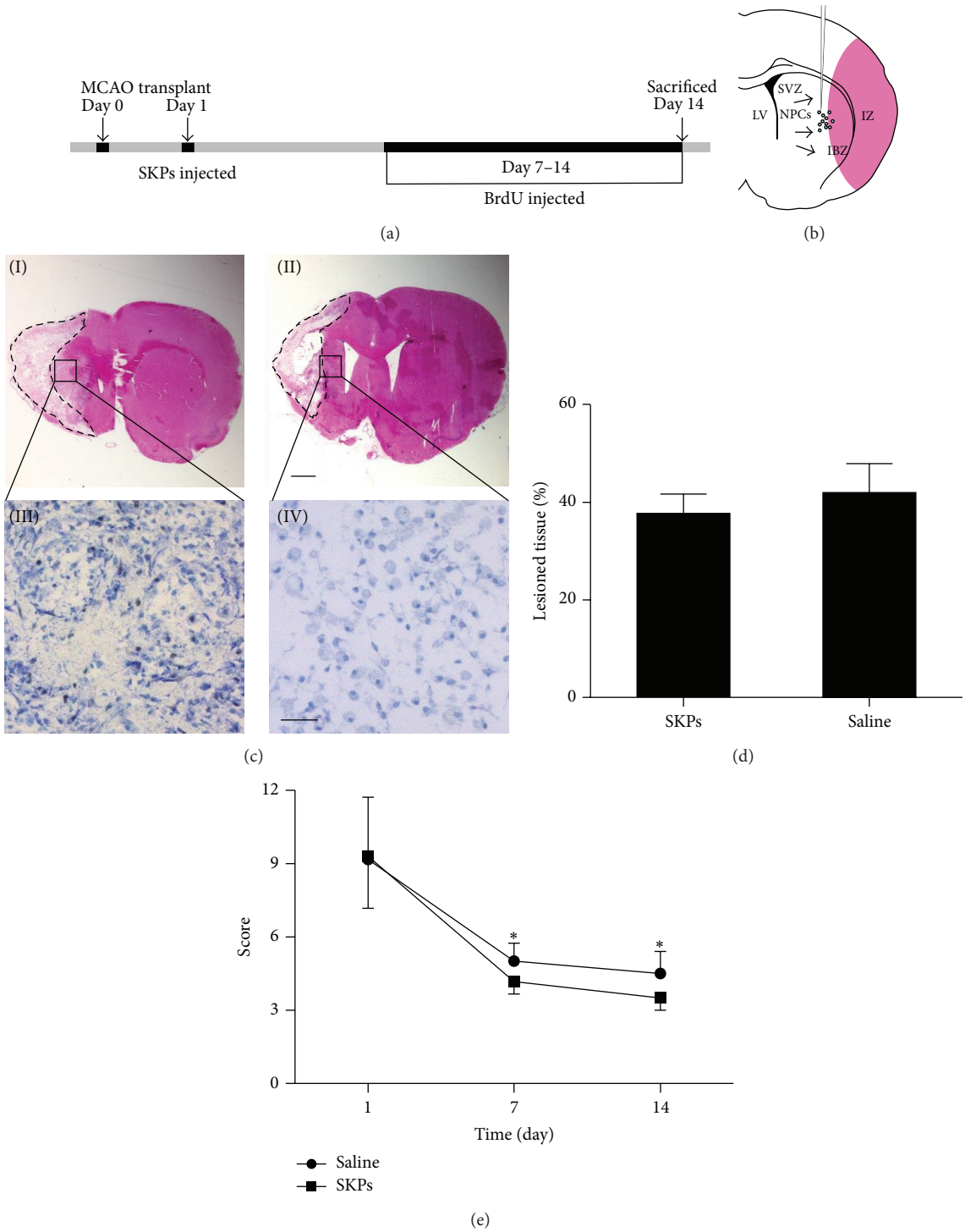

Figure 2: Transplantation of SKPs ameliorates the behavioral impairments and reduces infarct volume in stroke model of rats. (a) Experimental study design. MCAO: middle cerebral artery occlusion; BrdU: bromodeoxyuridine. (b) Representation of the lateral ventricle wall that includes the stem cells injection site, neural progenitor cells (NPCs), the lateral ventricle (LV), the subventricular zone (SVZ), the ischemic boundary zone (IBZ), and the ischemic zone (IZ). ((c)(I), (c)(II)) Representative pictures of HE from animals treated with PBS or SKPs after MCAO. Scale bar, 1 mm. ((c)(III), (c)(IV)) Higher magnification showed that SKPs increased the number of cells with normal neuronal morphology and decreased the number of shrunken and misshapen cells in cresyl violet–stained sections. Scale bar, 10 μm. (d) Infarct size was measured on HE brain sections. Relative infarct size of PBS or SKPs-treated animals is presented as the mean ± S.D. The percentage of lesion tissue in the two groups (SKPs, Saline) at 14 days after occlusion. Two-way ANOVA with repeated measurements followed by one-way ANOVA and post hoc multiple comparison tests using Fisher's PLSD. (e) Behavioral performance in the neurological score (NSS) tests of PBS or SKPs injected animals from 1 to 14 days after ischemia. Statistically significant differences between the SKPs group with PBS group were determined by ANOVA, $^{*}P < 0.05$.

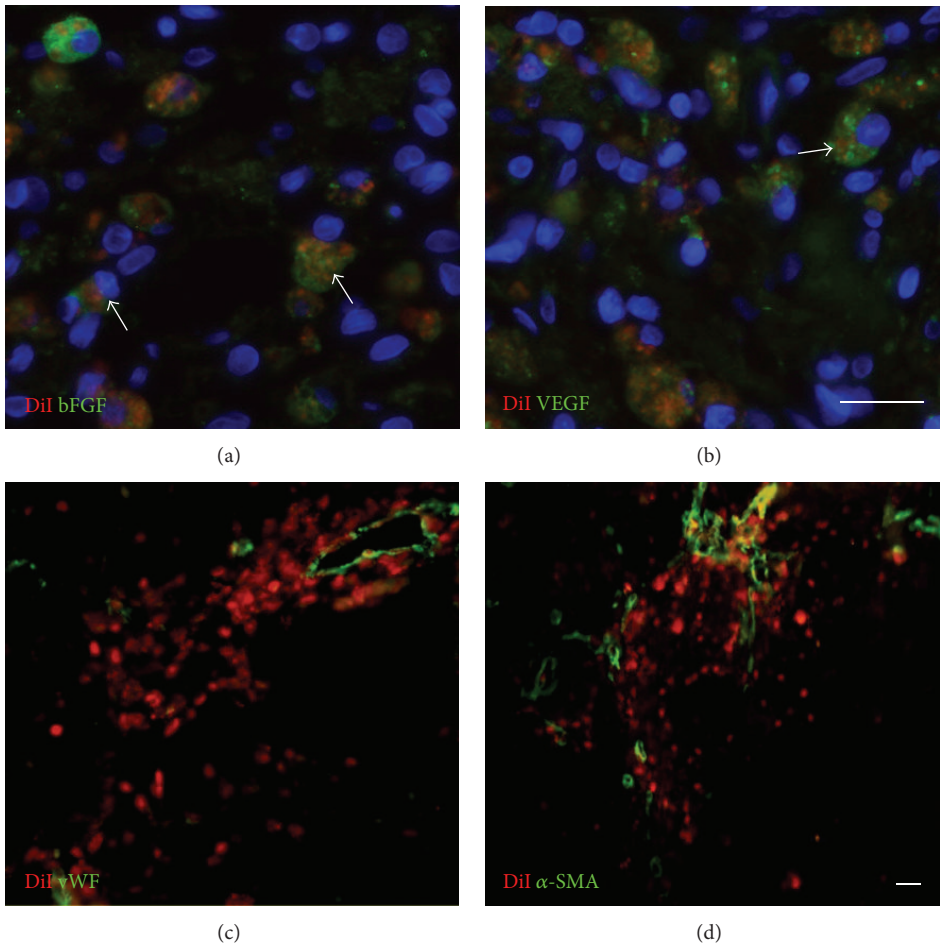

Figure 3: Implanted SKPs secrete growth factors and differentiate into blood vessel in vivo. Immunostaining of DiI and growth factor bFGF, VEGF and blood vessel maker vWF, α-SMA in implantation site of IBZ. Brain sections were immunostained for ((a), (b)) bFGF, VEGF (green) or for ((c), (d)) vWF, α-SMA (green). Arrowhead shows DiI positive cells (red) that were colocalized with bFGF and VEGF (green). Scale bars, 10 μm.

stroke. The number of total BrdU$^+$ cells had no significant difference between cell therapy group and control group in SVZ (Figure 4(d)). Meanwhile, BrdU$^+$ cells also are widely distributed in areas from SVZ to infarct boundary in both groups. Compared with control group, the BrdU$^+$ cells had a 2.5-fold increase in IBZ. Moreover, nestin$^+$ cells had a 2-fold increase in IBZ of SKPs treated groups, but no significant difference between two groups in SVZ (Figure 4(f)). β-III tubulin is a marker that is expressed in newborn neuroblasts and used to trace the nascent cells. At second week after stroke, we observed that β-III tubulin$^+$ cells are distributed in SVZ (Figures 4(b)(II) and 4(b)(IV)) and IBZ (Figures 4(b)(II) and 4(b)(IV)). Compared with control group, the number of β-III tubulin$^+$ cells was increased 2-fold in SVZ, 1.4-fold in IBZ of SKPs group (Figure 4(e)). The increased BrdU$^+$ cells and migrated neuroblasts indicated ameliorated microenvironment in the infract region which promoted neurogenesis in SVZ.

The number of α-SMA$^+$, vWF$^+$ vessels and vWF$^+$/BrdU$^+$ cells at 14 days after transplantation in IBZ (Figure 5(a)) and ischemic zone (IZ) (Figure 5(b)) were analyzed by double immunofluorescence staining and visualized by laser scanning confocal microscopy respectively. By counting the number of α-SMA$^+$ vessels, which represent large blood vessel, the results were significantly higher than that of control group in IBZ but not in IZ (Figure 4(d)). Meanwhile, the vWF$^+$ vessel density of SKPs group has followed the same trend (Figure 5(e)). However, the numbers of vWF$^+$/BrdU$^+$ cells were increased 2.3-fold in IBZ, 2-fold in IZ (Figure 5(f)). These data demonstrate that SKPs have an obvious effect on revascularization of ischemic damage.

4. Discussion

In this study, we demonstrated that injection of 0.5×10^6 SKPs (24 h after brain ischemia) significantly improved functional outcome compared with control group at day 7 and day 14. Morphological analysis indicated that paracrine signaling of SKPs played a major role to enhance vessel density, cellular proliferation, and neurogenesis along the lateral ventricle and in the striatal ischemic boundary zone, which likely

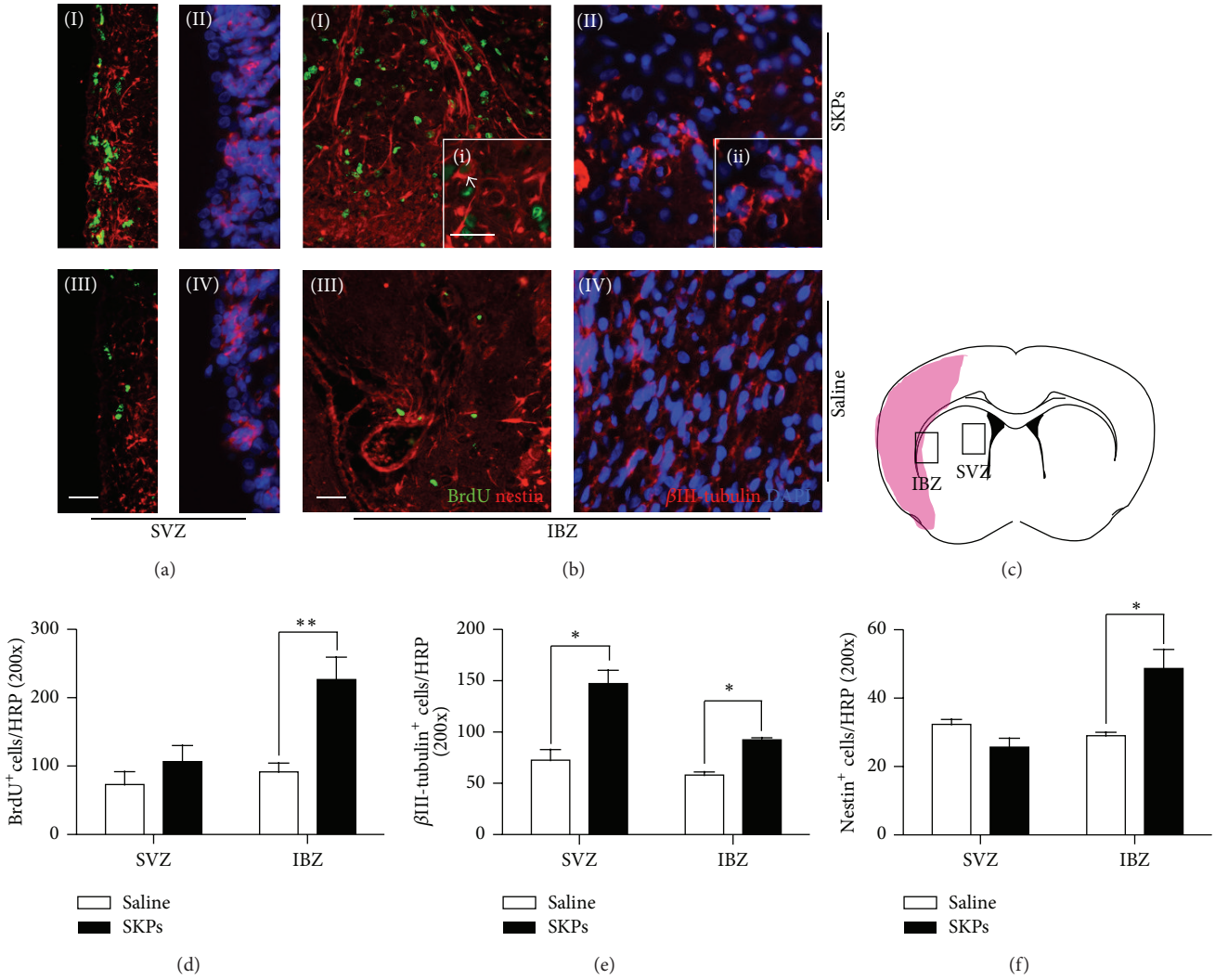

Figure 4: SKPs increase SVZ and IBZ neurogenesis and neuronal progenitor migration to the ischemic lesion 14 days after MCAO. Immunostaining of neural stem cells markers and colocalization of BrdU in (a) SVZ and (b) IBZ of the ischemic rat brain. Brain sections were immunostained for both ((a)(I); (a)(III); (b)(I); (b)(III)) BrdU (green) and nestin (red) or for ((a)(II); (a)(IV); (b)(II); (b)(IV)) βIII-tubulin in SKPs group (top) and PBS (bottom). ((i), (ii)) Higher magnification of indicated by the white box. Arrowhead shows BrdU positive cells that were colocalized with nestin. Scale bars, 10 μm. (c) The pattern of implanted SKPs after cerebral brain ischemia. SVZ and IBZ were indicated by the black box, shadow area, and infracted zone. Quantitative analysis of (d) BrdU, (e) βIII-tubulin, and (f) nestin positive cells in the SVZ and IBZ ($n = 5$ for control and SKPs group). $^{*}P < 0.05$, $^{**}P < 0.01$ versus control.

contributed to the improvement of neurological functional recovery in rat after stroke.

SKPs were initially derived from neural crest and displayed multidirectional differentiation capacity including mesodermal and neural progeny during long-term culture [24]. However, the ability of differentiation into electrophysiologically active neural cells has not been proved by animal model just through hippocampal slices culture [14]. Here, we do not observe any DiI^{+} neural cells differentiation in injection area perhaps due to low cell viability after transplantation. In the present research, the fact that transplanted SKPs improved functional restoration without the reduction of lesion area in the ischemic brain of rats would be more probably due to neurorestorative effects of proteins released by transplanted SKPs, which resulted in neurogenesis and angiogenesis in the ischemic boundary zone.

It was known that NSCs reside in the specific region of brain. When damaged, NSCs will be mobilized and migrate toward injury site immediately in the first two weeks [25] and yet were hard to survive due to low blood-supply level and hypoxia in the local microenvironment [26]. To overcome this problem, MSCs [27] and olfactory ensheathing cells [28] were applied to neuroprotective in stroke animal models of stroke. Noteworthy this is the first report in which the treatment outcome was found in ischemic brain tissue after SKPs transplantation. Results showed that SKPs also secrete VEGF and bFGF, which could help in vascular remolding. Increased vWF-immunoreactive vessel density

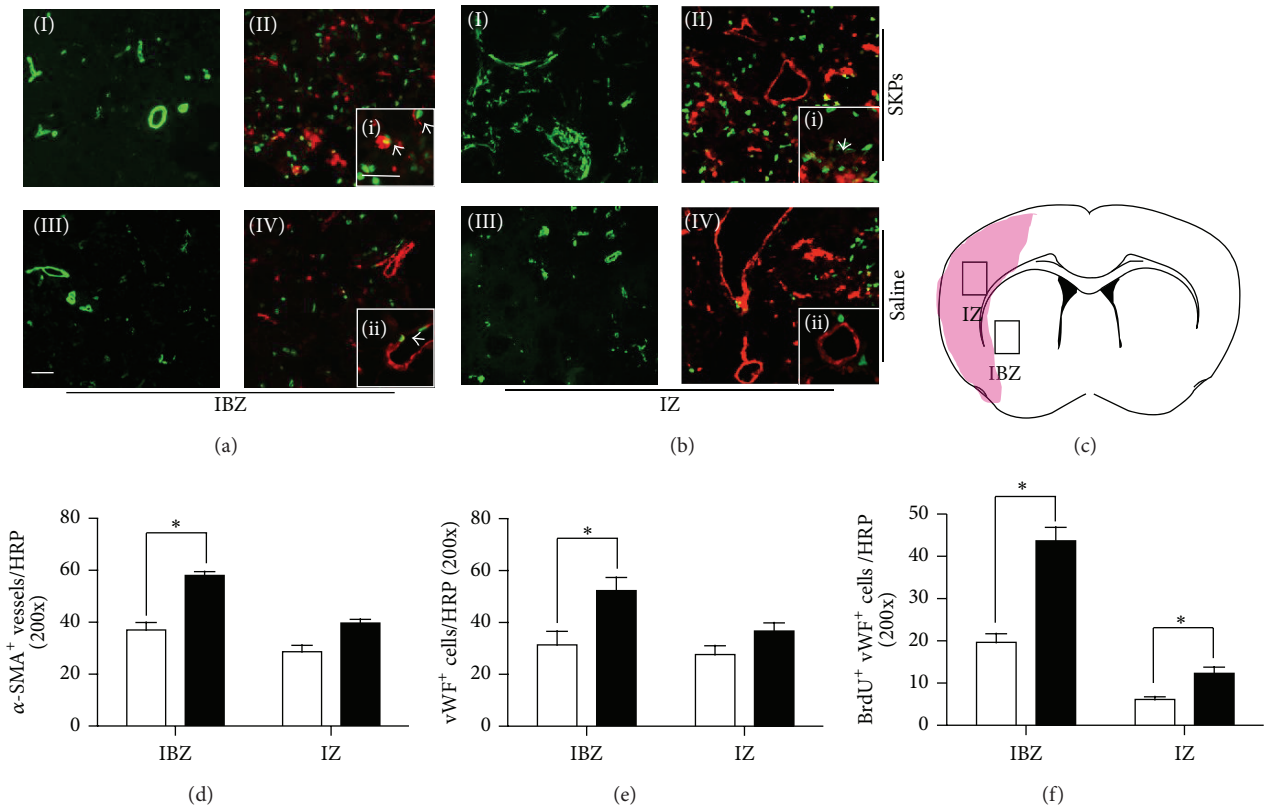

FIGURE 5: SKPs increase IZ and IBZ revascularization in MCAO model of rats. BrdU immunoreactive endothelial cells, α-SMA, and vWF vessels were detected in (a) IBZ and (b) IZ. Brain sections were immunostained for ((a)(I), (a)(III); (b)(I), (b)(III)) α-SMA or for ((a)(II), (a)(IV); (b)(II), (b)(IV)) both BrdU (green) and vWF (red) in SKPs group (top) and PBS (bottom). ((i), (ii), (iii), and (iv)) Higher magnification of indicated by the white box. Arrowhead shows BrdU positive cells that were colocalized with vWF. Scale bars, 10 μm. (c) The pattern of implanted SKPs after cerebral brain ischemia. SVZ and IZ were indicated by the black box, shadow area, and infracted zone. Quantitative data of number of (d) vWF or (e) α-SMA immunoreactive vessels and (f) BrdU immunoreactive endothelial cells. Injected SKPs ($n = 5$) significantly ($P < 0.05$) increased the number of endothelial cells and the density of vessels in the IZ and IBZ compared with group treated with PBS ($n = 5$).

and the number of $BrdU^+$ vWF^+ cells in the rats treated with SKPs indicated that SKPs modulated vascular system and stimulated endothelial cells proliferation.

Previous study reported that, compared to MSCs, SKPs were able to secrete more neurotrophic molecules (like BDNFs, GDNFs, and bFGF) that exhibit substantial effects on neuron survival and functions [29]. Neurotrophic molecules not only stimulates neurite outgrowth for several neuronal cell types in vitro but also stimulates regrowth of multiple descending axon tracts within the spinal cord following injury [30]. In addition, transplantation of neural stem cells overexpressing GDNF enhanced neurogenesis in rats after stroke [31]. We also demonstrated that treatment with SKPs significantly increased the number of BrdU incorporating cells, nestin-immunoreactive cells, and the β-III tubulin-immunoreactive cells in the SVZ suggesting that SKPs treatment enhanced endogenous neurogenesis. Moreover, H&E and toluidine blue staining showed that most neuron exhibited relatively homogenous oval shaped nuclei in SKPs group and less extent of inflammation in SKPs group than the control group. It has been reported that extracellular matrix (ECM) affects cells survival, proliferation, and migration [32]. Fibronectin is a crucial component of the ECM that has been demonstrated to stimulate nerve fiber growth in vitro and exert a neural protective effect after stroke [33]. In our study, SKPs expressed fibronectin in culture. Therefore, it is possible that fibronectin may participate in neuron survival and differentiation and involve the functional restoration by activating integrin signal transduction and reestablishing new neuronal circuits in host brain tissue. Taken together, these data further explain why SKPs could enhance neurological function recovery.

5. Conclusion

Transplantation of SKPs into rat brain after stroke improved neurological function recovery by promoting neurogenesis and neovascularization, because SKPs are readily accessible pluripotent sources and possess various therapeutic capacities, which may become a promising candidate cell source for treatment of stroke.

Conflict of Interests

The authors declare that there is no conflict of interests regarding the publication of this paper.

Authors' Contribution

Duo Mao and Xinpeng Yao contributed equally to this work.

Acknowledgments

The work was partially supported by National Program on Key Basic Research Project (973 Program, no. 2011CB964903), the National Natural Science Foundation of China (NSFC) projects (31260223, 81220108015), and Program for Changjiang Scholars and Innovative Research Team in University (no. IRT13023).

References

[1] R. McKay, "Stem cells in the central nervous system," *Science*, vol. 276, no. 5309, pp. 66–71, 1997.

[2] M. Grabowski, P. Brundin, and B. B. Johansson, "Functional integration of cortical grafts placed in brain infarcts of rats," *Annals of Neurology*, vol. 34, no. 3, pp. 362–368, 1993.

[3] Y. Li, J. Chen, L. Wang, M. Lu, and M. Chopp, "Treatment of stroke in rat with intracarotid administration of marrow stromal cells," *Neurology*, vol. 56, no. 12, pp. 1666–1672, 2001.

[4] S. I. Savitz, D. M. Rosenbaum, J. H. Dinsmore, L. R. Wechsler, and L. R. Caplan, "Cell transplantation for stroke," *Annals of Neurology*, vol. 52, no. 3, pp. 266–275, 2002.

[5] C. Suárez-Monteagudo, P. Hernández-Ramírez, L. Alvarez-González et al., "Autologous bone marrow stem cell neurotransplantation in stroke patients. An open study," *Restorative Neurology and Neuroscience*, vol. 27, no. 3, pp. 151–161, 2009.

[6] J. Chen, Y. Li, L. Wang et al., "Therapeutic benefit of intravenous administration of bone marrow stromal cells after cerebral ischemia in rats," *Stroke*, vol. 32, no. 4, pp. 1005–1011, 2001.

[7] K. J. L. Fernandes, I. A. McKenzie, P. Mill et al., "A dermal niche for multipotent adult skin-derived precursor cells," *Nature Cell Biology*, vol. 6, no. 11, pp. 1082–1093, 2004.

[8] K. J. L. Fernandes, J. G. Toma, and F. D. Miller, "Multipotent skin-derived precursors: adult neural crest-related precursors with therapeutic potential," *Philosophical Transactions of the Royal Society B: Biological Sciences*, vol. 363, no. 1489, pp. 185–198, 2008.

[9] J. A. Biernaskie, I. A. McKenzie, J. G. Toma, and F. D. Miller, "Isolation of skin-derived precursors (SKPs) and differentiation and enrichment of their Schwann cell progeny," *Nature Protocols*, vol. 1, no. 6, pp. 2803–2812, 2007.

[10] J. G. Toma, I. A. McKenzie, D. Bagli, and F. D. Miller, "Isolation and characterization of multipotent skin-derived precursors from human skin," *Stem Cells*, vol. 23, no. 6, pp. 727–737, 2005.

[11] Y. Amoh, L. Li, K. Katsuoka, and R. M. Hoffman, "Multipotent hair follicle stem cells promote repair of spinal cord injury and recovery of walking function," *Cell Cycle*, vol. 7, no. 12, pp. 1865–1869, 2008.

[12] Y. Amoh, L. Li, R. Campillo et al., "Implanted hair follicle stem cells form Schwann cells that support repair of severed peripheral nerves," *Proceedings of the National Academy of Sciences of the United States of America*, vol. 102, no. 49, pp. 17734–17738, 2005.

[13] I. A. McKenzie, J. Biernaskie, J. G. Toma, R. Midha, and F. D. Miller, "Skin-derived precursors generate myelinating Schwann cells for the injured and dysmyelinated nervous system," *The Journal of Neuroscience*, vol. 26, no. 24, pp. 6651–6660, 2006.

[14] K. J. L. Fernandes, N. R. Kobayashi, C. J. Gallagher et al., "Analysis of the neurogenic potential of multipotent skin-derived precursors," *Experimental Neurology*, vol. 201, no. 1, pp. 32–48, 2006.

[15] J. Chen, Z. G. Zhang, Y. Li et al., "Intravenous administration of human bone marrow stromal cells induces angiogenesis in the ischemic boundary zone after stroke in rats," *Circulation Research*, vol. 92, no. 6, pp. 692–699, 2003.

[16] Y. Li, J. Chen, X. G. Chen et al., "Human marrow stromal cell therapy for stroke in rat: Neurotrophins and functional recovery," *neurology*, vol. 59, no. 4, pp. 514–523, 2002.

[17] R. Pili, J. Chang, J. Muhlhauser et al., "Adenovirus-mediated gene transfer of fibroblast growth factor-1: angiogenesis and tumorigenicity in nude mice," *International Journal of Cancer*, vol. 73, no. 2, pp. 258–263, 1997.

[18] J. A. Gorski, S. R. Zeiler, S. Tamowski, and K. R. Jones, "Brain-derived neurotrophic factor is required for the maintenance of cortical dendrites," *The Journal of Neuroscience*, vol. 23, no. 17, pp. 6856–6865, 2003.

[19] S. K. Steinbach, O. El-Mounayri, R. S. Dacosta et al., "Directed differentiation of skin-derived precursors into functional vascular smooth muscle cells," *Arteriosclerosis, Thrombosis, and Vascular Biology*, vol. 31, no. 12, pp. 2938–2948, 2011.

[20] Y. Amoh, L. Li, M. Yang et al., "Nascent blood vessels in the skin arise from nestin-expressing hair-follicle cells," *Proceedings of the National Academy of Sciences of the United States of America*, vol. 101, no. 36, pp. 13291–13295, 2004.

[21] R. Aki, Y. Amoh, N. Li, K. Katsuoka, and R. M. Hoffman, "Nestin-expressing interfollicular blood vessel network contributes to skin transplant survival and wound healing," *Journal of Cellular Biochemistry*, vol. 110, no. 1, pp. 80–86, 2010.

[22] S. T. Chen, C. Y. Hsu, E. L. Hogan, H. Maricq, and J. D. Balentine, "A model of focal ischemic stroke in the rat: reproducible extensive cortical infarction," *Stroke*, vol. 17, no. 4, pp. 738–743, 1986.

[23] P. Taupin, "BrdU immunohistochemistry for studying adult neurogenesis: paradigms, pitfalls, limitations, and validation," *Brain Research Reviews*, vol. 53, no. 1, pp. 198–214, 2007.

[24] A. Joannides, P. Gaughwin, C. Schwiening et al., "Efficient generation of neural precursors from adult human skin: astrocytes promote neurogenesis from skin-derived stem cells," *The Lancet*, vol. 364, no. 9429, pp. 172–178, 2004.

[25] T. Yamashita, M. Ninomiya, P. H. Acosta et al., "Subventricular zone-derived neuroblasts migrate and differentiate into mature neurons in the post-stroke adult striatum," *The Journal of Neuroscience*, vol. 26, no. 24, pp. 6627–6636, 2006.

[26] A. Arvidsson, T. Collin, D. Kirik, Z. Kokaia, and O. Lindvall, "Neuronal replacement from endogenous precursors in the adult brain after stroke," *Nature Medicine*, vol. 8, no. 9, pp. 963–970, 2002.

[27] S.-W. Yoo, S.-S. Kim, S.-Y. Lee et al., "Mesenchymal stem cells promote proliferation of endogenous neural stem cells and survival of newborn cells in a rat stroke model," *Experimental and Molecular Medicine*, vol. 40, no. 4, pp. 387–397, 2008.

[28] W. C. Shyu, D. D. Liu, S. Z. Lin et al., "Implantation of olfactory ensheathing cells promotes neuroplasticity in murine models of stroke," *The Journal of Clinical Investigation*, vol. 118, no. 7, pp. 2482–2495, 2008.

[29] M. Li, J. Y. Liu, S. Wang et al., "Multipotent neural crest stem cell-like cells from rat vibrissa dermal papilla induce neuronal differentiation of PC12 cells," *BioMed Research International*, vol. 2014, Article ID 186239, 13 pages, 2014.

[30] W. Gu, F. Zhang, Q. Xue, Z. Ma, P. Lu, and B. Yu, "Bone mesenchymal stromal cells stimulate neurite outgrowth of spinal neurons by secreting neurotrophic factors," *Neurological Research*, vol. 34, no. 2, pp. 172–180, 2012.

[31] M. Yuan, S. J. Wen, C. X. Yang et al., "Transplantation of neural stem cells overexpressing glial cell line-derived neurotrophic factor enhances Akt and Erk1/2 signaling and neurogenesis in rats after stroke," *Chinese Medical Journal*, vol. 126, no. 7, pp. 1302–1309, 2013.

[32] K. M. Yamada, S. Aota, S. K. Akiyama, and S. E. LaFlamme, "Mechanisms of fibronectin and integrin function during cell adhesion and migration," *Cold Spring Harbor Symposia on Quantitative Biology*, vol. 57, pp. 203–212, 1992.

[33] T. Sakai, K. J. Johnson, M. Murozono et al., "Plasma fibronectin supports neuronal survival and reduces brain injury following transient focal cerebral ischemia but is not essential for skin-wound healing and hemostasis," *Nature Medicine*, vol. 7, no. 3, pp. 324–330, 2001.

Hindawi Publishing Corporation
BioMed Research International
Volume 2015, Article ID 974615, 8 pages
http://dx.doi.org/10.1155/2015/974615

Research Article

Activating Transcription Factor 4 Promotes Angiogenesis of Breast Cancer through Enhanced Macrophage Recruitment

Chen Liu,[1] Zongjin Li,[2] Lina Wang,[3] Lingling Tong,[4] Ningning He,[2] Yanan Chen,[2] Yanhua Liu,[2] Zhongjun Wu,[1] Peiqing Sun,[5] Rong Xiang,[1,2] Guosheng Ren,[1] and Weijun Su[2]

[1] *The First Affiliated Hospital of Chongqing Medical University, Chongqing 400016, China*
[2] *School of Medicine, Nankai University, Tianjin 300071, China*
[3] *State Key Lab of Experimental Hematology, Institute of Hematology and Blood Diseases Hospital, Chinese Academy of Medical Sciences, Tianjin 300052, China*
[4] *Department of Clinical Laboratory, Xiamen International Travel Healthcare Center, Xiamen 361012, China*
[5] *Department of Cell and Molecular Biology, The Scripps Research Institute, La Jolla, CA 92037, USA*

Correspondence should be addressed to Guosheng Ren; rengs726@126.com and Weijun Su; suweijun@nankai.edu.cn

Received 4 September 2014; Accepted 30 November 2014

Academic Editor: Betti Giusti

Angiogenesis plays an important role in the progression of tumor. Besides being regulated by tumor cells per se, tumor angiogenesis is also influenced by stromal cells in tumor microenvironment (TME), for example, tumor associated macrophages (TAMs). Activating transcription factor 4 (ATF4), a member of the ATF/CREB family, has been reported to be related to tumor angiogenesis. In this study, we found that exogenous overexpression of ATF4 in mouse breast cancer cells promotes tumor growth via increasing tumor microvascular density. However, ATF4 overexpression failed to increase the expression level of a series of proangiogenic factors including vascular endothelial growth factor A (VEGFA) in tumor cells in this model. Thus, we further investigated the infiltration of proangiogenic macrophages in tumor tissues and found that ATF4-overexpressing tumors could recruit more macrophages via secretion of macrophage colony stimulating factor (M-CSF). Overall, we concluded that exogenous overexpression of ATF4 in breast cancer cells may facilitate the recruitment of macrophages into tumor tissues and promote tumor angiogenesis and tumor growth indirectly.

1. Introduction

Angiogenesis plays an important role in the progression of tumor. Insufficient oxygen supply to meet the demands of proliferating cancer cells gives rise to hypoxic tumor microenvironment (TME). And oxygen-deprived cancer cells respond to the hypoxic stress by inducing a series of cellular responses leading to angiogenesis [1–4]. Besides being regulated by tumor cells per se, it has been found that stromal cells in TME also play significant roles in tumor angiogenesis [5–8]. Among them, tumor associated macrophages (TAMs) are most intensively studied. Via either producing proangiogenic factors or physically assisting angiogenic sprouting, TAMs have been found to promote tumor angiogenesis directly or indirectly [8–11].

Activating transcription factor 4 (ATF4) belongs to the ATF/CREB family. It has been found that ATF4 expression is increased in response to tumor microenvironment stresses including oxygen deprivation [12–15], and it takes part in the adaptation to hypoxia [16, 17]. In previous studies, ATF4 was shown to mediate the VEGF-dependent tumor growth and angiogenesis triggered by osteopontin (OPN) [18]. However, it has not been discussed before whether exogenous overexpression of ATF4 in tumor cells can also influence tumor angiogenesis via regulating stromal cells in TME.

In this study, we overexpressed ATF4 in mouse breast cancer 4T1 and 4TO7 cells. In these two models, ATF4 overexpression facilitates the macrophage infiltration into breast cancer tissues via enhanced secretion of M-CSF and thus

promotes tumor angiogenesis and tumor growth indirectly via recruiting proangiogenic macrophages.

2. Materials and Methods

2.1. Cell Culture. Mouse breast cancer cell lines 4T1 and 4TO7 and mouse macrophage cell line Raw264.7 were cultured with 1640 medium (ThermoFisher Scientific, Hudson, NH) supplemented with 10% fetal bovine serum (FBS) (Corning, Lowell, MA) and 1% penicillin-streptomycin solution (Gibco, Rockville, MD). All cell lines were maintained at 37°C in a 5% CO2 incubator. To be tracked *in vivo*, 4T1 cells were transduced with a self-inactivating lentiviral vector carrying a ubiquitin promoter driving firefly luciferase reporter gene to obtain the 4T1-Luc cells.

2.2. Plasmid Constructs. The lentivirus system including three packaging vectors (pCMV-VSVG, pRRE, and pRSV-REV) and the expression vector (pLV-EF1α-MCS-IRES-Bsd) were purchased from Biosettia Company (San Diego, CA, USA). Full-length mouse ATF4 was cloned from 4T1 cell cDNA, and the PCR-amplified fragment was inserted into the MCS of pLV-EF1α-MCS-IRES-Bsd vector to obtain the pLV-ATF4-Bsd plasmid.

2.3. Lentivirus Packaging and Generation of Stable Transfectants. 293T cells were transfected with the lentivirus packaging vectors and pLV-ATF4-Bsd plasmid using Lipo-2000 (Invitrogen, Carlsbad, CA) according to the manufacturer's instructions. 40 hours after transfection, the supernatant was collected and stored at −80°C until use.

4T1-Luc or 4TO7 cells were seeded into 6-well plates at a density of 10^5 per well. 24 hours later, the medium was changed with the mixture of 2 mL complete medium and 1 mL lentivirus supernatant, and the cells were centrifuged at 1600 rpm for 1 h at 37°C. After centrifugation, the lentivirus was discarded, and the tumor cells were cultured for another 48 h before the selection medium with Bsd (Sigma, St. Louis, MO) was added. Four days later, the protein of the selected 4T1-Luc-ATF4 or 4TO7-ATF4 cells was collected to detect the ATF4 expression level.

2.4. Cell Counting Kit-8 (CCK-8) Assay. CCK-8 assay kit was bought from Dojindo Molecular Technologies (Kumamoto, Japan). Cells for assay were cultured in 96-well plates, and the culture medium was changed with 100 μL fresh medium per well before each measurement. 10 μL CCK-8 working solution was added to each well, and the cells were incubated for another 2 hours. Two hours later, the absorbance of the samples at 450 nm was measured using GloMax-Multi Detection System (Promega, Madison, WI).

2.5. Western Blot Analysis. Total cell protein was prepared by lysis of cells with the radioimmunoprecipitation assay (RIPA) buffer, and the protein concentrations were determined by the bicinchoninic acid (BCA) protein assay kit (ThermoFisher Scientific). Proteins were examined with specific antibodies against ATF4 (1 : 1000 dilution, Santa Cruz Biotechnology, Santa Cruz, CA), luciferase (1 : 1000 dilution, Promega), Ki67 (1 : 1000 dilution, Abcam, Cambridge, MA), M-CSF (1 : 1000 dilution, Santa Cruz Biotechnology), and β-actin (1 : 5000 dilution, Santa Cruz Biotechnology), followed by peroxidase-conjugated secondary antibodies (Abcam). The reactions were detected using Immobilon Western Chemiluminescent HRP Substrate (Millipore, Billerica, MA).

2.6. Real-Time PCR. Total RNA was extracted using TRIzol reagent (Invitrogen) and reverse transcribed with PrimeScript RT reagent (TaKaRa, Shiga, Japan). SYBR Premix Ex Taq (TaKaRa) was used to amplify cDNA for real-time PCR. The primers used for real-time PCR are as follows: mouse hypoxia inducible factor 1 alpha (mHIF-1alpha) (5′-GTGCACCCTAACAAGCCGGGG-3′/5′-AGCACCAAGCACGTCATGGGT-3′), mouse vascular endothelial growth factor A (mVEGFA) (5′-AGGGCTATACTGCCCTCCAA-3′/5′-ACGCGAGTCTGTGTTTTTGC-3′), mouse placenta growth factor (mPlGF) (5′-CACTTGCTTCTTACAGGTCC-3′/5′-CACCTCATCAGGCTATTCAT-3′), mouse platelet derived growth factor, B polypeptide (mPDGF-B) (5′-TGTAATCGCCGAGTGCAAGA-3′/5′-CATTGCACATTGCGGTTATTG-3′), mouse angiopoietin 1 (mANG-1) (5′-AGCTACCAACAACAACAGCA-3′/5′-GCAAAGGCTGATAAGGTTATGA-3′), mouse angiopoietin 2 (mANG-2) (5′-AGCCACGGTCAACAACTCGC-3′/5′-TCTTCTTTACGGATAGCAAC-3′), mouse granulocyte colony stimulating factor (mG-CSF) (5′-CGTTCCCCTGGTCACTGTC-3′/5′-TAGAGCCTGCAGGAGACCTT-3′), mouse macrophage colony stimulating factor (mM-CSF) (5′-GCAACTCAGCCACCCCCGTT-3′/5′-AAAACGGGCCACAGGCCTGG-3′), and mouse granulocyte-macrophage colony stimulating factor (mGM-CSF) (5′-CTCCGGAAACGGACTGTGAA-3′/5′-AGGGCTATACTGCCCTCCAA-3′). Data analysis was performed using GelDoc XR (BioRad, Berkeley, CA, USA).

2.7. Transwell Migration Assay. 1×10^5 Raw264.7 cells in 200 μL basic medium were seeded upon the 24-well Millicell Hanging Cell Culture Inserts (Millipore) with conditioned medium of ATF4 overexpressing tumor cells or control cells in the lower chamber. After incubation for 24 hours, the inserts were taken out, and the cells were removed from the upper chamber with a cotton swab. Cells which have migrated through the pores and attached to the reverse side of the membrane were fixed with 4% formaldehyde in PBS, followed by staining with 0.5% crystal violet for 20 min. Cells of 5 randomly chosen fields per membrane were counted under the microscope at 200x and statistically analyzed.

2.8. Animal Works. Six-week-old female Balb/c mice were purchased from the Experimental Animal Institute, Chinese Academy of Medical Sciences (Beijing, China). All experimental procedures were conducted in conformity with institutional guidelines for The Care and Use of Laboratory Animals in Nankai University, Tianjin, China, and conformed to the National Institutes of Health (NIH) Guide for Care and Use of Laboratory Animals. 4T1-Luc-ATF4

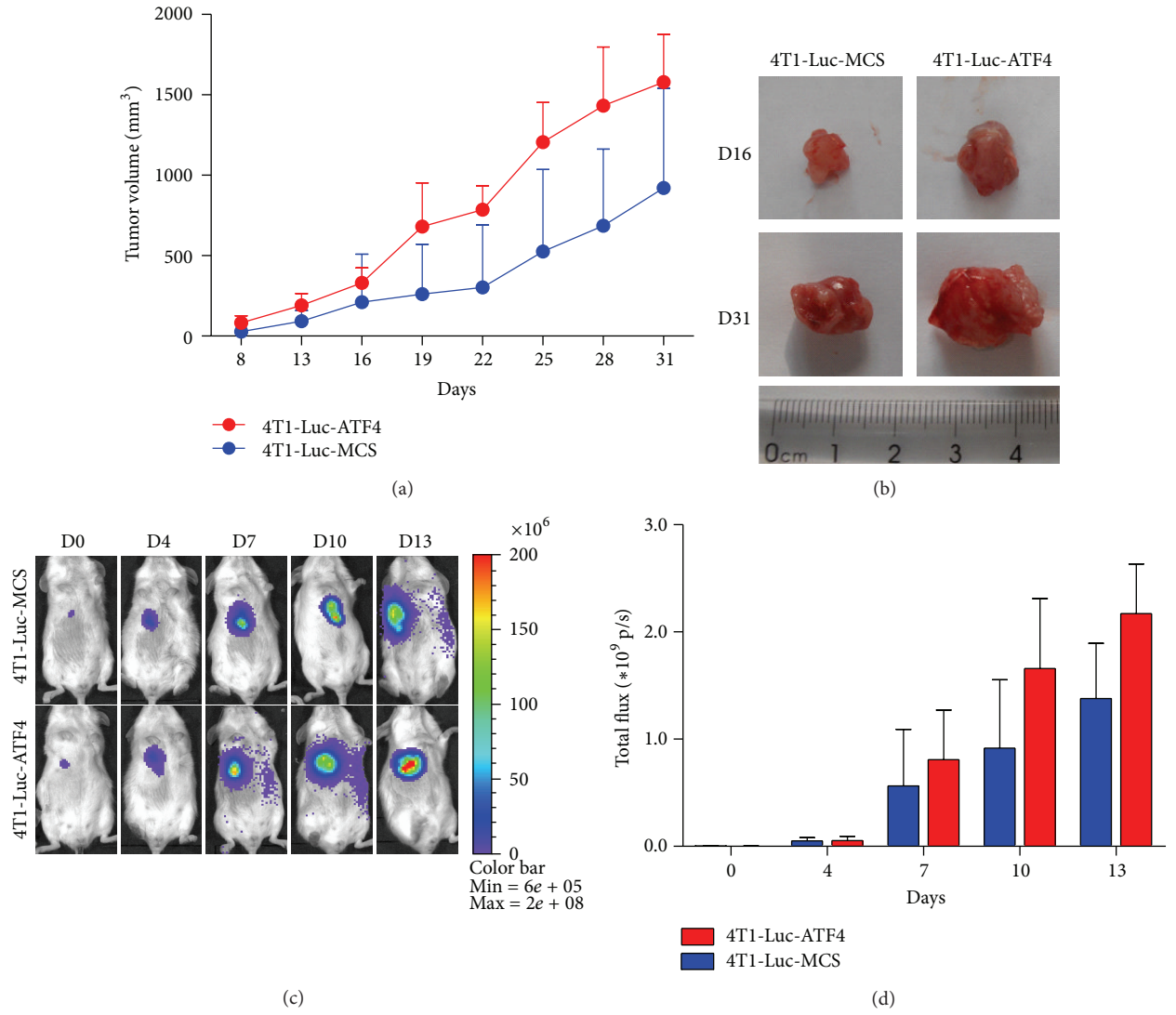

FIGURE 1: ATF4 promotes the growth of breast cancer *in vivo*. (a) ATF4-overexpressing breast cancer grew faster than MCS group *in vivo*. (b) Representative tumor tissues from ATF4 group and MCS group on day 16 and day 31. (c) Fluc imaging of subcutaneous breast cancers from ATF4 group and MCS group on day 0, day 4, day 7, day 10, and day 13. For each group, a representative mouse at each time point was shown. (d) Quantitative analysis of BLI signals in (c) was shown as photons/sec/cm^2/sr. MCS is the abbreviation of multiple cloning sites, and MCS group is used as control here.

or 4T1-Luc-MCS cells (5×10^4 per mouse) were injected subcutaneously to the mice. Bioluminescence imaging was performed on day 0, day 4, day 7, day 10, and day 13. The tumor volume was measured with microcalipers from day 8 to day 31. Mice were sacrificed on day 16 or day 31, and the tumor tissues were embedded within OCT and stored at −80°C until use.

2.9. Bioluminescence Imaging. Bioluminescence imaging of Fluc was performed using the IVIS Lumina II system (Xenogen, Alameda, CA). After intraperitoneal injection of D-Luciferin (150 mg/kg) (Invitrogen), each mouse was imaged for 1–5 minutes under anesthesia with isoflurane. Bioluminescence signals were quantified in units of maximum photons per second per cm square per steradian (photons/sec/cm^2/sr).

2.10. Immunofluorescence Staining. For immunofluorescence staining, specific antibodies against F4/80 (1 : 50 dilution, Abcam) and mouse CD31 (1 : 100 dilution, BD Biosciences, Bedford, MA), followed by Alexa Fluor 594 labeled-secondary antibodies (Invitrogen), were used for detection. Then the sections were counterstained with 4′,6-diamidino-2-phenylindole (DAPI), mounted, and observed under the microscope.

2.11. Immunohistochemical Staining. Specific antibody against M-CSF (1 : 50 dilution, Santa Cruz Biotechnology) followed by peroxidase-conjugated goat anti-mouse IgG (Vector Laboratories, Burlingame, CA) was used. DAB Peroxidase Substrate Kit (Vector Laboratories) was employed for detection. Then the sections were costained with hematoxylin, hydrated, mounted, and observed under the microscope.

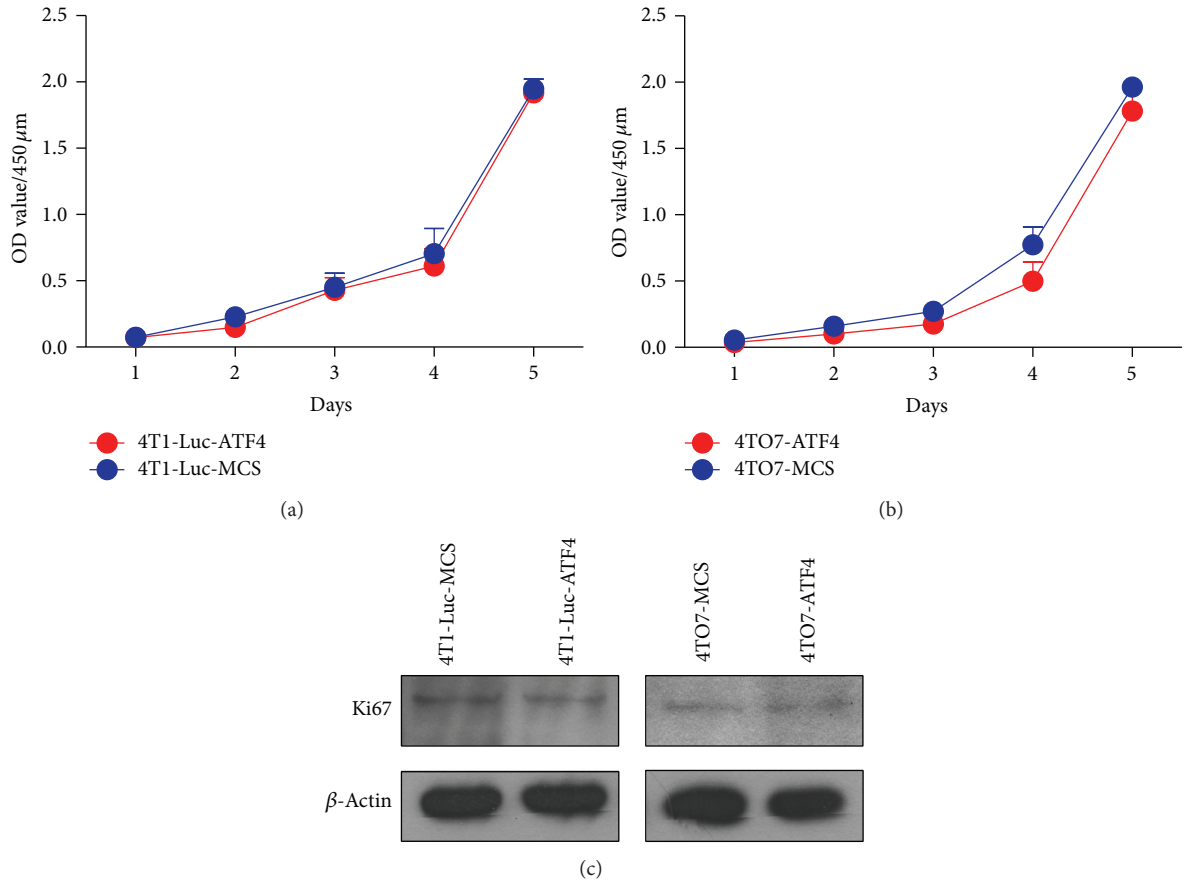

Figure 2: ATF4 does not influence the proliferation of mouse breast cancer cells *in vitro*. (a) ATF4 overexpression did not influence the proliferation of 4T1-Luc cells *in vitro*. (b) ATF4 overexpression did not influence the proliferation of 4TO7 cells *in vitro*. (c) ATF4 overexpression did not influence Ki67 expression level in 4T1-Luc and 4TO7 cells.

2.12. Statistical Analysis. Statistics were calculated using SigmaStat for Windows Version 3.5. For comparison between two groups, two-tailed Student's t-test was used. Differences were considered as significant at P values of less than 0.05.

3. Results and Discussion

3.1. ATF4 Promotes the Growth of Breast Cancer In Vivo without Influencing Breast Cancer Cell Proliferation In Vitro. First, to study the influence of ATF4 on the growth of breast cancer, we overexpressed ATF4 in mouse breast cancer 4T1-Luc cells and injected the 4T1-Luc-ATF4 cells subcutaneously to Balb/c mice. Western blots were used to confirm the overexpression of ATF4 (Figure S1(a), available online at http://dx.doi.org/10.1155/2014/974615). And the expression level of Luc was not influenced by ATF4 overexpression (Figure S1(b)).

The growth rate of ATF4-overexpressing tumors was significantly enhanced compared to MCS tumors (used as control here), and the average volume of ATF4-overexpressing tumors was nearly twice that of MCS tumors on day 31 (Figure 1(a)). Figure 1(b) shows the representative tumor tissues from ATF4 group and MCS group on day 16 and day 31. For it is not an exact method to measure the volume of tumors with microcalipers in early stage, we also employed bioluminescence imaging (BLI) to assess the growth rate of tumors. Via BLI, we found that even in early stage ATF4-overexpressing tumors grew with a much higher rate (Figures 1(c) and 1(d)).

To investigate whether the promotion effect on breast cancer growth depends on the influence of ATF4 on cancer cell proliferation, CCK-8 cell proliferation assay was performed. Figure 2(a) shows that ATF4 overexpression did not significantly influence the proliferation of 4T1-Luc cells *in vitro*. Similarly, overexpression of ATF4 in another mouse breast cancer cell line, 4TO7, also did not obviously influence its proliferation (Figures S1(a) and 2(b)). We also detected the expression of Ki67, a proliferation marker in ATF4-overexpressing breast cancer cells by western blots. In either 4T1-Luc cells or 4TO7 cells, ATF4 overexpression failed to enhance the Ki67 expression level (Figure 2(c)). Overall, these data demonstrated that ATF4 could not influence the proliferation of mouse breast cancer cells. Thus, we hypothesized that ATF4 may promote the growth of breast cancer *in vivo* through regulation of TME.

3.2. ATF4 Increases the Microvascular Density of Breast Cancer but Fails to Upregulate the Expression of Proangiogenic Factors

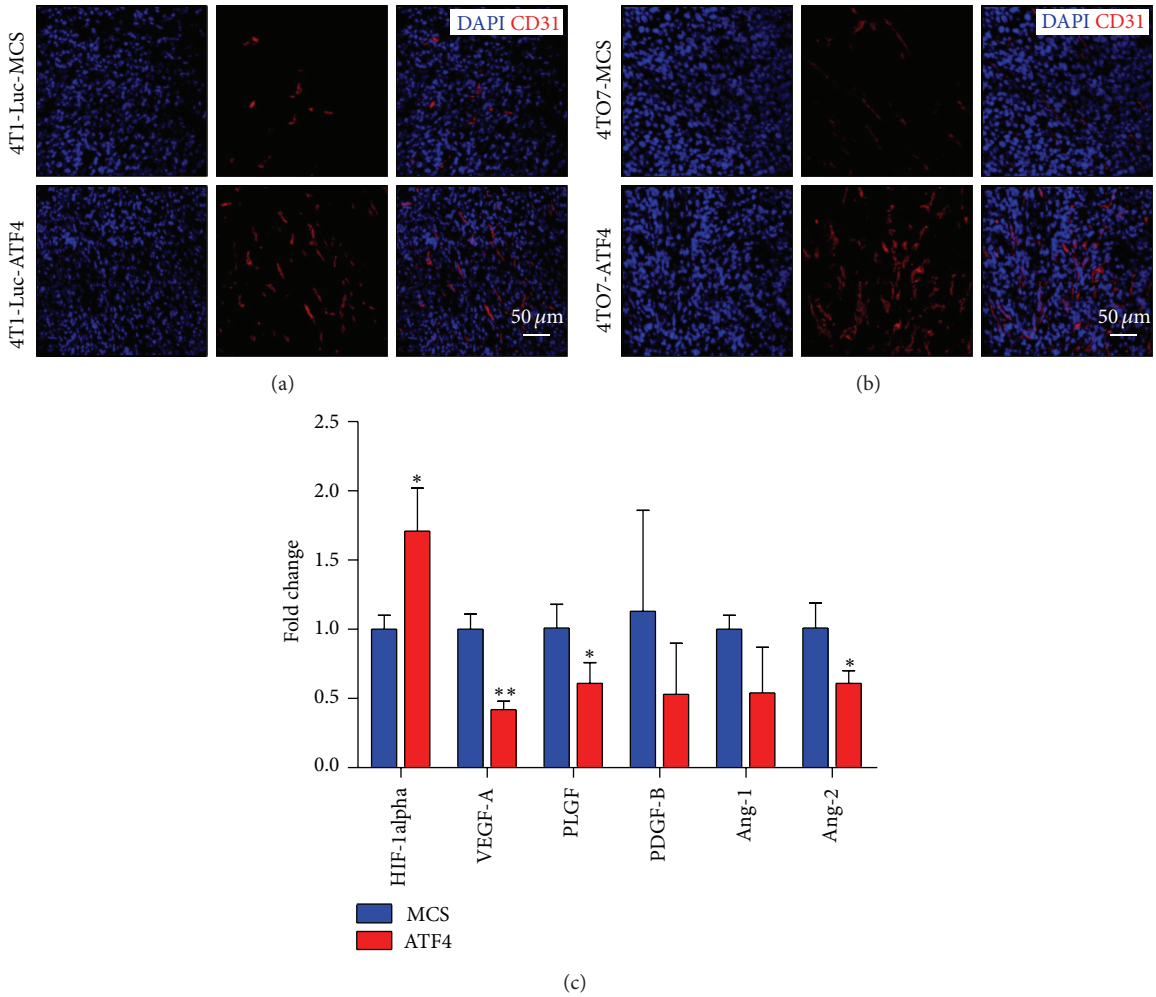

Figure 3: ATF4 increases the microvascular density in breast cancer tissue. (a) Immunofluorescence staining of CD31 showed the increased microvascular density in ATF4-overexpressing 4T1-Luc breast cancers. (b) Immunofluorescence staining of CD31 showed the increased microvascular density in ATF4-overexpressing 4TO7 breast cancers. (c) ATF4 did not significantly influence the expression of proangiogenic factors.

in Breast Cancer Cells. Angiogenesis is an important limiting factor on tumor growth. There have been reports that ATF4 relates to tumor angiogenesis. This leads us to investigate whether ATF4 overexpression can regulate breast cancer angiogenesis and also promote breast cancer growth *in vivo*. We sacrificed 4T1-Luc or 4TO7 tumor-bearing mice on day 31 and detected microvascular density in tumor tissues. Figures 3(a) and 3(b) show that the microvascular density of ATF4-overexpressing tumors is much higher than MCS groups in these two models.

For there have been reports that ATF4 can regulate the expression of VEGF [16–18], we initially speculated that maybe exogenous ATF4 overexpression can promote tumor angiogenesis via upregulation of proangiogenic factors in breast cancer cells. However, to our surprise, real-time PCR showed that ATF4 failed to enhance the mRNA level of most proangiogenic factors we detected in breast cancer cells. In fact, the expression level of VEGF-A, PlGF, PDGF-B, Ang-1, and Ang-2 even tended to decrease in ATF4-overexpressing breast cancer cells. The only exception was HIF-1alpha, whose expression level was upregulated by ATF4 less than two times (Figure 3(c)). Consistent with our results, it has been reported that ablation of ATF4 in mice leads to dramatic decrease of HIF-1alpha expression in osteoblasts [17].

3.3. ATF4 Facilitates the Recruitment of Macrophages via Enhanced Secretion of M-CSF. Besides being regulated by tumor cells per se, tumor angiogenesis can also be influenced by stromal cells in TME. In previous studies, it has been reported that TAMs in TME are proangiogenic. Thus we detected whether the infiltration of macrophages in tumor tissues was influenced by ATF4 overexpression. Immunofluorescence staining for F4/80, a macrophage marker, showed that there were more macrophages recruited into ATF4-overexpressing breast cancer tissues in both 4T1-Luc and 4TO7 model (Figures 4(a) and 4(b)). And this phenomenon

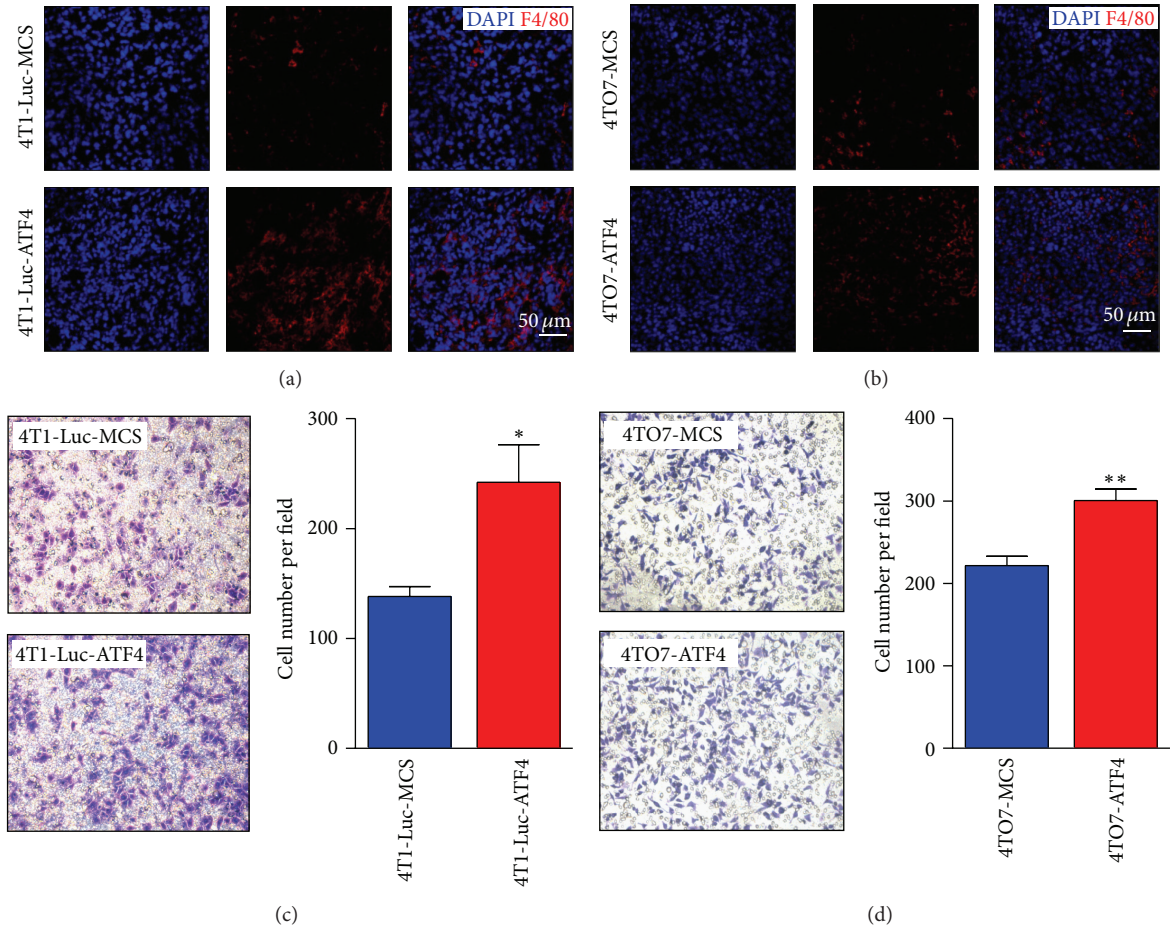

Figure 4: ATF4 facilitates the recruitment of macrophages both *in vitro* and *in vivo*. (a) Immunofluorescence staining of F4/80 showed more macrophages infiltrating into ATF4-overexpressing 4T1-Luc breast cancer tissue compared to MCS group. (b) Immunofluorescence staining of F4/80 showed more macrophages infiltrating into ATF4-overexpressing 4TO7 breast cancer tissue compared to MCS group. (c) More Raw264.7 cells were recruited by the conditioned medium of ATF4-overexpressing 4T1-Luc cells. Data were representative of three independent experiments. (d) More Raw264.7 cells were recruited by the conditioned medium of ATF4-overexpressing 4TO7 cells. Data were representative of three independent experiments.

was further confirmed by transwell migration assay *in vitro*. Compared to MCS groups, more mouse macrophage Raw264.7 cells were recruited to the lower chamber by the conditioned medium of ATF4-overexpressing breast cancer cells (Figures 4(c) and 4(d)).

In most malignant tumors, macrophages compose the most prominent component of stromal cells in TME. Once infiltrated into tumor tissues, macrophages undergo profound changes in gene transcription, thus resulting in the proangiogenic "tumor associated macrophages (TAMs)." The overall TAMs number has been found to be correlated with increased microvascular density in a variety of tumors, for example, pulmonary adenocarcinoma [19], endometrial carcinoma [20], and also breast cancer [21]. And our results further confirmed this phenomenon in breast cancer.

Further, we wanted to uncover the soluble factors through which more macrophages were recruited to ATF4-overexpressing tumors. By real-time PCR, we found that among G-CSF, M-CSF, and GM-CSF, which have been reported to be related to the recruitment and development of macrophages, only M-CSF expression level was significantly elevated in ATF4-overexpressing breast cancer cells (Figure 5(a)), which was also confirmed in protein level by western blots (Figure 5(b)). Furthermore, immunohistochemical staining also demonstrated the elevated level of M-CSF in ATF4-overexpressing breast cancer tissues (Figure 5(c)).

A series of previous studies implicate M-CSF derived from breast cancer cells as a potent chemoattractant for macrophages [22–25]. There have been reports that ATF4 was largely modulated by M-CSF signaling and was also crucial for M-CSF induction of RANK expression in bone marrow monocytes [26]. However, there have been no reports whether M-CSF can also be regulated by ATF4 before. In our study, ectopic overexpression of ATF4 in breast cancer cells led to the enhanced expression of M-CSF and also the increased infiltration of macrophages into tumor tissues. And it needs further investigation to reveal the underlying mechanisms.

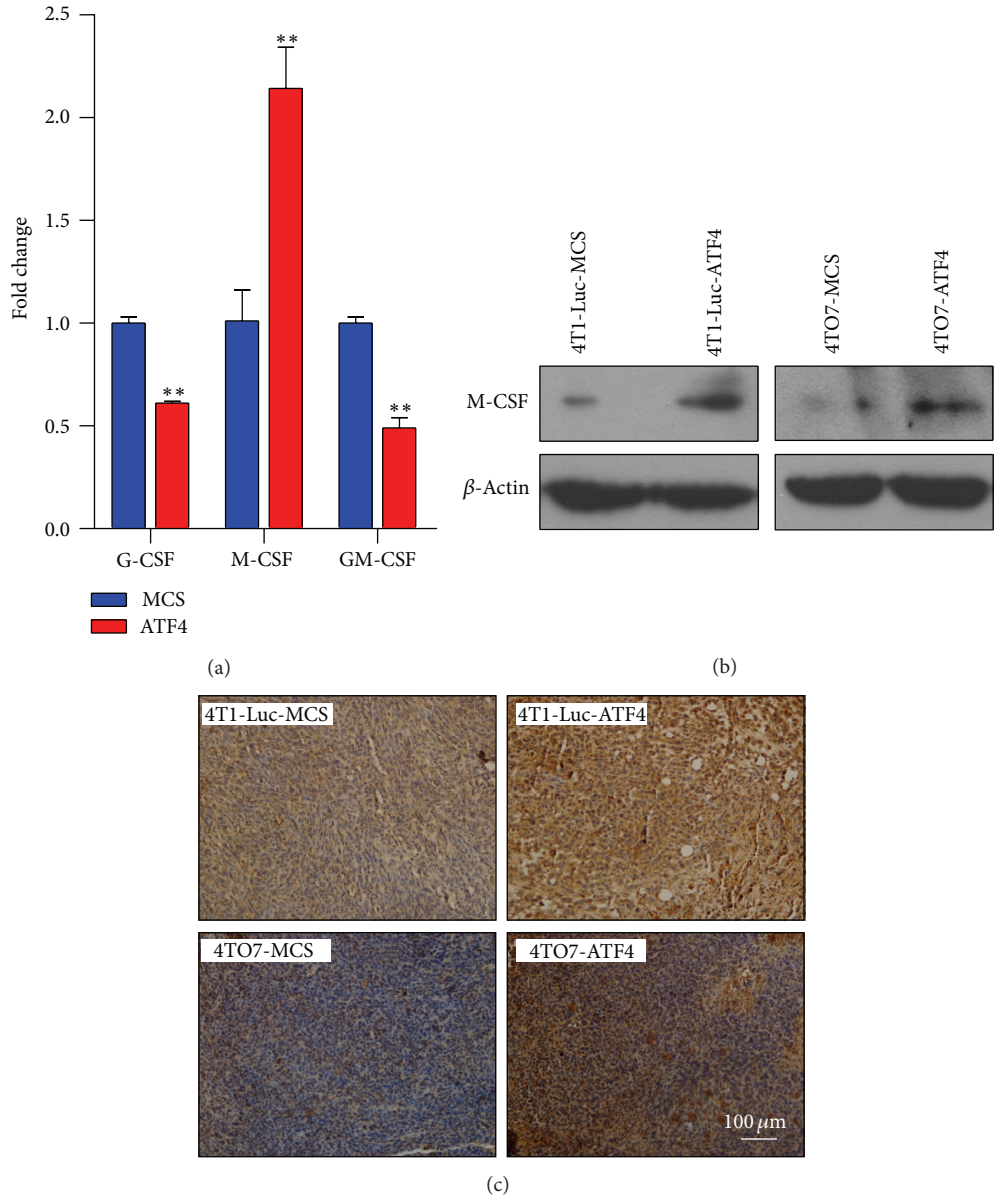

Figure 5: ATF4 increases the expression of M-CSF in breast cancer cells. (a) The mRNA level of M-CSF was increased in ATF4-overexpressing breast cancer cells. (b) The protein level of M-CSF was increased in ATF4-overexpressing breast cancer cells. (c) Immunohistochemical staining showed increased M-CSF level in ATF4-overexpressing breast cancer tissues.

4. Conclusions

In this study, we demonstrated that exogenous overexpression of ATF4 in mouse breast cancer cells can increase proangiogenic macrophages infiltrating into tumor tissues via the secretion of M-CSF, thus promoting the tumor angiogenesis and also tumor growth indirectly. These results provide interesting observations that ATF4 can affect tumor angiogenesis via the recruitment of macrophages into TME of breast cancer and also novel insights into the role of ATF4 on tumor angiogenesis besides the direct regulation of proangiogenic factors.

Conflict of Interests

The authors declare that there is no conflict of interests regarding the publication of this paper.

Acknowledgments

This work was partially supported by grants from the National Key Scientific Research Projects of China (2013CB967201), China International Cooperation Research Program (2012DFA10650), and National Natural Science Foundation of China (81402407) and General Financial

Grant from the China Postdoctoral Science Foundation (2014M551016).

References

[1] L. Marignol, K. Rivera-Figueroa, T. Lynch, and D. Hollywood, "Hypoxia, notch signalling, and prostate cancer," *Nature Reviews Urology*, vol. 10, no. 7, pp. 405–413, 2013.

[2] Y. Yang, M. Sun, L. Wang, and B. Jiao, "HIFs, angiogenesis, and cancer," *Journal of Cellular Biochemistry*, vol. 114, no. 5, pp. 967–974, 2013.

[3] G.-H. Fong, "Mechanisms of adaptive angiogenesis to tissue hypoxia," *Angiogenesis*, vol. 11, no. 2, pp. 121–140, 2008.

[4] J. A. Bertout, S. A. Patel, and M. C. Simon, "The impact of O_2 availability on human cancer," *Nature Reviews Cancer*, vol. 8, no. 12, pp. 967–975, 2008.

[5] G. L. Semenza, "Cancer-stromal cell interactions mediated by hypoxia-inducible factors promote angiogenesis, lymphangiogenesis, and metastasis," *Oncogene*, vol. 32, no. 35, pp. 4057–4063, 2013.

[6] S. B. Coffelt, C. E. Lewis, L. Naldini, J. M. Brown, N. Ferrara, and M. de Palma, "Elusive identities and overlapping phenotypes of proangiogenic myeloid cells in tumors," *The American Journal of Pathology*, vol. 176, no. 4, pp. 1564–1576, 2010.

[7] M. Egeblad, E. S. Nakasone, and Z. Werb, "Tumors as organs: complex tissues that interface with the entire organism," *Developmental Cell*, vol. 18, no. 6, pp. 884–901, 2010.

[8] C. Murdoch, M. Muthana, S. B. Coffelt, and C. E. Lewis, "The role of myeloid cells in the promotion of tumour angiogenesis," *Nature Reviews Cancer*, vol. 8, no. 8, pp. 618–631, 2008.

[9] M. de Palma, M. A. Venneri, R. Galli et al., "Tie2 identifies a hematopoietic lineage of proangiogenic monocytes required for tumor vessel formation and a mesenchymal population of pericyte progenitors," *Cancer Cell*, vol. 8, no. 3, pp. 211–226, 2005.

[10] R. Mazzieri, F. Pucci, D. Moi et al., "Targeting the ANG2/TIE2 axis inhibits tumor growth and metastasis by impairing angiogenesis and disabling rebounds of proangiogenic myeloid cells," *Cancer Cell*, vol. 19, no. 4, pp. 512–526, 2011.

[11] W. Chen, T. Ma, X.-N. Shen et al., "Macrophage-induced tumor angiogenesis is regulated by the TSC2-mTOR pathway," *Cancer Research*, vol. 72, no. 6, pp. 1363–1372, 2012.

[12] X. Tang, J. E. Lucas, J. L.-Y. Chen et al., "Functional interaction between responses to lactic acidosis and hypoxia regulates genomic transcriptional outputs," *Cancer Research*, vol. 72, no. 2, pp. 491–502, 2012.

[13] H. P. Harding, Y. Zhang, H. Zeng et al., "An integrated stress response regulates amino acid metabolism and resistance to oxidative stress," *Molecular Cell*, vol. 11, no. 3, pp. 619–633, 2003.

[14] J. D. Blais, V. Filipenko, M. Bi et al., "Activating transcription factor 4 is translationally regulated by hypoxic stress," *Molecular and Cellular Biology*, vol. 24, no. 17, pp. 7469–7482, 2004.

[15] K. Ameri, C. E. Lewis, M. Raida, H. Sowter, T. Hai, and A. L. Harris, "Anoxic induction of ATF-4 through HIF-1-independent pathways of protein stabilization in human cancer cells," *Blood*, vol. 103, no. 5, pp. 1876–1882, 2004.

[16] E. R. Pereira, K. Frudd, W. Awad, and L. M. Hendershot, "Endoplasmic reticulum (ER) stress and hypoxia response pathways interact to potentiate hypoxia-inducible factor 1 (HIF-1) transcriptional activity on targets like vascular endothelial growth factor (VEGF)," *The Journal of Biological Chemistry*, vol. 289, no. 6, pp. 3352–3364, 2014.

[17] K. Zhu, H. Jiao, S. Li et al., "ATF4 promotes bone angiogenesis by increasing vegf expression and release in the bone environment," *Journal of Bone and Mineral Research*, vol. 28, no. 9, pp. 1870–1884, 2013.

[18] G. Chakraborty, S. Jain, and G. C. Kundu, "Osteopontin promotes vascular endothelial growth factor-dependent breast tumor growth and angiogenesis via autocrine and paracrine mechanisms," *Cancer Research*, vol. 68, no. 1, pp. 152–161, 2008.

[19] I. Takanami, K. Takeuchi, and S. Kodaira, "Tumor-associated macrophage infiltration in pulmonary adenocarcinoma: association with angiogenesis and poor prognosis," *Oncology*, vol. 57, no. 2, pp. 138–142, 1999.

[20] H. B. Salvesen and L. A. Akslen, "Significance of tumour-associated macrophages, vascular endothelial growth factor and thrombospondin-1 expression for tumour angiogenesis and prognosis in endometrial carcinomas," *International Journal of Cancer*, vol. 84, no. 5, pp. 538–543, 1999.

[21] R. D. Leek, C. E. Lewis, R. Whitehouse, M. Greenall, J. Clarke, and A. L. Harris, "Association of macrophage infiltration with angiogenesis and prognosis in invasive breast carcinoma," *Cancer Research*, vol. 56, no. 20, pp. 4625–4629, 1996.

[22] E. Y. Lin, V. Gouon-Evans, A. V. Nguyen, and J. W. Pollard, "The macrophage growth factor CSF-1 in mammary gland development and tumor progression," *Journal of Mammary Gland Biology and Neoplasia*, vol. 7, no. 2, pp. 147–162, 2002.

[23] E. Y. Lin, A. V. Nguyen, R. G. Russell, and J. W. Pollard, "Colony-stimulating factor 1 promotes progression of mammary tumors to malignancy," *The Journal of Experimental Medicine*, vol. 193, no. 6, pp. 727–740, 2001.

[24] C. E. Lewis, R. Leek, A. Harris, and J. O. McGee, "Cytokine regulation of angiogenesis in breast cancer: the role of tumor-associated macrophages," *Journal of Leukocyte Biology*, vol. 57, no. 5, pp. 747–751, 1995.

[25] B. C. Zhang, J. Gao, J. Wang, Z. G. Rao, B. C. Wang, and J. F. Gao, "Tumor-associated macrophages infiltration is associated with peritumoral lymphangiogenesis and poor prognosis in lung adenocarcinoma," *Medical Oncology*, vol. 28, no. 4, pp. 1447–1452, 2011.

[26] H. Cao, S. Yu, Z. Yao et al., "Activating transcription factor 4 regulates osteoclast differentiation in mice," *The Journal of Clinical Investigation*, vol. 120, no. 8, pp. 2755–2766, 2010.

Hindawi Publishing Corporation
BioMed Research International
Volume 2015, Article ID 132086, 1 page
http://dx.doi.org/10.1155/2015/132086

Corrigendum

Corrigendum to "SIRT1 Inhibition Affects Angiogenic Properties of Human MSCs"

Chiara Botti,[1] Ilaria Caiafa,[2] Antonietta Coppola,[2] Francesca Cuomo,[2] Marco Miceli,[3] Lucia Altucci,[2,3] and Gilda Cobellis[2]

[1]*Istituto Nazionale Tumori, Struttura Complessa Oncologia Medica Melanoma Immunoterapia Oncologica e Terapia Innovativa, Via Mariano Semmola, 80131 Napoli, Italy*
[2]*Department of Biochemistry, Biophysics and General Pathology, Second University of Napoli, Via L. De Crecchio 7, 80138 Napoli, Italy*
[3]*Institute of Genetics and Biophysics "A. Buzzati-Traverso", CNR, Via P. Castellino 111, 80131 Napoli, Italy*

Correspondence should be addressed to Chiara Botti; chiara_botti@yahoo.it and Gilda Cobellis; g.cobellis@unina2.it

Received 22 December 2014; Accepted 22 December 2014

In the paper titled "SIRT1 Inhibition Affects Angiogenic Properties of Human MSCs" the authors were listed with their surnames followed by first names erroneously, and the affiliation of Dr. Chiara Botti was not correctly inserted.

The corrected authors' list and affiliations are shown above.

Hindawi Publishing Corporation
BioMed Research International
Volume 2015, Article ID 314178, 9 pages
http://dx.doi.org/10.1155/2015/314178

Review Article

Actin-Tethered Junctional Complexes in Angiogenesis and Lymphangiogenesis in Association with Vascular Endothelial Growth Factor

Dimitar P. Zankov and Hisakazu Ogita

Division of Molecular Medical Biochemistry, Department of Biochemistry and Molecular Biology, Shiga University of Medical Science, Seta Tsukinowa-cho, Shiga, Otsu 520-2192, Japan

Correspondence should be addressed to Dimitar P. Zankov; dzankoff@belle.shiga-med.ac.jp and Hisakazu Ogita; hogita@belle.shiga-med.ac.jp

Received 11 September 2014; Revised 23 October 2014; Accepted 31 October 2014

Academic Editor: Qiang Zhao

Vasculature is present in all tissues and therefore is indispensable for development, biology, and pathology of multicellular organisms. Endothelial cells guarantee proper function of the vessels and are the original component in angiogenesis. Morphogenesis of the vascular system utilizes processes like cell adhesion, motility, proliferation, and survival that are closely related to the dynamics of actin filaments and actin-tethered adhesion complexes. Here we review involvement of actin cytoskeleton-associated junctional molecules of endothelial cells in angiogenesis and lymphangiogenesis. Particularly, we focus on F-actin binding protein afadin, an adaptor protein involved in broad range of signaling mechanisms. Afadin mediates the pathways of vascular endothelial growth factor- (VEGF-) and sphingosine 1-phosphate-triggered angiogenesis and is essential for embryonic development of lymph vessels in mice. We propose that targeting actin-tethered junctional molecules, including afadin, may present a new approach to angiogenic therapy that in combination with today used medications like VEGF inhibitors will benefit against development of pathological angiogenesis.

1. Introduction

Endothelial cells (ECs) in mature vascular system are quiescent, nonproliferating (with some exceptions, e.g., uterus) heterogenic population. The endothelium generated by a single layer of ECs separates the blood and lymph from other components of the vessel wall and serves wide variety of functions, specific not only for the vascular bed but also for the tissue they populate [1, 2]. ECs are the first component of blood vasculature that is formed in the embryo by differentiation of mesodermal precursor cells angioblasts (process defined as vasculogenesis, VG), thus creating the primary capillary plexus [3]. Subsequently, the embryonic vasculature evolves from the existing vessels by remodeling (termed as angiogenesis, AG) [4]. In contrast, lymphangiogenesis (LAG) starts with migration, proliferation, and differentiation of ECs pool residing in cardinal vein [5, 6].

Intercellular junctions between the adjacent ECs and between ECs and surrounding non-EC wall components (e.g., pericytes) maintain the organization of EC layer and vessel integrity. Their function is beyond just mechanical support involving at least inhibition of ECs proliferation and neovasculogenesis in mature vessels as well as regulation of ECs gene expression and survival [7]. Adhesive machinery of ECs includes adherens and tight junctions and focal adhesions [8], all associated with intracellular F-actin network. Morphogenesis of vasculature relies on processes like cell adhesion, motility, and proliferation that inevitably include the actin cytoskeleton and associated junctional molecules, making the majority of these complexes a requisite of VG, AG, and LAG [9–14].

In this review we focus on the involvement of actin-associated molecules at the junctional apparatus in AG and LAG and, in particular, afadin, an adaptor protein with multiple roles in cellular physiology [15]. Small GTP-binding proteins (GTPases) Rap1 and RhoA are discussed in the context of afadin signaling. The role of GTPases related to actin cytoskeleton organization and AG is beyond the

scope of this paper. The interested readers may refer to a number of outstanding publications [16–18]. We have selected this particular view on vascular development, because those adherent complexes are deeply interwoven with the signaling of the "prime switches" of AG: vascular endothelial growth factors (VEGFs) and their receptor-tyrosine kinase VEGF receptors [19], which makes them appealing target for pro/antiangiogenic therapy.

2. Afadin in the Pathways Controlling AG and LAG

Afadin is an adaptor protein discovered in 1997 by Mandai et al. and holds two RA (Ras association), a FHA (forkhead-associated), a DIL (dilute), a PDZ (postsynaptic density, Drosophila disk large tumor suppressor, zonula occludens-1), three PR (proline-rich), and F-actin structural domains (Figure 1) [20]. Two isoforms are described at present: l-afadin and s-afadin. s-Afadin truncates the C-terminal F-actin and the third PR domains. l-Afadin is expressed ubiquitously, whereas s-afadin is expressed mainly in the nerve tissue [21]. F-actin and PDZ domains link actin filaments and Ig-like transmembrane junctional proteins nectins, respectively. Resulting cell-cell adhesion assembly is crucial for establishment and part of adherens and tight junctions in epithelia, fibroblasts, and ECs [15, 22]. In addition, afadin functions independently of nectins to promote cell movement and neuronal physiology [23–26]. Due to the multitude of interacting domains and fundamental role of cell-cell junctions for tissue organization [27], afadin is involved in various biological phenomena ranging from embryonic development to cancer progression. Complexity of those processes creates a broad field of constantly increasing information of afadin roles [28–32].

Physiological AG, the formation of blood vessels from existing ones, occurs not only in the embryo but also in postnatal life (e.g., in uterus, during wound healing). Pathological AG accompanies some chronic inflammatory diseases (e.g., rheumatoid arthritis), cancer, and atherosclerosis [4, 33, 34]. During physiological AG, there is fine-tuned balance between stimulating and suppressing factors in order to maintain vascular and tissue integrity and assure effective vessel formation [35]. Pathological AG results in disorganized, abnormal vasculature with disturbed regulation [4].

Undeniably, the prime molecular machinery that stimulates VG and sprouting AG is comprised of VEGF and VEGF receptor in ECs [4, 33, 34, 36]. VEGF receptor interacts with key ECs adhesion molecules (e.g., VE-cadherin, neuropilin, and integrins), guides tip ECs to VEGF signal, and activates a myriad of intracellular signaling during all phases of AG. Genetic inhibition of VEGF or VEGF receptor in mice prevents successful vessel formation and cause embryonic death [37–39].

VEGF signaling is also critical for tumor AG. At present the most extensively applied medication in human cancer treatment is VEGF inhibitors [40]. One of the downstream targets of activated VEGF receptor is Rap1 GTPase that is also indispensable for the vessel formation [41]. In epithelial cells Rap1 associates with afadin and recruits epithelial (E)-cadherin to adherens junctions [42]. Understanding of the partners of activated Rap1 in ECs had not been extensive when we investigated Rap1-driven mechanisms in VEGF and sphingosine 1-phosphate- (S1P-) induced AG [43]. By studying VEGF- or S1P-stimulated human umbilical vein ECs (HUVECs) and conditional knockout (cKO) mice with endothelial-specific afadin gene disruption, we found that (i) in HUVECs, intracellular localization of afadin was Rap1-dependent and colocalization of activated (GTP-containing) Rap1 and afadin was observed in the cell-cell contacts and the leading edge of polarized moving cells; (ii) afadin or Rap1 knockdown in HUVECs reduced VEGF- or S1P-stimulated capillary-like network formation in Matrigel and 3D gels, suppressed migration and proliferation of HUVECs, and increased the number of apoptotic cells; (iii) equivalent to the epithelial cells, Rap1 and afadin played key roles in accumulation of adherens and tight junction proteins since absence of afadin or Rap1 in HUVECs removed the fluorescent signal in the cell membrane for nectin-2, VE-cadherin, claudin-5, and junctional adhesion molecule A; (iv) in VEGF- or S1P-stimulated HUVECs, afadin and Rap1 controlled specifically phosphorylation of Akt and endothelial nitric oxide synthase (eNOS) but not extracellular signal-regulated kinase or p38. The subsequent experiments revealed that afadin is essential for the interaction between phosphoinositide 3-kinase (PI3K) regulatory subunit p85 and VEGF or S1P receptors. That interaction recruits catalytic subunit p110 of PI3K and Akt/eNOS phosphorylation follows (schematically drawn in Figure 2). Akt/eNOS signaling is proangiogenic and downstream of VEGF and S1P in ECs [44, 45].

We have also found that, in endothelial afadin cKO mice, postnatal development of retinal vessels is initially delayed, that small vessels network decreased, and that VE-cadherin staining in ECs became discontinuous. Even in heterozygous KO mice, recovery of blood flow and neoformation of capillary networks after hind limb ischemia were diminished compared to control mice. Those *in vivo* data validated the vital role of afadin in postnatal AG. Moreover, afadin is involved in maintaining epithelial and endothelial barrier function [46–48], migration of cancer cells [29, 32], elongation and lumen formation of the developing nephron [49], and modulation of integrin levels in epithelial cells [50]. All those findings provide evidence that afadin is one of the main participants in the mechanisms of cellular adhesion, motility, and proliferation, processes implicated in AG but also in a broad variety of other physiological and pathological events.

VEGF receptor-Rap1 activation signal in ECs is transmitted not only to afadin/Akt but also to p42/44 ERK1/2 and p38 MAPK [51]. Those tyrosine kinases are important for ECs proliferation and actin cytoskeleton remodeling and are absolutely required for placental AG [52, 53]. In Rap1b-deficient mice AG is disturbed resulting in embryonic and perinatal mortality [54]. The mechanisms for the defective AG comprise ECs dysfunction (decreased activation, migration, and proliferation) that coincides with lower levels of p42/44 ERK1/2 and p38 MAPK in ECs. Another downstream target of Rap1 in ECs is RAPL, protein that associates with

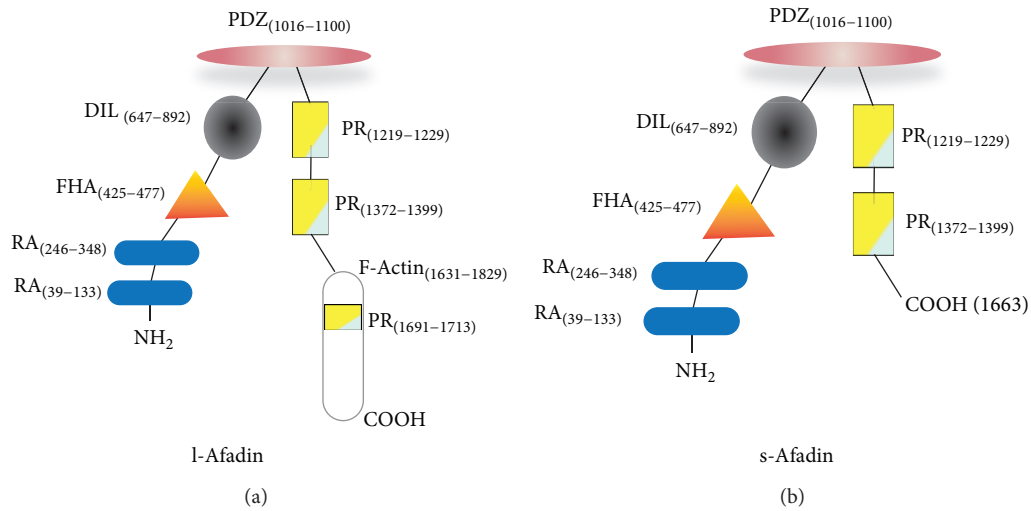

Figure 1: Anatomy of afadin molecule. The modular structure of l-afadin (a) and s-afadin (b) is schematically shown. Numbers in parentheses indicate the first and last amino acid of the structural domains. RA: Ras associated domain; FHA: forkhead associated domain; DIL: dilute domain; PDZ: postsynaptic density, Drosophila disk large tumor suppressor, zonula occludens-1 domain; PR: proline rich domain; F-actin: F-actin binding domain. PDZ domain interacts with nectin molecules.

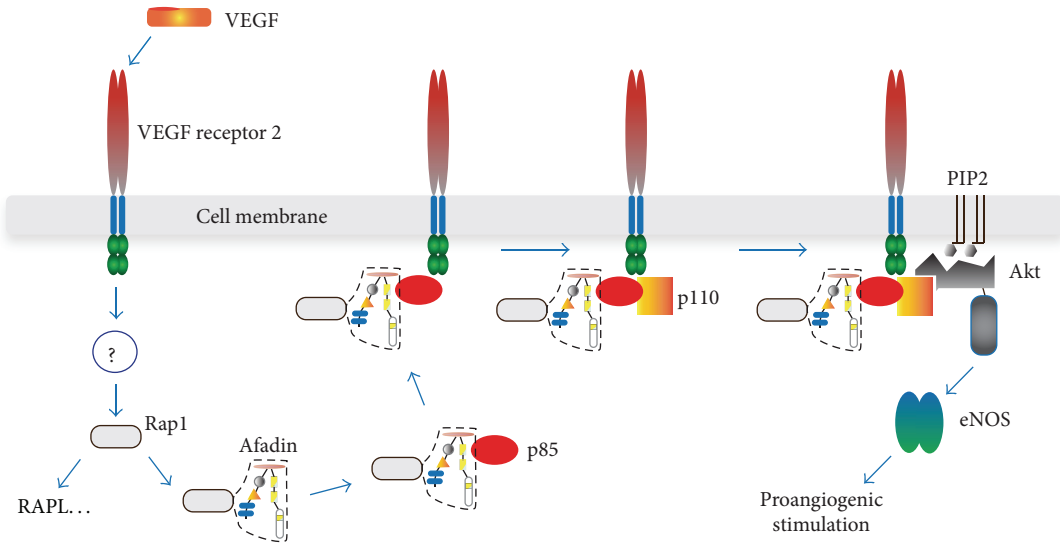

Figure 2: Proposed function of afadin in the VEGF or S1P receptor signaling during AG. In HUVECs, activated Rap1 (by still unknown mechanism) binds and recruits afadin to cell membrane where the complex between VEGF receptor, afadin, Rap1, and sequentially p85 and p110 subunits of PI3K assembles. Activated PI3K phosphorylates Akt and downstream signaling follows. Similar events occur after S1P receptor activation (not drawn). In addition, Rap1 stimulates different proteins (e.g., RAPL) that may contribute to proangiogenic signal.

GTP-bound Rap1 to activate integrins [55]. This pathway has proved essential in angiogenic sprouting, ECs migration (HUVECs), adhesion, and *in vivo* neovascularization (hind limb ischemia model in mice) [56]. The role of RAPL in AG is attributed to inside-out integrin signaling: RAPL promotes β1 integrin affinity, thereby stimulating ECs adhesion and migration (for the role of integrins in AG and LAG, see the next section of this review).

The mice with EC-targeted deletion of afadin [43] were born in a significantly reduced ratio (3.6% versus 25% expected), showing that afadin is also important for embryonic AG. That observation became the topic of our investigation [57], in which we found that most of the endothelial afadin cKO mouse embryos died at embryonic day (E) 16.5. Until E13.5, no detectable dissimilarities between cKO and control embryos could be observed, but at E14.5–E16.5, cKO mice developed diffuse subcutaneous edema and dot-like skin hemorrhages. Series of immunofluorescence experiments demonstrated that lymphatic vessels in the skin of afadin cKO embryos were largely dilated and that lymphatic endothelium exhibited defect in VE-cadherin staining but preserved ability to differentiate and

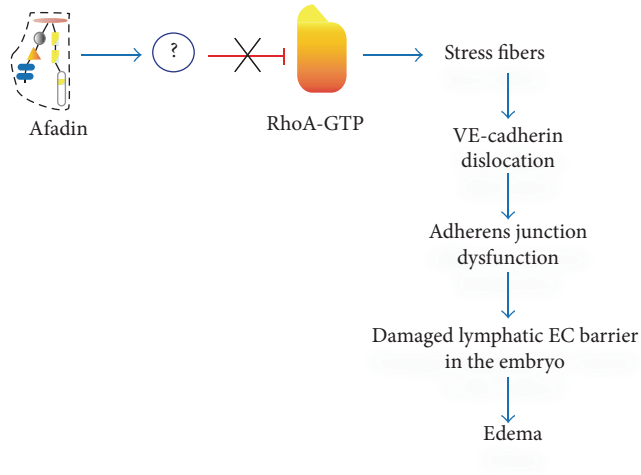

Figure 3: Sequence of regulatory steps leading to damage of lymph endothelial barrier in afadin cKO mouse embryos. In the absence of afadin-mediated inhibition of RhoA activity, actin stress fibers are formed. Thick actin filaments alter the cell shape, dislocate VE-cadherin from cell membrane, compromise adherent junctions, and damage lymph EC barrier. This results in generalized edema and embryonic death.

proliferate. To investigate afadin-induced dysfunction of lymphatic endothelium, human dermal blood and lymphatic microvascular ECs (BMVECs and LMVECs, resp.) were used as a model. Knockdown of afadin in LMVECs triggered cell-shape alteration, disorganization of cell-cell contacts, reduction of VE-cadherin staining, and formation of thick F-actin fibers at the cells periphery. All of these effects were not produced in BMVECs. Afadin-associated F-actin/VE-cadherin rearrangements in LMVECs depended on RhoA activity: GTP-bound (active) RhoA was increased in afadin-knockdown LMVECs and dominant negative RhoA mutant rescued the phenotype in LVMECs. Thus, afadin stabilizes adherens junctions/VE-cadherin by suppressing RhoA activity and stress fibers formation to maintain EC barrier in embryonic lymphatic vessels (Figure 3). Actin fibers organization is reported as condition that defines the localization of VE-cadherin in cell junctions. Actin depolymerization or hyperpolymerization has been shown to decrease VE-cadherin in ECs and compromise endothelial barrier [58]. Contraction of cortical actin-myosin cytoskeleton in ECs stimulated by Rho GTPase has similar effect [59]. Actin bundles in ECs formed after cAMP/Epac/Rap1 stimulation anchor VE-cadherin and strengthen cell-cell adhesions, the effect that results in reduction of endothelial layer permeability [60, 61].

Our reports described above complement the knowledge about signaling in embryonic LAG and postnatal AG. Lack of afadin in lymphatic ECs of the mouse embryo does not impede vessel morphogenesis but compromises intercellular junctions of ECs. This effect is secondary to F-actin stress fiber synthesis and VE-cadherin dislocation. Contrary to adhesion structures in blood ECs, lymphatic ECs have "button-like" intercellular contacts that facilitate the transport of intercellular fluids [62]. This functional specialization may also include unique RhoA regulation by afadin. In addition, RhoA-dependent actin rearrangement and disruption of cell-cell adherens junction resemble the mechanism exploited by thrombin to damage barrier function in lung ECs [47]. Afadin/Rap1 complex was essential for recovery of cell-cell contacts and actin network in lung ECs.

Participation of afadin in the signaling downstream of VEGF and S1P receptors as well as its involvement in tubulogenesis and apoptosis might focus attention on this molecule in the context of tumor AG and cancer therapy. Afadin is also important antiapoptotic guard in embryogenesis, and platelet-derived growth factor (PDGF) receptor binds PI3K regulatory subunit p85/afadin in a similar way as shown for VEGF and S1P receptors to activate Akt [63].

3. Other Actin-Associated Adhesion Complexes in relation to AG and LAG

Many transmembrane adhesion molecules in ECs and their intracellular partners that link the molecular assembly to actin filaments contribute to the complex sequence of events in the process of VEGF-induced AG. Studies with cKO mice that eliminate the function of selected molecule in ECs demonstrated the individual role of excluded junctional component in AG or LAG and revealed its unique phenotype.

3.1. VE-Cadherin. VE-cadherin communicates through its cytoplasmic segment with β-catenin, plakoglobin, and p120-catenin. β-Catenin and plakoglobin interact with α-catenin that anchors (although recently questioned [64]) VE-cadherin to actin cytoskeleton [65, 66]. p120-Catenin stabilizes VE-cadherin by preventing its endocytosis [67]. VE-cadherin deficiency in ECs of mice created by cKO technique has caused embryonic lethality at E9.5 because of increased EC apoptosis and defective AG [68]. VG was not disturbed, but lack of VE-cadherin stopped the remodeling of primary capillary plexus. Some vessels of the embryos had narrow or

no lumen, whereas others were dilated. Throughout the vasculature, ECs were detached from the basement membranes, disconnected each other, and could be seen in the lumen of the vessels. Those observations resulted from a failure to form the EC survival complex amid VEGF, VE-cadherin, β-catenin, and PI3K, missing Akt phosphorylation and thus inactive antiapoptotic machinery [69].

VE-cadherin is crucial for the functional integrity of endothelial layer [70] and contributes to all phases of AG. Upon initiation of VEGF-mediated AG and activation of VEGF receptor, VE-cadherin is target for Src phosphorylation, a modulation that leads to adherens junction disassembly and increased permeability of ECs. Simultaneously, molecular complex consisting of integrin $\alpha v\beta 3$, syndecan-1, and insulin-like growth factor-1 receptor is activated. These molecular events facilitate early adhesion and migration of ECs in VEGF-induced AG [71]. During sprouting neovascularization, the tip and stalk ECs are recognized in the developing branches [72]. It has been found that tip and stalk ECs are not static but they exchange their positions and phenotypes in the process of elongation of the vessel [73]. VE-cadherin dynamics under contrasting control of VEGF and Notch signaling drives this ECs behavior and is necessary for the coordination of physiological AG. VE-cadherin mobility is lost in certain pathology, for example, cancer [74]. VE-cadherin is important for establishing the functional vessels by inhibiting VEGF-signaling (p44/p42 MAPK) and ECs proliferation after ECs contact and adherens junction formation [75].

3.2. β-Catenin. Mice embryos with inactivated β-catenin in ECs die at E11.5–E13.5 [10]. VG and early AG developed, but after E9.5 vessels showed lumen irregularities and hemorrhage. Vitelline vessels had smaller diameter. The pattern of the vasculature of primitive neural plexus was defective, and the placenta was less vascularized compared to control mice. ECs had morphological changes, impaired junctions, and abundant fenestrations. In cultured ECs of β-catenin cKO mice, immunofluorescence of plakoglobin was increased, α-catenin decreased, and desmoplakin was found at EC contacts but not at those of control mice. The shift of molecular composition of junctional proteins in the β-catenin cKO mice has led to the authors' interesting hypothesis: lack of β-catenin forces creation of extra VE-cadherin/plakoglobin complexes and plakoglobin/desmoplakin/vimentin interaction analogous to that in *complexus adhaerentes* in lymphatic vessels [76]. In addition, proliferation of cultured ECs stimulated by VEGF receptor was not inhibited by confluency in the absence of β-catenin [75]. ECs express an array of Frizzled/Lrp (low-density lipoprotein receptor-related protein) receptor complexes, a target of Wnt (Wingless and Int-1) ligand [77]. Canonical Wnt signaling includes β-catenin transcriptional activity through interaction with T-cell factor (Tcf)/Lef transcription factors [78]. Wnt canonical system is involved in embryonic AG [79] and the vascular phenotype of β-catenin cKO mice may partially be a result of Wnt signal failure. Interestingly, the constitutively active β-catenin mutant in ECs also impairs embryonic AG because of overactivity of Notch-related pathways [80].

3.3. p120-Catenin. p120-Catenin stabilizes membrane localization of VE-cadherin by preventing endocytosis [81]. Deletion of p120-catenin in ECs of mice is also embryonically lethal starting at E12.5 (40% of mutated embryos) [11]; however, some of them survive without obvious abnormalities. p120-Catenin deletion causes defects in microvasculature after E9.5; reduced microvascular density, disorganized vascular networks with impaired branching and blind-ending vessels, and hemorrhages were found in the brain and other organs. Pericytes recruitment, VE-cadherin, and N-cadherin expression were decreased. Cultured ECs from p120-catenin cKO mice exhibited proliferation deficiency.

3.4. Integrins. Integrins are large family of adhesive proteins that interact with extracellular matrix components and some adhesion molecules in the cell membranes and are critical for cell motility and survival [82]. They are heterodimers of α and β subunits that upon activation cluster to form focal adhesions and assemble intracellular signaling molecules that are linked to actin cytoskeleton and specific cellular functions. In addition, integrins regulate VE-cadherin/catenin complexes during cell movement [83]. A vast number of reports show the importance of particular integrins in AG [8, 84, 85]. Integrin $\alpha v\beta 3$ is coreceptor of VEGF receptor in AG [86] and null or cKO mice (ECs) for several integrin subunits like αv, α3, α5, β1, and β3 demonstrate their obligatory role in AG [87–89]. Deficiency of those subunits causes severe defects in vascular development: disturbed vessel organization, defective tubulogenesis, hemorrhage, vessel wall rupture, and embryonic death. Intracellular adaptor molecules linked to integrin dimers also control AG. Deletion of talin-1, which directly associates with β subunit of integrins and mediates coupling to actin, in ECs of mice produced severe defect in AG with diffuse hemorrhages and disrupted vascular trees, leading to embryonic death [90]. Kindlin-2, the newly discovered β subunit partner important for integrin activation [91], is also critical for AG. In mice, heterozygous deletion of kindlin-2 resulted in formation of immature vessels in implanted tumors. ECs from those mice showed reduction of integrin β3-dependent adhesion, migration, and tube formation. Another key component of integrin activation, focal adhesion kinase (FAK), induced tumor AG [91].

Integrin $\alpha 9\beta 1$ appears to have specific role in LAG. Integrin α9-null mice suffered insufficiency of the valves in collecting lymph vessels, developed chylothorax, and inexorably died by postnatal day 12 because of respiratory failure [92]. The valves had malformed leaflets due to missing integrin $\alpha 9\beta 1$/fibronectin interaction that is necessary for the leaflets matrix organization [93]. Integrin $\alpha 9\beta 1$ has unique property of binding directly VEGF to promote ECs adhesion and migration [94].

ECs in lymphatic microvasculature have specialized junctions that apparently reflect specific functionality of lymph capillaries [62]. Those "button-like" structures form discontinuous line of adhesions that allow easy flow of interstitial constituents into the lumen. During embryonic development ECs in lymphatic capillaries have continuous intercellular junctions that evolve to the "buttons" soon after birth [95].

The molecular composition of the junctions in lymphatic ECs is mixture of adherens and tight junctional proteins (VE-cadherin, occluding, claudin, afadin, etc.). Contrary to the role of those proteins in AG, importance of actin-associated junctional molecules in LAG (except partially for afadin) remains to be elucidated.

4. Necessity for Clarifying the Role of Similar Molecules in Developmental and Pathological AG and LAG

Pathological AG and LAG are considered dysregulated processes utilizing similar molecular repertoire as AG and LAG during embryogenesis [4]. However, there is still little knowledge about the specificity of signaling mechanisms in pathological AG and LAG. Available reports have demonstrated altered functionality of certain angiogenic molecules like placental growth factor (PIGF), VEGF receptor-1, and VEGF-B in the context of diseased state [96–98]. Those pathology-associated investigations of the key angiogenic molecules such as VEGF ligands and receptors are the actual basis for understanding and eventually discovering the targets for antiangiogenic therapy. Actin-related junctional molecules are probably not exception and they may have additional/changed functionality in diseased conditions: for example, VE-cadherin in neoplastic vascular ECs expresses epitope that normally is obscured and this molecular segment allows specific targeting of tumor ECs [99]. Promising objective for antiangiogenic therapy especially in cancer is integrin $\alpha v\beta 3$, essential molecule for tumor AG. At present, several groups of pharmacological inhibitors of integrin $\alpha v\beta 3$ are in the different stages of testing and the results show favorable effects in preclinical and clinical settings [100].

5. Conclusion

AG and LAG are attractive targets for influencing pathological conditions that present with excessive/abnormal vascular proliferation (chronic inflammation, cancer) or ischemia (atherosclerosis). The growth of vessels in AG demands fundamental processes of cell biology and morphogenesis: cellular adhesion, migration, proliferation, and survival. All of these functions utilize as essential effector actin filaments and associated junctional molecules that assure intercellular or cell-matrix communication. As a part of the same machinery, actin-tethered molecular complexes appear to be highly integrated, and they cooperate to regulate organization or disorganization of particular adhesion structure. Furthermore, the main switch of AG, VEGF signaling, is intimately dependent on these molecular complexes. Because of these properties, molecular assemblies including VE-cadherin, integrin, and nectin as well as actin may be considered as (co)targets of VEGF-related pro- or antiangiogenic therapy.

Afadin functions downstream of angiogenic signals translated by VEGF and S1P in ECs and also may represent target for modulating AG. Afadin has multiple roles in cellular processes, which may broaden the effects of its inhibition. Not only physiological AG but also pathological AG (e.g., neovascularization in tumors) might be affected by modulating the afadin-related signals. However, there are many unanswered questions at present to justify this strategy: compromising intercellular adhesions may promote metastasis in cancer, whereas dysfunctional actin-related machinery might have opposite effects by preventing cell adhesion and promoting apoptosis; fundamental roles of cell junctions most probably will require targeted approach, delivery of active substances only to the diseased location; mechanisms involving afadin in pathological AG could have altered effects. Nevertheless, the proposed hypotheses might be worth testing in translational studies with hope that it will help in reducing the resistance to VEGF receptor inhibitors in VEGF-induced (or other) pathological AG.

Conflict of Interests

All the authors declare that there is no conflict of interests regarding the publication of this paper.

References

[1] W. C. Aird, "Phenotypic heterogeneity of the endothelium: I. Structure, function, and mechanisms," *Circulation Research*, vol. 100, no. 2, pp. 158–173, 2007.

[2] K. L. Marcelo, L. C. Goldie, and K. K. Hirschi, "Regulation of endothelial cell differentiation and specification," *Circulation Research*, vol. 112, no. 9, pp. 1272–1287, 2013.

[3] L. Coultas, K. Chawengsaksophak, and J. Rossant, "Endothelial cells and VEGF in vascular development," *Nature*, vol. 438, no. 7070, pp. 937–945, 2005.

[4] A. S. Chung and N. Ferrara, "Developmental and pathological angiogenesis," *Annual Review of Cell and Developmental Biology*, vol. 27, pp. 563–584, 2011.

[5] T. Tammela and K. Alitalo, "Lymphangiogenesis: molecular mechanisms and future promise," *Cell*, vol. 140, no. 4, pp. 460–476, 2010.

[6] S. Schulte-Merker, A. Sabine, and T. V. Petrova, "Lymphatic vascular morphogenesis in development, physiology, and disease," *The Journal of Cell Biology*, vol. 193, no. 4, pp. 607–618, 2011.

[7] E. Dejana, "Endothelial cell-cell junctions: happy together," *Nature Reviews Molecular Cell Biology*, vol. 5, no. 4, pp. 261–270, 2004.

[8] C. Rüegg and A. Mariotti, "Vascular integrins: pleiotropic adhesion and signaling molecules in vascular homeostasis and angiogenesis," *Cellular and Molecular Life Sciences*, vol. 60, no. 6, pp. 1135–1157, 2003.

[9] G. H. Mahabeleshwar, W. Feng, K. Reddy, E. F. Plow, and T. V. Byzova, "Mechanisms of integrin-vascular endothelial growth factor receptor cross-activation in angiogenesis," *Circulation Research*, vol. 101, no. 6, pp. 570–580, 2007.

[10] A. Cattelino, S. Liebner, R. Gallini et al., "The conditional inactivation of the β-catenin gene in endothelial cells causes a defective vascular pattern and increased vascular fragility," *The Journal of Cell Biology*, vol. 162, no. 6, pp. 1111–1122, 2003.

[11] R. G. Oas, K. Xiao, S. Summers et al., "P120-catenin is required for mouse vascular development," *Circulation Research*, vol. 106, no. 5, pp. 941–951, 2010.

[12] Y. Luo and G. L. Radice, "N-cadherin acts upstream of VE-cadherin in controlling vascular morphogenesis," *The Journal of Cell Biology*, vol. 169, no. 1, pp. 29–34, 2005.

[13] K. J. Bayless and G. A. Johnson, "Role of the cytoskeleton in formation and maintenance of angiogenic sprouts," *Journal of Vascular Research*, vol. 48, no. 5, pp. 369–385, 2011.

[14] H. Schnittler, M. Taha, M. O. Schnittler, A. A. Taha, N. Lindemann, and J. Seebach, "Actin filament dynamics and endothelial cell junctions: the Ying and Yang between stabilization and motion," *Cell and Tissue Research*, vol. 355, no. 3, pp. 529–543, 2014.

[15] H. Ogita, Y. Rikitake, J. Miyoshi, and Y. Takai, "Cell adhesion molecules nectins and associating proteins: Implications for physiology and pathology," *Proceedings of the Japan Academy Series B: Physical and Biological Sciences*, vol. 86, no. 6, pp. 621–629, 2010.

[16] C. Kim, H. Yang, Y. Fukushima et al., "Vascular RhoJ is an effective and selective target for tumor angiogenesis and vascular disruption," *Cancer Cell*, vol. 25, no. 1, pp. 102–117, 2014.

[17] D. Gerald, I. Adini, S. Shechter et al., "RhoB controls coordination of adult angiogenesis and lymphangiogenesis following injury by regulating VEZF1-mediated transcription," *Nature Communications*, vol. 4, article 2824, 2013.

[18] B. A. Bryan, E. Dennstedt, D. C. Mitchell et al., "RhoA/ROCK signaling is essential for multiple aspects of VEGF-mediated angiogenesis," *The FASEB Journal*, vol. 24, no. 9, pp. 3186–3195, 2010.

[19] N. Ferrara, H.-P. Gerber, and J. LeCouter, "The biology of VEGF and its receptors," *Nature Medicine*, vol. 9, no. 6, pp. 669–676, 2003.

[20] K. Mandai, H. Nakanishi, A. Satoh et al., "Afadin: a novel actin filament-binding protein with one PDZ domain localized at cadherin-based cell-to-cell adherens junction," *The Journal of Cell Biology*, vol. 139, no. 2, pp. 517–528, 1997.

[21] Y. Takai and H. Nakanishi, "Nectin and afadin: novel organizers of intracellular junctions," *Journal of Cell Science*, vol. 116, no. 1, pp. 17–27, 2003.

[22] Y. Takai, K. Irie, K. Shimizu, T. Sakisaka, and W. Ikeda, "Nectins and nectin-like molecules: roles in cell adhesion, migration, and polarization," *Cancer Science*, vol. 94, no. 8, pp. 655–667, 2003.

[23] M. Miyata, H. Ogita, H. Komura et al., "Localization of nectin-free afadin at the leading edge and its involvement in directional cell movement induced by platelet-derived growth factor," *Journal of Cell Science*, vol. 122, no. 23, pp. 4319–4329, 2009.

[24] Y. Fukumoto, S. Kurita, Y. Takai, and H. Ogita, "Role of scaffold protein afadin dilute domain-interacting protein (ADIP) in platelet-derived growth factor-induced cell movement by activating Rac protein through Vav2 protein," *The Journal of Biological Chemistry*, vol. 286, no. 50, pp. 43537–43548, 2011.

[25] T. Majima, H. Ogita, T. Yamada et al., "Involvement of afadin in the formation and remodeling of synapses in the hippocampus," *Biochemical and Biophysical Research Communications*, vol. 385, no. 4, pp. 539–544, 2009.

[26] J.-E. van Leeuwen, I. Rafalovich, K. Sellers et al., "Coordinated nuclear and synaptic shuttling of afadin promotes spine plasticity and histone modifications," *The Journal of Biological Chemistry*, vol. 289, no. 15, pp. 10831–10842, 2014.

[27] B. M. Gumbiner, "Cell adhesion: the molecular basis of tissue architecture and morphogenesis," *Cell*, vol. 84, no. 3, pp. 345–357, 1996.

[28] A. B. Zhadanov, D. W. Provance Jr., C. A. Speer et al., "Absence of the tight junctional protein AF-6 disrupts epithelial cell-cell junctions and cell polarity during mouse development," *Current Biology*, vol. 9, no. 16, pp. 880–888, 1999.

[29] G. Fournier, O. Cabaud, E. Josselin et al., "Loss of AF6/afadin, a marker of poor outcome in breast cancer, induces cell migration, invasiveness and tumor growth," *Oncogene*, vol. 30, no. 36, pp. 3862–3874, 2011.

[30] G. M. J. Beaudoin III, C. M. Schofield, T. Nuwal et al., "Afadin, a Ras/Rap effector that controls cadherin function, promotes spine and excitatory synapse density in the hippocampus," *The Journal of Neuroscience*, vol. 32, no. 1, pp. 99–110, 2012.

[31] M. Tanaka-Okamoto, K. Hori, H. Ishizaki et al., "Involvement of afadin in barrier function and homeostasis of mouse intestinal epithelia," *Journal of Cell Science*, vol. 124, no. 13, pp. 2231–2240, 2011.

[32] S. Elloul, D. Kedrin, N. W. Knoblauch, A. H. Beck, and A. Toker, "The adherens junction protein Afadin is an AKT substrate that regulates breast cancer cell migration," *Molecular Cancer Research*, vol. 12, no. 3, pp. 464–476, 2014.

[33] M. Potente, H. Gerhardt, and P. Carmeliet, "Basic and therapeutic aspects of angiogenesis," *Cell*, vol. 146, no. 6, pp. 873–887, 2011.

[34] P. Carmeliet, "Mechanisms of angiogenesis and arteriogenesis," *Nature Medicine*, vol. 6, no. 4, pp. 389–395, 2000.

[35] R. H. Adams and K. Alitalo, "Molecular regulation of angiogenesis and lymphangiogenesis," *Nature Reviews Molecular Cell Biology*, vol. 8, no. 6, pp. 464–478, 2007.

[36] M. Jeltsch, V.-M. Leppänen, P. Saharinen, and K. Alitalo, "Receptor tyrosine kinase-mediated angiogenesis," *Cold Spring Harbor Perspectives in Biology*, vol. 5, no. 9, Article ID a009183, 2013.

[37] P. Carmeliet, V. Ferreira, G. Breier et al., "Abnormal blood vessel development and lethality in embryos lacking a single VEGF allele," *Nature*, vol. 380, no. 6573, pp. 435–439, 1996.

[38] G.-H. Fong, J. Rossant, M. Gertsenstein, and M. L. Breitman, "Role of the Flt-1 receptor tyrosine kinase in regulating the assembly of vascular endothelium," *Nature*, vol. 376, no. 6535, pp. 66–70, 1995.

[39] F. Shalaby, J. Rossant, T. P. Yamaguchi et al., "Failure of blood-island formation and vasculogenesis in Flk-1-deficient mice," *Nature*, vol. 376, no. 6535, pp. 62–66, 1995.

[40] S. Moens, J. Goveia, P. C. Stapor, A. R. Cantelmo, and P. Carmeliet, "The multifaceted activity of VEGF in angiogenesis—implications for therapy responses," *Cytokine & Growth Factor Reviews*, vol. 25, no. 4, pp. 473–482, 2014.

[41] M. R. H. Kooistra, N. Dubé, and J. L. Bos, "Rap1: a key regulator in cell-cell junction formation," *Journal of Cell Science*, vol. 120, no. 1, pp. 17–22, 2007.

[42] T. Sato, N. Fujita, A. Yamada et al., "Regulation of the assembly and adhesion activity of E-cadherin by nectin and afadin for the formation of adherens junctions in Madin-Darby canine kidney cells," *The Journal of Biological Chemistry*, vol. 281, no. 8, pp. 5288–5299, 2006.

[43] H. Tawa, Y. Rikitake, M. Takahashi et al., "Role of afadin in vascular endothelial growth factor-and sphingosine 1-phosphate-induced angiogenesis," *Circulation Research*, vol. 106, no. 11, pp. 1731–1742, 2010.

[44] Y. Rikitake, K.-I. Hirata, S. Kawashima et al., "Involvement of endothelial nitric oxide in sphingosine-1-phosphate—induced angiogenesis," *Arteriosclerosis, Thrombosis, and Vascular Biology*, vol. 22, no. 1, pp. 108–114, 2002.

[45] E. Ackah, J. Yu, S. Zoellner et al., "Akt1/protein kinase Bα is critical for ischemic and VEGF-mediated angiogenesis," *The Journal of Clinical Investigation*, vol. 115, no. 8, pp. 2119–2127, 2005.

[46] A. C. Monteiro, R. Sumagin, C. R. Rankin et al., "JAM-A associates with ZO-2, afadin, and PDZ-GEF1 to activate Rap2c and regulate epithelial barrier function," *Molecular Biology of the Cell*, vol. 24, no. 18, pp. 2849–2860, 2013.

[47] A. A. Birukova, X. Tian, Y. Tian, K. Higginbotham, and K. G. Birukov, "Rap-afadin axis in control of Rho signaling and endothelial barrier recovery," *Molecular Biology of the Cell*, vol. 24, no. 17, pp. 2678–2688, 2013.

[48] A. A. Birukova, P. Fu, T. Wu et al., "Afadin controls p120-catenin-ZO-1 interactions leading to endothelial barrier enhancement by oxidized phospholipids," *Journal of Cellular Physiology*, vol. 227, no. 5, pp. 1883–1890, 2012.

[49] Z. Yang, S. Zimmerman, P. R. Brakeman, G. M. Beaudoin, L. F. Reichardt, and D. K. Marciano, "De novo lumen formation and elongation in the developing nephron: a central role for afadin in apical polarity," *Development*, vol. 140, no. 8, pp. 1774–1784, 2013.

[50] E. A. Severson, W. Y. Lee, C. T. Capaldo, A. Nusrat, and C. A. Parkos, "Junctional adhesion molecule a interacts with afadin and PDZ-GEF2 to activate RaplA, regulate β1 integrin levels, and enhance cell migration," *Molecular Biology of the Cell*, vol. 20, no. 7, pp. 1916–1925, 2009.

[51] M. Chrzanowska-Wodnicka, A. E. Kraus, D. Gale, G. C. White II, and J. Vansluys, "Defective angiogenesis, endothelial migration, proliferation, and MAPK signaling in Rap1b-deficient mice," *Blood*, vol. 111, no. 5, pp. 2647–2656, 2008.

[52] J. S. Mudgett, J. Ding, L. Guh-Siesel et al., "Essential role for p38α mitogen-activated protein kinase in placental angiogenesis," *Proceedings of the National Academy of Sciences of the United States of America*, vol. 97, no. 19, pp. 10454–10459, 2000.

[53] N. Hatano, Y. Mori, M. Oh-hora et al., "Essential role for ERK2 mitogen-activated protein kinase in placental development," *Genes to Cells*, vol. 8, no. 11, pp. 847–856, 2003.

[54] M. Chrzanowska-Wodnicka, S. S. Smyth, S. M. Schoenwaelder, T. H. Fischer, and G. C. White II, "Rap1b is required for normal platelet function and hemostasis in mice," *The Journal of Clinical Investigation*, vol. 115, no. 3, pp. 680–687, 2005.

[55] K. Katagiri, A. Maeda, M. Shimonaka, and T. Kinashi, "RAPL, a Rap1-binding molecule that mediates Rap1-induced adhesion through spatial regulation of LFA-1," *Nature Immunology*, vol. 4, no. 8, pp. 741–748, 2003.

[56] G. Carmona, S. Göttig, A. Orlandi et al., "Role of the small GTPase Rap1 for integrin activity regulation in endothelial cells and angiogenesis," *Blood*, vol. 113, no. 2, pp. 488–497, 2009.

[57] T. Majima, K. Takeuchi, K. Sano et al., "An adaptor molecule afadin regulates lymphangiogenesis by modulating RhoA activity in the developing mouse embryo," *PLoS ONE*, vol. 8, no. 6, Article ID e68134, 2013.

[58] J. Waschke, F. E. Curry, R. H. Adamson, and D. Drenckhahn, "Regulation of actin dynamics is critical for endothelial barrier functions," *American Journal of Physiology—Heart and Circulatory Physiology*, vol. 288, no. 3, pp. H1296–H1305, 2005.

[59] K. J. Whitehead, A. C. Chan, S. Navankasattusas et al., "The cerebral cavernous malformation signaling pathway promotes vascular integrity via Rho GTPases," *Nature Medicine*, vol. 15, no. 2, pp. 177–184, 2009.

[60] M. R. H. Kooistra, M. Corada, E. Dejana, and J. L. Bos, "Epac1 regulates integrity of endothelial cell junctions through VE-cadherin," *FEBS Letters*, vol. 579, no. 22, pp. 4966–4972, 2005.

[61] K. Noda, J. Zhang, S. Fukuhara, S. Kunimoto, M. Yoshimura, and N. Mochizuki, "Vascular endothelial-cadherin stabilizes at cell-cell junctions by anchoring to circumferential actin bundles through α- and β-catenins in cyclic AMP-Epac-Rap1 signal-activated endothelial cells," *Molecular Biology of the Cell*, vol. 21, no. 4, pp. 584–596, 2010.

[62] P. Baluk, J. Fuxe, H. Hashizume et al., "Functionally specialized junctions between endothelial cells of lymphatic vessels," *The Journal of Experimental Medicine*, vol. 204, no. 10, pp. 2349–2362, 2007.

[63] N. Kanzaki, H. Ogita, H. Komura et al., "Involvement of the nectin-afadin complex in PDGF-induced cell survival," *Journal of Cell Science*, vol. 121, no. 12, pp. 2008–2017, 2008.

[64] N. Rudini and E. Dejana, "Adherens junctions," *Current Biology*, vol. 18, no. 23, pp. R1080–R1082, 2008.

[65] J. E. Nieset, A. R. Redfield, F. Jin, K. A. Knudsen, K. R. Johnson, and M. J. Wheelock, "Characterization of the interactions of α-catenin with α-actinin and β-catenin/plakoglobin," *Journal of Cell Science*, vol. 110, no. 8, pp. 1013–1022, 1997.

[66] L. Shapiro and W. I. Weis, "Structure and biochemistry of cadherins and catenins," *Cold Spring Harbor Perspectives in Biology*, vol. 1, no. 3, Article ID a003053, 2009.

[67] A. B. Reynolds and R. H. Carnahan, "Regulation of cadherin stability and turnover by p120ctn: implications in disease and cancer," *Seminars in Cell and Developmental Biology*, vol. 15, no. 6, pp. 657–663, 2004.

[68] P. Carmeliet, M.-G. Lampugnani, L. Moons et al., "Targeted deficiency or cytosolic truncation of the *VE-cadherin* gene in mice impairs VEGF-mediated endothelial survival and angiogenesis," *Cell*, vol. 98, no. 2, pp. 147–157, 1999.

[69] I. Shiojima and K. Walsh, "Role of Akt signaling in vascular homeostasis and angiogenesis," *Circulation Research*, vol. 90, no. 12, pp. 1243–1250, 2002.

[70] M. Corada, M. Mariotti, G. Thurston et al., "Vascular endothelial-cadherin is an important determinant of microvascular integrity in vivo," *Proceedings of the National Academy of Sciences of the United States of America*, vol. 96, no. 17, pp. 9815–9820, 1999.

[71] A. C. Rapraeger, B. J. Ell, M. Roy et al., "Vascular endothelial-cadherin stimulates syndecan-1-coupled insulin-like growth factor-1 receptor and cross-talk between αvβ3 integrin and vascular endothelial growth factor receptor 2 at the onset of endothelial cell dissemination during angiogenesis," *FEBS Journal*, vol. 280, no. 10, pp. 2194–2206, 2013.

[72] M. Hellström, L.-K. Phng, J. J. Hofmann et al., "Dll4 signalling through Notch1 regulates formation of tip cells during angiogenesis," *Nature*, vol. 445, no. 7129, pp. 776–780, 2007.

[73] L. Jakobsson, C. A. Franco, K. Bentley et al., "Endothelial cells dynamically compete for the tip cell position during angiogenic sprouting," *Nature Cell Biology*, vol. 12, no. 10, pp. 943–953, 2010.

[74] K. Bentley, C. A. Franco, A. Philippides et al., "The role of differential VE-cadherin dynamics in cell rearrangement during angiogenesis," *Nature Cell Biology*, vol. 16, no. 4, pp. 309–321, 2014.

[75] M. G. Lampugnani, A. Zanetti, M. Corada et al., "Contact inhibition of VEGF-induced proliferation requires vascular endothelial cadherin, β-catenin, and the phosphatase DEP-1/CD148," *The Journal of Cell Biology*, vol. 161, no. 4, pp. 793–804, 2003.

[76] B. Hämmerling, C. Grund, J. Boda-Heggemann, R. Moll, and W. W. Franke, "The *Complexus adhaerens* of mammalian lymphatic endothelia revisited: a junction even more complex than hitherto thought," *Cell and Tissue Research*, vol. 324, no. 1, pp. 55–67, 2006.

[77] A. M. Goodwin, K. M. Sullivan, and P. A. D'Amore, "Cultured endothelial cells display endogenous activation of the canonical Wnt signaling pathway and express multiple ligands, receptors, and secreted modulators of Wnt signaling," *Developmental Dynamics*, vol. 235, no. 11, pp. 3110–3120, 2006.

[78] H. Clevers, "Wnt/β-Catenin Signaling in Development and Disease," *Cell*, vol. 127, no. 3, pp. 469–480, 2006.

[79] C. A. Franco, S. Liebner, and H. Gerhardt, "Vascular morphogenesis: a Wnt for every vessel?" *Current Opinion in Genetics and Development*, vol. 19, no. 5, pp. 476–483, 2009.

[80] M. Corada, D. Nyqvist, F. Orsenigo et al., "The Wnt/β-catenin pathway modulates vascular remodeling and specification by upregulating Dll4/notch signaling," *Developmental Cell*, vol. 18, no. 6, pp. 938–949, 2010.

[81] C. M. Chiasson, K. B. Wittich, P. A. Vincent, V. Faundez, and A. P. Kowalczyk, "P120-catenin inhibits VE-cadherin internalization through a Rho-independent mechanism," *Molecular Biology of the Cell*, vol. 20, no. 7, pp. 1970–1980, 2009.

[82] F. G. Giancotti and E. Ruoslahti, "Integrin signaling," *Science*, vol. 285, no. 5430, pp. 1028–1032, 1999.

[83] Y. Wang, G. Jin, H. Miao, J. Y. S. Li, S. Usami, and S. Chien, "Integrins regulate VE-cadherin and catenins: dependence of this regulation on Src, but not on Ras," *Proceedings of the National Academy of Sciences of the United States of America*, vol. 103, no. 6, pp. 1774–1779, 2006.

[84] N. L. Malinin, E. Pluskota, and T. V. Byzova, "Integrin signaling in vascular function," *Current Opinion in Hematology*, vol. 19, no. 3, pp. 206–211, 2012.

[85] C. J. Avraamides, B. Garmy-Susini, and J. A. Varner, "Integrins in angiogenesis and lymphangiogenesis," *Nature Reviews Cancer*, vol. 8, no. 8, pp. 604–617, 2008.

[86] P. R. Somanath, N. L. Malinin, and T. V. Byzova, "Cooperation between integrin $\alpha v\beta 3$ and VEGFR2 in angiogenesis," *Angiogenesis*, vol. 12, no. 2, pp. 177–185, 2009.

[87] A. C. Zovein, A. Luque, K. A. Turlo et al., "$\beta 1$ integrin establishes endothelial cell polarity and arteriolar lumen formation via a Par3-dependent mechanism," *Developmental Cell*, vol. 18, no. 1, pp. 39–51, 2010.

[88] A. van der Flier, K. Badu-Nkansah, C. A. Whittaker et al., "Endothelial $\alpha 5$ and αv integrins cooperate in remodeling of the vasculature during development," *Development*, vol. 137, no. 14, pp. 2439–2449, 2010.

[89] K. M. Hodivala-Dilke, K. P. McHugh, D. A. Tsakiris et al., "$\beta 3$-integrin-deficient mice are a model for Glanzmann thrombasthenia showing placental defects and reduced survival," *Journal of Clinical Investigation*, vol. 103, no. 2, pp. 229–238, 1999.

[90] S. J. Monkley, V. Kostourou, L. Spence et al., "Endothelial cell talin1 is essential for embryonic angiogenesis," *Developmental Biology*, vol. 349, no. 2, pp. 494–502, 2011.

[91] M. Moser, K. R. Legate, R. Zent, and R. Fässler, "The tail of integrins, talin, and kindlins," *Science*, vol. 324, no. 5929, pp. 895–899, 2009.

[92] X. Z. Huang, J. F. Wu, R. Ferrando et al., "Fatal bilateral chylothorax in mice lacking the integrin $\alpha 9\beta 1$," *Molecular and Cellular Biology*, vol. 20, no. 14, pp. 5208–5215, 2000.

[93] E. Bazigou, S. Xie, C. Chen et al., "Integrin-$\alpha 9$ is required for fibronectin matrix assembly during lymphatic valve morphogenesis," *Developmental Cell*, vol. 17, no. 2, pp. 175–186, 2009.

[94] N. E. Vlahakis, B. A. Young, A. Atakilit et al., "Integrin $\alpha 9\beta 1$ directly binds to vascular endothelial growth factor (VEGF)-A and contributes to VEGF-A-induced angiogenesis," *The Journal of Biological Chemistry*, vol. 282, no. 20, pp. 15187–15196, 2007.

[95] L.-C. Yao, P. Baluk, R. S. Srinivasan, G. Oliver, and D. M. McDonald, "Plasticity of button-like junctions in the endothelium of airway lymphatics in development and inflammation," *The American Journal of Pathology*, vol. 180, no. 6, pp. 2561–2575, 2012.

[96] M. Dewerchin and P. Carmeliet, "PlGF: a multitasking cytokine with disease-restricted activity," *Cold Spring Harbor Perspectives in Medicine*, vol. 2, no. 8, Article ID a011056, 2012.

[97] E. Boscolo, J. B. Mulliken, and J. Bischoff, "VEGFR-1 mediates endothelial differentiation and formation of blood vessels in a murine model of infantile hemangioma," *The American Journal of Pathology*, vol. 179, no. 5, pp. 2266–2277, 2011.

[98] R. Serpi, A. M. Tolonen, J. Huusko et al., "Vascular endothelial growth factor-B gene transfer prevents angiotensin II-induced diastolic dysfunction via proliferation and capillary dilatation in rats," *Cardiovascular Research*, vol. 89, no. 1, pp. 204–213, 2011.

[99] C. May, J. R. Doody, R. Abdullah et al., "Identification of a transiently exposed VE-cadherin epitope that allows for specific targeting of an antibody to the tumor neovasculature," *Blood*, vol. 105, no. 11, pp. 4337–4344, 2005.

[100] Z. Liu, F. Wang, and X. Chen, "Integrin $\alpha v\beta 3$-targeted cancer therapy," *Drug Development Research*, vol. 69, no. 6, pp. 329–339, 2008.

Hindawi Publishing Corporation
BioMed Research International
Volume 2015, Article ID 865076, 10 pages
http://dx.doi.org/10.1155/2015/865076

Research Article

Enhanced Vascularization in Hybrid PCL/Gelatin Fibrous Scaffolds with Sustained Release of VEGF

Kai Wang, Xuejiao Chen, Yiwa Pan, Yun Cui, Xin Zhou, Deling Kong, and Qiang Zhao

State Key Laboratory of Medicinal Chemical Biology, Key Laboratory of Bioactive Materials, Ministry of Education, College of Life Sciences, Nankai University, Tianjin 300071, China

Correspondence should be addressed to Qiang Zhao; qiangzhao@nankai.edu.cn

Received 7 August 2014; Revised 13 October 2014; Accepted 3 November 2014

Academic Editor: Ian Chen

Creating a long-lasting and functional vasculature represents one of the most fundamental challenges in tissue engineering. VEGF has been widely accepted as a potent angiogenic factor involved in the early stages of blood vessel formation. In this study, fibrous scaffolds that consist of PCL and gelatin fibers were fabricated. The gelatin fibers were further functionalized by heparin immobilization, which provides binding sites for VEGF and thus enables the sustained release of VEGF. *In vitro* release test confirms the sustained releasing profile of VEGF, and stable release was observed over a time period of 25 days. *In vitro* cell assay indicates that VEGF release significantly promoted the proliferation of endothelial cells. More importantly, *in vivo* subcutaneous implantation reflects that vascularization has been effectively enhanced in the PCL/gelatin scaffolds compared with the PCL counterpart due to the sustained release of VEGF. Therefore, the heparinized PCL/gelatin scaffolds developed in this study may be a promising candidate for regeneration of complex tissues with sufficient vascularization.

1. Introduction

Blood vessels can provide necessary oxygen and nutrients to cell by diffusion processes, but the effective distance of diffusion is 100–200 μm around a capillary [1]. Sufficient vascularization has a decisive effect on maintaining the survival of regenerated tissue in the field of tissue engineering. So far, only a few thin tissues, such as skin, cartilage, or cornea, can successfully survive after implantation [2]. Vascularization in three-dimensional tissue engineering scaffolds, such as bones, remained an important challenge in both research and clinic practice [3]. For the regeneration of blood vessels, immature and regressed capillaries within the wall of blood vessel also led to calcification after a long period of implantation, which resulted in the restenosis failure finally [4].

Recently, several approaches have been employed to improve vascularization of tissue engineering scaffolds, including optimization of 3D structures [5, 6]; preseeding of mesenchymal stem cells (MSCs) [7], endothelial cells (ECs) [2], and endothelial progenitor cells (EPCs) [8]; and the loading of bioactive molecules, such as NO donor [9], angiogenic factors [10, 11], or peptides [12] to the scaffold. However, until now none of them have been proven fully successful in development of long-lasting vasculature (blood vessels).

Rational design of physical structure of tissue engineering scaffold (pore size and interconnectivity) is fundamental for tissue regeneration and vascularization. Published results indicate that enhancing pore sizes within fibrous scaffolds fabricated by electrospinning can effectively promote cellular infiltration [13, 14]; thus, the vascularization has been improved thereafter. However, due to the bioinert characteristic of scaffolds, the integrity and stability of de novo vasculature are not satisfactory. More importantly, the capillaries will regress over long-term implantation as mentioned before.

In addition to the physical structure, bioactivity and function of the scaffold are more important for the vascularization. Of the known angiogenic factors, vascular endothelial growth factor (VEGF) is the most studied and effective one. It has been reported that loading VEGF onto tissue engineering scaffolds is an effective strategy to promote vascularization. However, due to the short half-life (about 50 min), high

doses are often required, which results in a number of side effects (such as vasodilation and hypertension, inappropriate blood vessel growth, atherosclerotic plaque development, and neovascularization of tumors) [15, 16]. In addition, sustained local concentration of VEGF is also necessary for the development of mature blood vessels. Therefore, it is very important to develop functional fibrous scaffold that could load and release VEGF in a sustained and controlled manner.

Heparin possesses a special binding affinity to a variety of growth factors, including platelet-derived growth factor-BB (PDGF-BB) [17], fibroblast growth factor (FGF) [18], transforming growth factor-β (TGF-β) [19], and VEGF [20]. The binding affinity of heparin-binding growth factors with heparin is mainly based on electrostatic interactions [21], which is critical for storage, release, and protection of the growth factor from degradation [22]. For these reasons, heparin has been widely utilized as a functional molecule for the delivery of growth factors to achieve sustained releasing property.

In this study, a hybrid scaffold that consists of synthetic PCL fibers and native gelatin fibers was designed and prepared by coelectrospinning. Gelatin fiber was further crosslinked and functionalized by heparin in one step. Then VEGF was immobilized onto the heparinized PCL/Gel scaffolds by the aid of affinity interaction between heparin and VEGF. The sustained release of VEGF was confirmed by *in vitro* releasing test. The effect of released VEGF from the heparinized PCL/Gel scaffolds on enhancing vascularization has been investigated by both *in vitro* cell experiment and *in vivo* subcutaneous implantation.

2. Materials and Methods

2.1. Materials. Poly(ε-caprolactone) (PCL: M_n = 80,000), gelatin, and 1-ethyl-3-(3-dimethylaminopropyl) carbodiimide (EDC) were purchased from Sigma-Aldrich (Shanghai, China). 1,1,1,3,3,3-Fluoro-2-propanol (HFIP) was purchased from Tianli Technology Co. Ltd (Zhuhai, China). Heparin and 3-(4,5)-dimethylthiahiazo(-z-y1)-3,5-diphenytetrazoliumromide (MTT) were bought from Lianxing Biotechnology Company (Tianjin, China). 3,3′-Dioctadecyloxacarbocyanine perchlorate (DiO) and 1,1′-dioctadecyl-3,3,3′,3′-tetramethylindocarbocyanine perchlorate (DiI) were products of Molecular Probes (Eugene, OR). Human vascular endothelial growth factor (VEGF) was purchased from R&D Systems (Minneapolis, MN). Other reagents were purchased from Tianjin Sixth Reagent Company and used as received without further purification.

2.2. Electrospinning of PCL/Gel Fibrous Scaffolds. The hybrid fibrous scaffolds were prepared by coelectrospinning. A 25% w/v solution of PCL was prepared in a 5 : 1 (V/V) mixture of chloroform and methanol by stirring overnight. Gelatin was dissolved in the HFIP with stirring at room temperature for 6 h to obtain 6% w/v solution. Two 10-mL syringes were filled with PCL or gelatin solution and connected to a 21 G blunt-ended needle that served as the charged spinneret. The apparatus consists of a syringe pump (Cole Parmer, Vernon Hills, IL), a high-voltage generator (DWP503-1AC, Dong-Wen High Voltage power supply Factory, Tianjin, China), and a spinneret-mandrel as collector. The voltages between the needle tip and the rotating mandrel were set as 11 kV for PCL and 17 kV for gelatin. The distances between the needle tip and collector were 25 and 15 cm, respectively. The obtained electrospun scaffolds were vacuum-dried over 48 h at room temperature before further treatment.

2.3. Functionalization of PCL/Gel Fibrous Scaffolds. Crosslinking and heparization of electrospun PCL/Gel scaffolds were performed in 50% ethanol (v/v) containing 30 mM EDC and 0.5 mg/mL heparin for 12 h with gentle shaking in ice bath. The heparinized PCL/Gel scaffolds were washed 3 times with distilled water for 24 h in order to remove unreacted EDC and heparin completely. Then, the scaffolds were dried at room temperature before use.

The heparinized PCL/Gel scaffolds were cut into circular discs (1 cm in diameter) and placed in 48-well cell culture plate. Samples were sterilized by immersion in 75% v/v ethanol solution for 1 h and air-dried at room temperature. They were incubated in VEGF solution (100 ng/100 μL in PBS) at 4°C overnight. Then, samples were quickly washed three times with fresh PBS.

2.4. Fiber Morphology and Distribution. The electrospun PCL/Gel scaffolds were mounted on an aluminum stubs and sputter coated with gold and palladium. They were observed by scanning electron microscope (SEM, HITACHI, X-650, Japan) at an accelerating voltage of 15 kV. Based on the SEM images, the pore diameter was determined according to the method described by Wang et al. [23]. At least six pores per image, three images per sample, and three samples per group were included to perform the calculation.

To visualize the distribution of the PCL and gelatin fibers, two different fluorescent dyes were incorporated into each fibers of the scaffold. DiI (1 mg/mL, orange-red fluorescent) was added to PCL solution and DiO (1 mg/mL, green fluorescent) was added to gelatin solution. After coelectrospinning, the PCL/Gel scaffolds were visualized using a laser scanning confocal microscope (CLSM; Zeiss LSM710).

2.5. Water Contact Angle (WCA) Measurements. The sessile drop method was used to measure WCA at room temperature through an optical contact goniometer (Harke-SPCA, Beijing, China). The scaffolds were pasted on glass slides and fixed onto the sample holder. Each measurement was performed using a 10 μL drop of ddH_2O on the surfaces of the scaffolds after 20 s. The average values of WCA were averaged based on four values at different positions of the sample surface.

2.6. Quantification of Immobilized Heparin. Circular samples (1 cm in diameter) of heparinized PCL/Gel were incubated with 5 mL of toluidine blue solution (0.04 g/100 mL 0.1 M HCl) for 4 h at room temperature with gentle agitation to form dye-heparin complex. Samples were rinsed with PBS twice for 5 min, and the residual dye that was bound to the

heparin was solubilized with 5 mL mixed solution of ethanol and 0.1 M NaOH (4 : 1 v/v). The absorbance of the resulting solution was measured at 530 nm using a spectrophotometer, and the results were used to calculate the heparin concentration based on a calibration curve obtained from a series of graded dye-heparin complexes. The final heparin amount was normalized to the dry weight of each sample ($n = 3$).

2.7. Mechanical Test. Mechanical properties were measured on a tensile-testing machine with a load capacity of 100 N (Instron-5865, Norwood, MA). The 1 cm × 4 cm electrospun PCL/Gel scaffolds were clamped and pulled longitudinally at a rate of 10 mm/min. The tensile strength and elongation at break were measured. The Young's modulus was obtained by measuring the slope of the stress-strain curve in the elastic region.

2.8. VEGF Release. The VEGF loaded specimens were placed in 5 mL centrifugal tube, and 2 mL of release media (0.1% sodium azide in PBS) was added to each tube. They were maintained at 37°C with gentle shaking for up to 25 days. At predetermined time points, buffer in each tube was collected and replaced with fresh PBS. The amount of released VEGF was analyzed using a human VEGF ELISA kit according to the manufacturer's instructions. The cumulative amount of VEGF released from each scaffold was normalized to the dry weight of each sample ($n = 3$).

2.9. Cell Proliferation. Specimens were cut into circular discs (1 cm in diameter) and then placed in 48-well plate. Human umbilical vein endothelial cells (HUVECs) (ScienCell, USA) were seeded on the scaffolds at a density of 5.0×10^3 cells/well. The endothelial culture medium (ECM, ScienCell, USA) was changed every 24 h. After cell culture for 1, 3, and 5 days, 50 μL of MTT reagents (5 mg/mL in PBS) was added to each well and incubated for 4 h. Then, the supernatant was discarded and the cell-scaffold constructs were washed with PBS. 300 μL of DMSO was added, and the plate was placed on a shaker for 15 min to dissolve the formazan salts. Finally, 100 μL of dissolved solution from each well was transferred to a 96-well plate. The absorbance at 490 nm was measured with a Bio-Rad Microplate Reader (iMark, Bio-Rad, USA).

2.10. Subcutaneous Implantation in Rats. Sprague Dawley (SD) rats (male, weight 250–300 g) were purchased from the laboratory animal center of the Academy of Military Medical Sciences (Beijing, China). All animal experiments were approved by the Animal Care and Use Committee of Nankai University. The rats were anesthetized with intraperitoneal injection of chloral hydrate (0.3 mg/kg body weight). Three circular specimens (1 cm in diameter) were implanted subcutaneously at one side of the backbone. The grouping of animals was based on the type of scaffolds and duration of observation for 2 and 4 weeks.

2.11. Histological Analysis. Upon explantation, the surrounding tissues of the scaffolds were excised together and then fixed with 4% paraformaldehyde at 4°C overnight, dehydrated in a 30% sucrose solution for 24 h, and finally embedded in optimal cutting temperature compound (OCT) for sectioning. One part of sections was stained by H&E to assess cellularization. The cell migration rate was calculated by the following equation:

$$\text{The cell migration rate} = \frac{W}{W_0}\%, \quad (1)$$

where W is the area of the cell migration into scaffolds and W_0 is the area of the scaffold. The other sections were stained by immunofluorescence to assess vascularization. Monoclonal antibody to vWF was used as primary antibodies, and Alexa Fluor 488-conjugated anti-rabbit IgG (Invitrogen) was used as the secondary antibody. The nuclei were counterstained with DAPI containing mounting solution (Dapi-Fluoromount-G, Southern Biotech, England). The sections without incubation with primary antibody were used as negative controls. Slides were observed under a fluorescence microscope (Zeiss Axio Imager Z1, Germany) and a digital camera (AxioCam MRm, Germany). The mean blood vessel number was determined based on the fluorescence images. At least six images per section, four sections per sample, and three samples per group were included to obtain the calculation.

2.12. Statistical Analysis. All data were presented as means ± standard deviations. A two-tailed paired Student's t-test was used to compare the differences. A value of $P < 0.05$ was considered statistically significant.

3. Results and Discussion

3.1. Characterization of the Structure and Composition of the Scaffolds. In this study, PCL/gelatin scaffolds with hybrid fibrous structure were designed and fabricated by coelectrospinning. Of the two fiber components, synthetic polymer PCL provides mechanical support, while native polymer gelatin contributes the functional groups for further heparization and VEGF loading. By controlling the flow rate of PCL solution (Table 1), two types of PCL/Gel scaffolds with different compositons were prepared.

SEM images show two types of fibers with contrast in fiber size (Figures 1(a) and 1(d)). The fibers of large diameter are attributed to PCL, while those of small diameter correspond to gelatin, by comparing with the SEM images of neat PCL and gelatin [24]. The pore size of scaffolds was also determined based on the SEM images (Table 2).

In order to better discern the fibers distribution, two types of fibers were fluorescently stained, respectively. As shown in Figure 1(i), red PCL and green gelatin fibers were distributed randomly and uniformly. The relative ratio of two fiber componets was quantified through selective leaching of gelatin. Results indicate that the gelatin ratio was 6.87 wt% and 19.00 wt% for PCL/Gel-1 and PCL/Gel-2, respectively, which agrees well with the theoretical value determined according to the feeding ratio [25].

Table 1: Preparation of heparinized PCL/Gel fibrous scaffolds.

Sample code	C_{PCL} (g/mL)	C_{Gel} (g/mL)	Flow rate PCL (mL/h)	Flow rate Gel (mL/h)	Immobilized heparin ($\mu g/cm^2$)
PCL	0.25	0	8	0	0
PCL/Gel-1	0.25	0.06	8	4	0
PCL/Gel-2	0.25	0.06	4	4	0
Hep-PCL/Gel-1	0.25	0.06	8	4	39.28 ± 4.24
Hep-PCL/Gel-2	0.25	0.06	4	4	84.11 ± 9.24

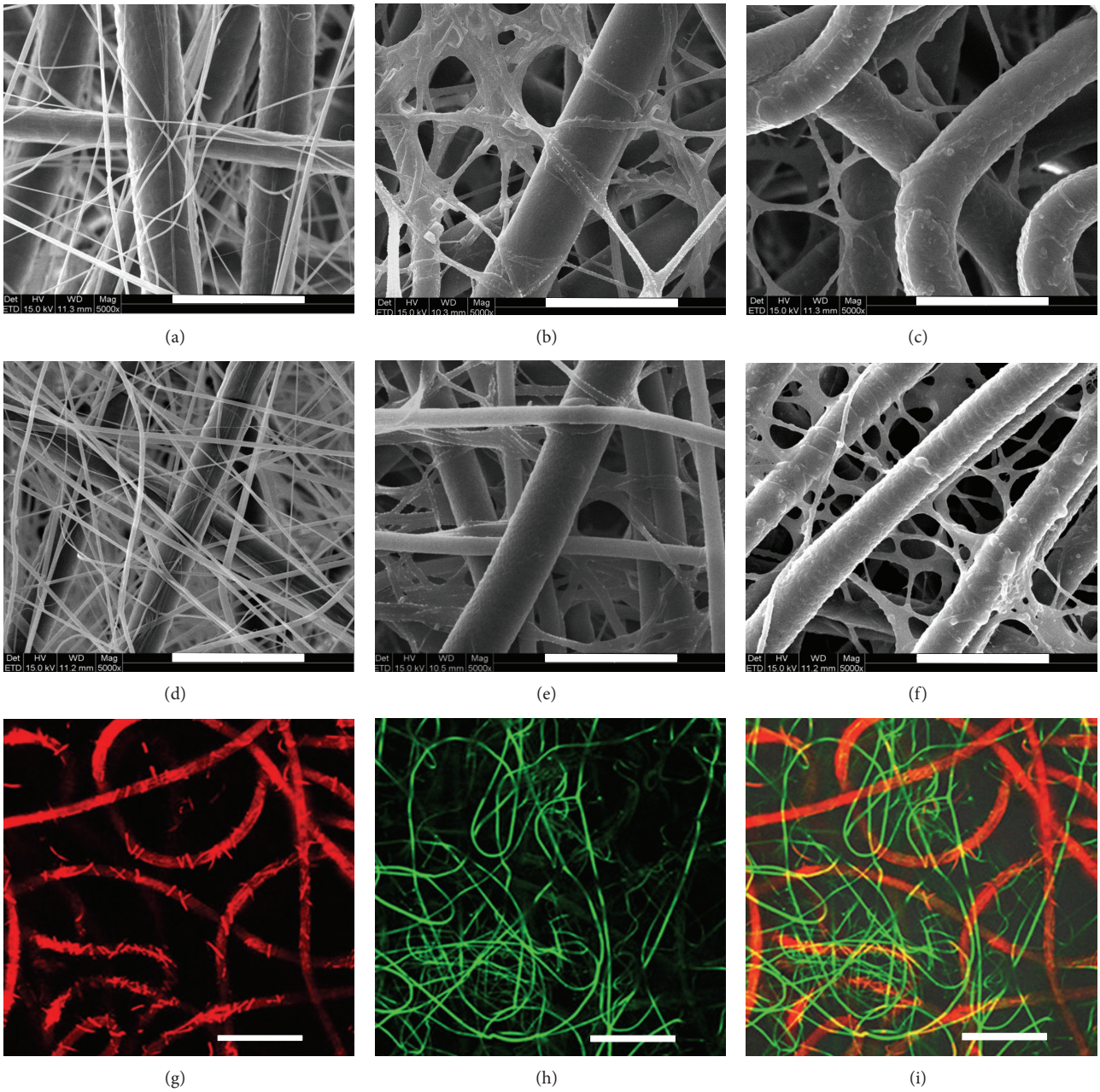

Figure 1: Structure characterization of electrospun PCL/Gel scaffolds. SEM images of PCL/Gel-1 (a), Hep-PCL/Gel-1 (b), and Hep-PCL/Gel-1 degraded in PBS for 14 days (c) and PCL/Gel-2 (d), Hep-PCL/Gel-2 (e), and Hep-PCL/Gel-2 degraded in PBS for 14 days (f) (scale bar = 20 μm). Fluorescent images of PCL/Gel-1 with red PCL fibers labled with DiI (g), and green gelatin fibers labled with DiO (h), as well as the merge one (i) (scale bar = 20 μm).

Table 2: The average pore sizes of the scaffolds.

Scaffolds	Averaged pore size (μm)
PCL	37.61 ± 12.19
PCL/Gel-1	12.43 ± 5.96
PCL/Gel-2	8.07 ± 3.31
Hep-PCL/Gel-1	13.37 ± 6.46
Hep-PCL/Gel-2	8.46 ± 4.24
Hep-PCL/Gel-1 in PBS for 14 d	26.94 ± 14.76
Hep-PCL/Gel-2 in PBS for 14 d	20.94 ± 16.57

The electrospun scaffolds were further functionalized by immobilizing heparin under the catalysis of zero-length crosslinking agent, 1-ethyl-3-(3-dimethylaminopropyl) carbodiimide (EDC). Within this process, gelatin component was also crosslinked, which is necessary for gelatin fibers to maintain the stable structure [20, 26, 27]. After the functionalization, PCL fibers remained the well-fined morphology, whereas the gelatin fibers showed some degree of collapse and deformation, but fiber morphology could still be identified (Figures 1(b) and 1(e)). The average pore size did not show detectable change before and after the functionalization (Table 2).

The stability of heparinized PCL/Gel scaffolds was evaluated by *in vitro* degradation for 14 days. Significant degradation of gelatin fibers could be identified based on the SEM images (Figures 1(c) and 1(f)), which results in enhanced pore size of the scaffold (Table 2).

The heparization was quantified by Toluidine blue assay, and results indicate that the amount of immobilized heparin was consistent with the gelatin content (Table 1).

3.2. Surface Hydrophobic/Hydrophilic Property. Surface hydrophilicity was analyzed by static contact angle measurement. In general, PCL is a hydrophobic polymer with water contact angle (WCA) of 130.52 ± 1.56°. After the incorporation of gelatin component, the hydrophicity was improved; that is, the mean WCA of PCL/Gel-1 and PCL/Gel-2 decreased to 70.85 ± 1.93° and 58.18 ± 1.73°, respectively. Heparization further enhanced the surface hydrophilicity, and PCL/Gel-1 and PCL/Gel-2 became fully hydrophilic; that is, the drop was completely absorbed within 20 seconds (Figure 2).

3.3. Mechanical Properties. The mechanical properties were evaluated by tensile test (Figure 3 and Table 3). Neat PCL is a ductile polymer with high degree of elongation, that is, 614.90 ± 13.34%. The incorporation of gelatin component fails to alter the flexible mechanical characteristic; only tensile strength was slightly lowered because the weight ratio of the gelatin in the scaffold is relatively low. Heparization strengthens the PCL/Gel scaffolds effectively with evidently enhanced tensile strength and Young's modulus. At the same time, the elongation at break was adversely decreased due to the formation of 3D molecular network during the crosslinking. Similar trends in mechanical properties have been reported before [21]. However in this case the elongation

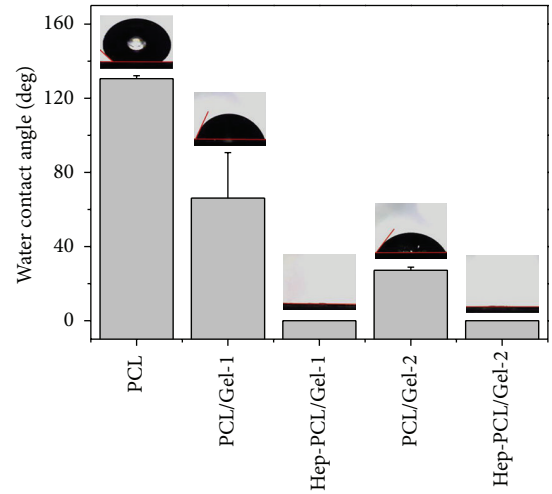

Figure 2: Surface hydrophilic/hydrophobic performance analyzed by water contact angle analysis ($n = 5$) and the corresponding images of water droplets on the different surfaces after contact of 20 seconds.

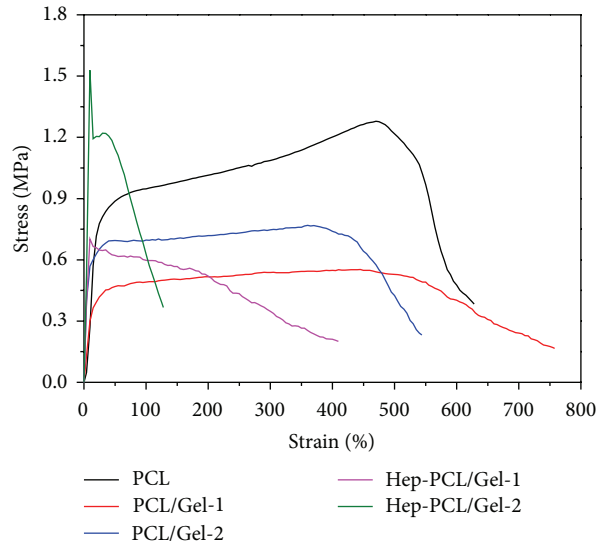

Figure 3: Mechanical properties of PCL and PCL/Gel scaffolds with or without heparization.

for heparinized PCL/Gel is still higher than 100%, which is higher than the normal displacement of the artery during the physiological dilation and constriction, and satisfies the requirement of artificial vascular grafts. In a word, the mechanical properties of the scaffolds could be readily tuned within a wide range to satisfy the requirement of vascular grafts.

3.4. In Vitro Release of VEGF. Figure 4 shows *in vitro* releasing profile of VEGF from heparinized PCL/Gel scaffolds with neat PCL as control. Sustained release of VEGF was observed in the Hep-PCL/Gel scaffolds within time period of 25 days. The release rate is quite stable, and the cumulative amounts of VEGF approach 2.48 ± 0.11 ng/mg for Hep-PCL/Gel-1 and

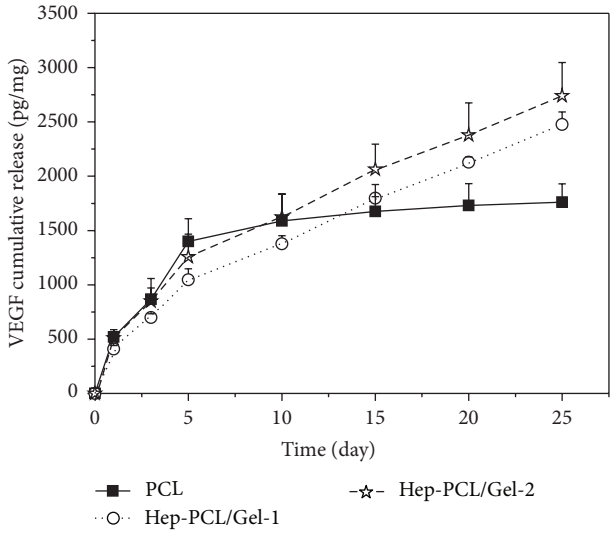

Figure 4: *In vitro* release of VEGF from heparinized PCL/Gel scaffolds and PCL ($n = 3$).

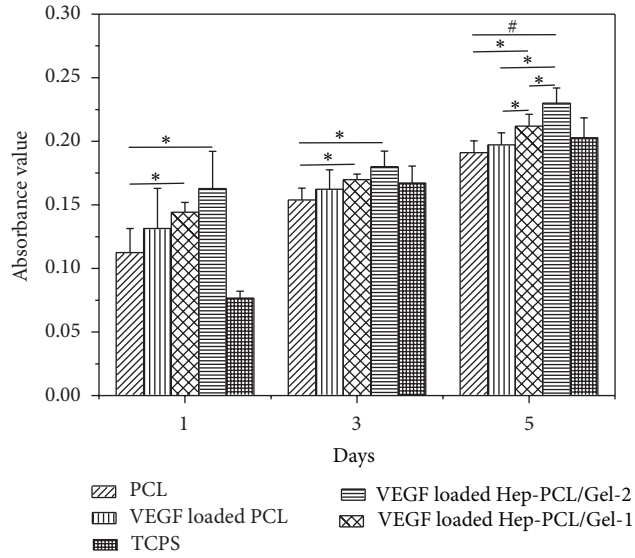

Figure 5: MTT assay for cell proliferation of human umbilical vein endothelial cells (HUVECs) on the VEGF loaded PCL and heparinized PCL/Gel scaffolds. Neat PCL and tissue culture plate (TCP) were used as control ($n = 5$). $^{*}P < 0.05$; $^{\#}P < 0.001$.

Table 3: Mechanical properties of the scaffolds ($n = 3$).

Sample code	Tensile strength (MPa)	Young's modulus (MPa)	Elongation at break (%)
PCL	1.18 ± 0.14	4.41 ± 2.05	614.90 ± 13.34
PCL/Gel-1	0.55 ± 0.04	3.02 ± 0.04	741.78 ± 35.12
PCL/Gel-2	0.76 ± 0.01	5.85 ± 0.01	551.37 ± 10.56
Hep-PCL/Gel-1	0.73 ± 0.02	7.57 ± 0.20	394.52 ± 29.36
Hep-PCL/Gel-2	1.42 ± 0.11	14.80 ± 1.47	126.69 ± 15.18

2.7±0.31 ng/mg for Hep-PCL/Gel-2, respectively. In contrast, PCL shows burst release during the initial 5 days due to the passive physical adsorption of VEGF on the scaffold, and nearly no additional release occurred within the following time period.

The sustained releasing behavior could be attributed to the stabilization effect provided by the heparin. The high binding affinity between VEGF and heparin could effectively delay the dissociation of VEGF from the scaffolds; thus, sustained release of VEGF has been realized.

Heparin also demonstrates high affinity towards a wide range of cytokines and growth factors; therefore, it has been widely utilized for the construction of biomaterial-based delivery system [20, 28–30]. The specific interaction also effectively protects growth factors from thermal denaturation, enzymatic degradation, and inactivation at acidic pH, which mainly comes from the conformational change in the growth factor molecule during the binding with heparin [31, 32]. In addition, it has been reported that heparin also shows binding affinity towards some cytokines secreted by the inflammatory response, which has a positive effect on inhibiting inflammatory reaction [33].

During the implantation of blood-contacting materials or devices in clinic, heparin was often administrated with the aim of anticoagulation. However, the half time of exogeneously supplied free heparin is short (less than 2.5 hours) [34]. They will be eliminated from the body rapidly [35]; hence, the presence of them cannot alter the releasing kinetics of VEGF from heparinized PCL/Gel scaffolds markedly.

3.5. In Vitro Endothelial Cell Proliferation. The effect of sustained release of VEGF on the endothelial cell proliferation was investigated by *in vitro* MTT assay. As shown in Figure 5, the cell proliferation was significantly ($P < 0.05$) accelerated on VEGF loaded Hep-PCL/Gel scaffolds compared with that on the neat PCL throughout the entire culture process. In addition, cells grew faster on the VEGF loaded Hep-PCL/Gel-2 than on the VEGF loaded Hep-PCL/Gel-1 scaffold, which may be due to the higher VEGF loading. VEGF loaded on the PCL scaffold slightly increases the cell proliferation, but the effect is not pronounced. The enhanced proliferation on the VEGF loaded Hep-PCL/Gel scaffolds also confirms that the bioactivity of VEGF released from the scaffolds was higher than PCL scaffolds due to the protective effect provided by immobilized heparin.

3.6. In Vivo Angiogenesis. Angiogenesis in the VEGF loaded PCL/Gel scaffolds was evaluated by subcutaneous implantation in rats. After 4 weeks of implantation, the H&E images clearly show that the scaffold was almost fully cellularized (Figures 6(b), 6(d), 6(f), and 6(h)). As mentioned before, rapid and sufficient cellularization is the prerequisite for vascularization. Previous studies have shown that the relatively small pore size in electrospun scaffolds often limits the cell infiltration. In this study, the pore size was optimized by the method previously developed [14], making the scaffold favorable for cell infiltration and migration. The cell migration rates in all groups exceed 90% after 4 weeks (Figure 6(i)).

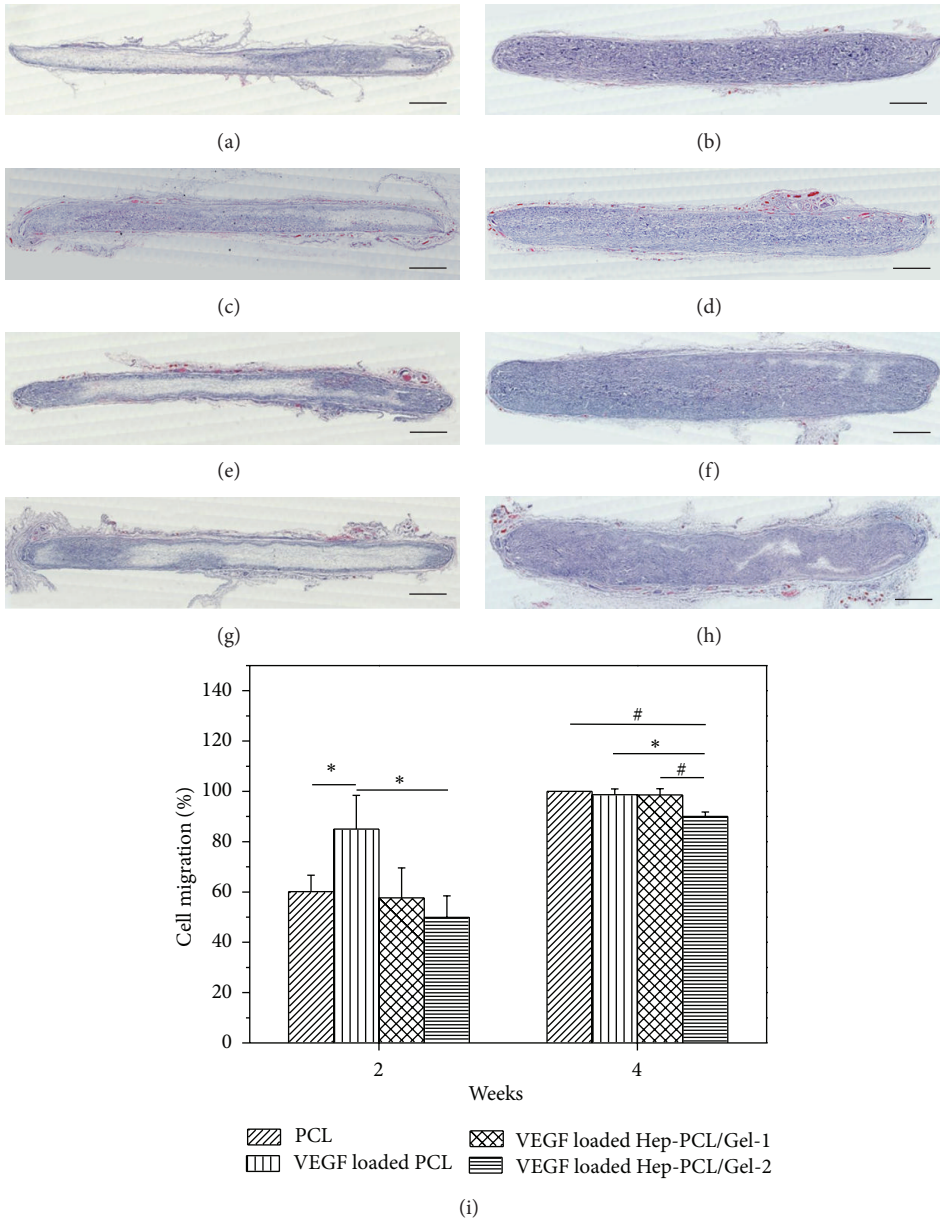

Figure 6: Representative hematoxylin and eosin (H&E) staining of explanted scaffolds after subcutaneous implantation for 2 (a, c, e, and g) and 4 (b, d, f, and h) weeks ($n = 3$): PCL (a and b); VEGF loaded PCL (c and d); VEGF loaded Hep-PCL/Gel-1 (e and f); VEGF loaded Hep-PCL/Gel-2 (g and h) (scale bars = 1 mm), and the corresponding quantitative analysis of cell migration (i). $^{*}P < 0.05$; $^{\#}P < 0.001$.

The blood vessels in the cellularized area were analyzed by immunofluorescent staining with vWF (Figures 7(a)–7(h)) and further quantified based on the image. More capillaries could be clearly identified on the VEGF loaded PCL/Gel scaffolds (arrow indicated). The quantitative result further demonstrates that VEGF loaded PCL/Gel scaffolds significantly enhanced the vessel density compared to PCL and VEGF loaded PCL ($P < 0.001$) after 4 weeks. This enhancement is closely associated with heparin for VEGF loading and protecting, which agrees well with *in vitro* cell proliferation (Figure 5).

Recently, numerous strategies have been developed to deliver VEGF in tissue engineering scaffolds in order to promote angiogenesis. Among these approaches, covalent binding is a robust one, achieving stable binding of VEGF [36]. However, it involves multiple steps, which is tedious and may compromise bioactivity of the protein [37]. The physical absorption by polymer-based carrier is a convenient and effective alternative [38]. This strategy can achieve sustained release of VEGF to some extent [37], but the simple adsorption fails to provide protection for VEGF. In contrast, the affinity delivery of VEGF based on the heparinized scaffold can not only effectively release VEGF in a controlled manner but also can protect it from degradation. The heparin conjugated PCL/Gel scaffolds therefore demonstrated excellent vascularization *in vivo*.

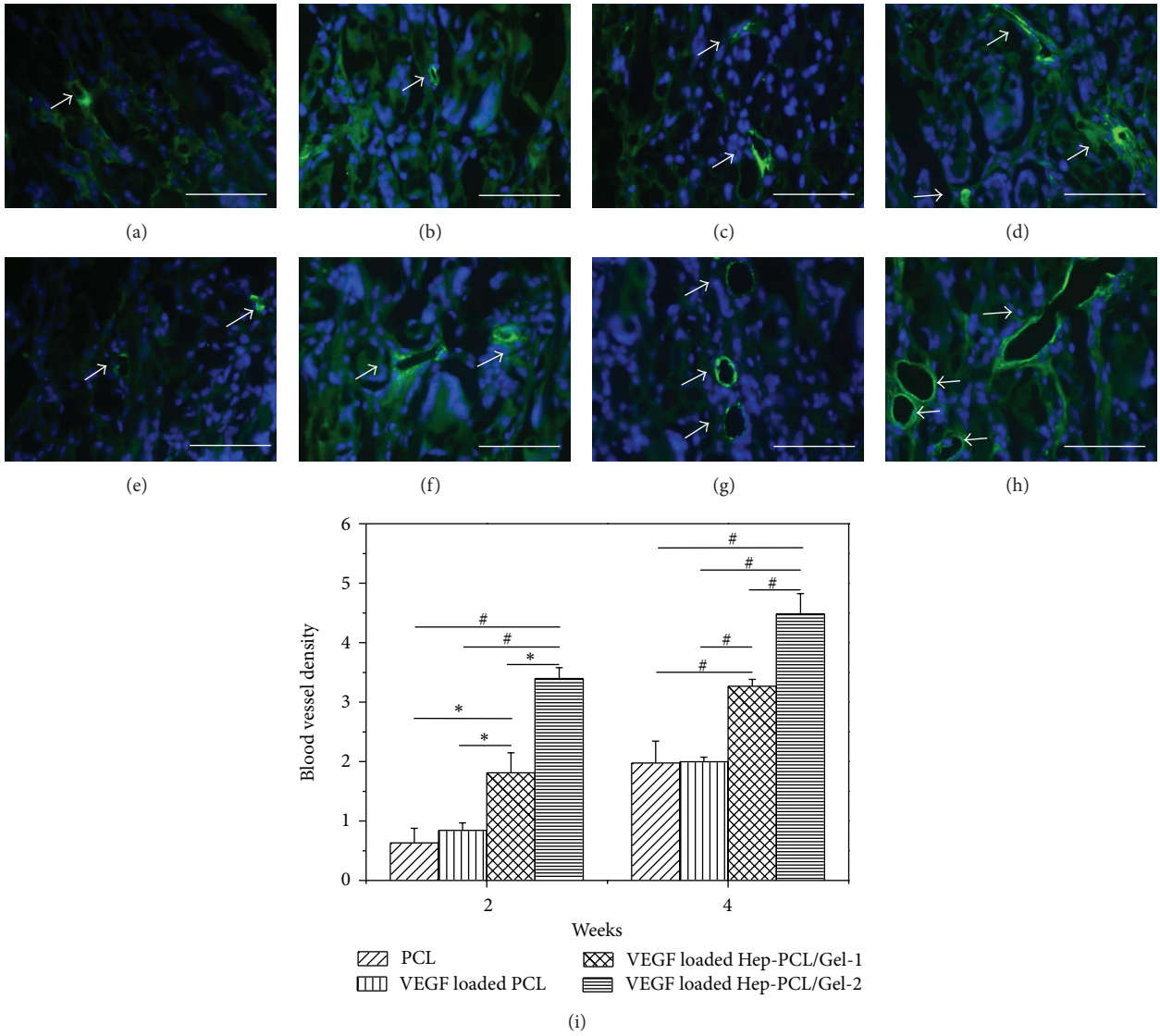

FIGURE 7: Representative microscopic images showing the blood vessels immunostained by vWF in the explanted scaffolds after subcutaneous implantation for 2 (a–d) and 4 (e–h) weeks ($n = 3$): PCL (a and e); VEGF loaded PCL (b and f); VEGF loaded Hep-PCL/Gel-1 (c and g); VEGF loaded Hep-PCL/Gel-2 (d and h) (scale bars = 50 μm). Quantitative analysis on the density of blood vessel (i). $^{*}P < 0.05$, $^{\#}P < 0.001$.

4. Conclusions

In summary, a type of tissue scaffold with hybrid fibrous structure was successfully prepared in this study using two fiber components. Synthetic PCL provides optimal mechanical strength, and native polymer gelatin has been further heparinized in order to deliver VEGF in a controlled manner. The scaffolds show well-defined fiber morphology and homogeneous distribution before and after heparin-functionalization. The physical properties of as-prepared scaffolds, including mechanical properties and surface hydrophilicity, have been evaluated and satisfy the requirement of tissue engineering scaffolds. Heparinized scaffolds demonstrate sustained release of VEGF, which proceeded beyond a time period of 25 days. The sustained release of VEGF can evidently promote the vascularization, which has been confirmed by both *in vitro* cell proliferation and *in vivo* subcutaneous implantation assay.

Conflict of Interests

The authors declare that there is no conflict of interests regarding the publication of this paper.

Acknowledgments

The work was financially supported by the National Natural Science Foundation of China (NSFC) Projects (81171478, 81371699, and 81401534), the Science & Technology Projects of Tianjin of China (12JCQNJC09300 and 14JCQNJC13900), the Program for Changjiang Scholars and Innovative

Research Team in University (IRT13023), and the China Postdoctoral Science Foundation (2014M561177).

References

[1] J. Rouwkema, N. C. Rivron, and C. A. van Blitterswijk, "Vascularization in tissue engineering," *Trends in Biotechnology*, vol. 26, no. 8, pp. 434–441, 2008.

[2] E. C. Novosel, C. Kleinhans, and P. J. Kluger, "Vascularization is the key challenge in tissue engineering," *Advanced Drug Delivery Reviews*, vol. 63, no. 4, pp. 300–311, 2011.

[3] P. C. Johnson, A. G. Mikos, J. P. Fisher, and J. A. Jansen, "Strategic directions in tissue engineering," *Tissue Engineering*, vol. 13, no. 12, pp. 2827–2837, 2007.

[4] S. de Valence, J.-C. Tille, D. Mugnai et al., "Long term performance of polycaprolactone vascular grafts in a rat abdominal aorta replacement model," *Biomaterials*, vol. 33, no. 1, pp. 38–47, 2012.

[5] D. Druecke, S. Langer, E. Lamme et al., "Neovascularization of poly(ether ester) block-copolymer scaffolds in vivo: long-term investigations using intravital fluorescent microscopy," *Journal of Biomedical Materials Research Part A*, vol. 68, no. 1, pp. 10–18, 2004.

[6] V. Karageorgiou and D. Kaplan, "Porosity of 3D biomaterial scaffolds and osteogenesis," *Biomaterials*, vol. 26, no. 27, pp. 5474–5491, 2005.

[7] K. Wang, Y. Guan, Y. Liu et al., "Fibrin glue with autogenic bone marrow mesenchymal stem cells for urethral injury repair in rabbit model," *Tissue Engineering Part A*, vol. 18, no. 23-24, pp. 2507–2517, 2012.

[8] A. Kawamoto, T. Asahara, and D. W. Losordo, "Transplantation of endothelial progenitor cells for therapeutic neovascularization," *Cardiovascular Radiation Medicine*, vol. 3, no. 3-4, pp. 221–225, 2002.

[9] Q. Zhao, J. Zhang, L. Song et al., "Polysaccharide-based biomaterials with on-demand nitric oxide releasing property regulated by enzyme catalysis," *Biomaterials*, vol. 34, no. 33, pp. 8450–8458, 2013.

[10] J. S. Pieper, T. Hafmans, P. B. van Wachem et al., "Loading of collagen-heparan sulfate matrices with bFGF promotes angiogenesis and tissue generation in rats," *Journal of Biomedical Materials Research*, vol. 62, no. 2, pp. 185–194, 2002.

[11] S. Nillesen, P. J. Geutjes, R. Wismans, J. Schalkwijk, W. F. Daamen, and T. H. van Kuppevelt, "Increased angiogenesis and blood vessel maturation in acellular collagen-heparin scaffolds containing both FGF2 and VEGF," *Biomaterials*, vol. 28, no. 6, pp. 1123–1131, 2007.

[12] M. T. Conconi, F. Ghezzo, M. Dettin et al., "Effects on in vitro and in vivo angiogenesis induced by small peptides carrying adhesion sequences," *Journal of Peptide Science*, vol. 16, no. 7, pp. 349–357, 2010.

[13] Y. M. Ju, J. S. Choi, A. Atala, J. J. Yoo, and S. J. Lee, "Bilayered scaffold for engineering cellularized blood vessels," *Biomaterials*, vol. 31, no. 15, pp. 4313–4321, 2010.

[14] Z. Wang, Y. Cui, J. Wang et al., "The effect of thick fibers and large pores of electrospun poly(ε-caprolactone) vascular grafts on macrophage polarization and arterial regeneration," *Biomaterials*, vol. 35, no. 22, pp. 5700–5710, 2014.

[15] M. Huang, S. N. Vitharana, L. J. Peek, T. Coop, and C. Berkland, "Polyelectrolyte complexes stabilize and controllably release vascular endothelial growth factor," *Biomacromolecules*, vol. 8, no. 5, pp. 1607–1614, 2007.

[16] Y.-I. Chung, S.-K. Kim, Y.-K. Lee et al., "Efficient revascularization by VEGF administration via heparin-functionalized nanoparticle-fibrin complex," *Journal of Controlled Release*, vol. 143, no. 3, pp. 282–289, 2010.

[17] B. Sun, B. Chen, Y. Zhao et al., "Crosslinking heparin to collagen scaffolds for the delivery of human platelet-derived growth factor," *Journal of Biomedical Materials Research B: Applied Biomaterials*, vol. 91, no. 1, pp. 366–372, 2009.

[18] H. Shen, X. Hu, F. Yang, J. Bei, and S. Wang, "Cell affinity for bFGF immobilized heparin-containing poly(lactide-co-glycolide) scaffolds," *Biomaterials*, vol. 32, no. 13, pp. 3404–3412, 2011.

[19] M. Lyon, G. Rushton, and J. T. Gallagher, "The interaction of the transforming growth factor-βs with heparin/heparan sulfate is isoform-specific," *The Journal of Biological Chemistry*, vol. 272, no. 29, pp. 18000–18006, 1997.

[20] S. Nakamura, T. Kubo, and H. Ijima, "Heparin-conjugated gelatin as a growth factor immobilization scaffold," *Journal of Bioscience and Bioengineering*, vol. 115, no. 5, pp. 562–567, 2013.

[21] J. Lee, J. J. Yoo, A. Atala, and S. J. Lee, "Controlled heparin conjugation on electrospun poly(ε-caprolactone)/gelatin fibers for morphology-dependent protein delivery and enhanced cellular affinity," *Acta Biomaterialia*, vol. 8, no. 7, pp. 2549–2558, 2012.

[22] R. Guan, X. L. Sun, S. Hou, P. Wu, and E. L. Chaikof, "A glycopolymer chaperone for fibroblast growth factor-2," *Bioconjugate Chemistry*, vol. 15, no. 1, pp. 145–151, 2004.

[23] S. Wang, Y. Zhang, H. Wang, G. Yin, and Z. Dong, "Fabrication and properties of the electrospun polylactide/silk fibroin-gelatin composite tubular scaffold," *Biomacromolecules*, vol. 10, no. 8, pp. 2240–2244, 2009.

[24] Y. Yao, J. Wang, Y. Cui et al., "Effect of sustained heparin release from PCL/chitosan hybrid small-diameter vascular grafts on anti-thrombogenic property and endothelialization," *Acta Biomaterialia*, vol. 10, no. 6, pp. 2739–2749, 2014.

[25] Y. Cui, *Fabrication and functionalization of small-diameter vascular grafts with hybrid fibrous structure [M.S. thesis]*, Nankai University, 2014.

[26] Y. Liu, M. An, L. Wang, and H. Qiu, "Preparation and characterization of chitosan-gelatin/glutaraldehyde scaffolds," *Journal of Macromolecular Science B: Physics*, vol. 53, no. 2, pp. 309–325, 2014.

[27] S. R. Gomes, G. Rodrigues, G. G. Martins, C. M. R. Henriques, and J. C. Silva, "In vitro evaluation of crosslinked electrospun fish gelatin scaffolds," *Materials Science and Engineering C*, vol. 33, no. 3, pp. 1219–1227, 2013.

[28] H. J. Chung, H. K. Kim, J. J. Yoon, and T. G. Park, "Heparin immobilized porous PLGA microspheres for angiogenic growth factor delivery," *Pharmaceutical Research*, vol. 23, no. 8, pp. 1835–1841, 2006.

[29] S. Reed and B. Wu, "Sustained growth factor delivery in tissue engineering applications," *Annals of Biomedical Engineering*, vol. 42, no. 7, pp. 1528–1536, 2014.

[30] F. Du, H. Wang, W. Zhao et al., "Gradient nanofibrous chitosan/poly ε-caprolactone scaffolds as extracellular microenvironments for vascular tissue engineering," *Biomaterials*, vol. 33, no. 3, pp. 762–770, 2012.

[31] S. J. Prestrelski, G. M. Fox, and T. Arakawa, "Binding of heparin to basic fibroblast growth factor induces a conformational change," *Archives of Biochemistry and Biophysics*, vol. 293, no. 2, pp. 314–319, 1992.

[32] A. Walker, J. E. Turnbull, and J. T. Gallagher, "Specific heparan sulfate saccharides mediate the activity of basic fibroblast growth factor," *The Journal of Biological Chemistry*, vol. 269, no. 2, pp. 931–935, 1994.

[33] N. Jiang, W. Xie, H. Wang et al., "Effects of low molecular weight heparin on the inflammatory response and vascular injury in rat after electric burn," *Chinese Journal of Burns*, vol. 30, pp. 128–133, 2014.

[34] T. J. McAvoy, "The biologic half-life of heparin," *Clinical Pharmacology and Therapeutics*, vol. 25, no. 3, pp. 372–379, 1979.

[35] H. R. Lijnen, M. Hoylaerts, and D. Collen, "Heparin binding properties of human histidine-rich glycoprotein," *Journal of Biological Chemistry*, vol. 258, no. 6, pp. 3803–3808, 1983.

[36] Y. Miyagi, L. L. Y. Chiu, M. Cimini, R. D. Weisel, M. Radisic, and R.-K. Li, "Biodegradable collagen patch with covalently immobilized VEGF for myocardial repair," *Biomaterials*, vol. 32, no. 5, pp. 1280–1290, 2011.

[37] C. del Gaudio, S. Baiguera, M. Boieri et al., "Induction of angiogenesis using VEGF releasing genipin-crosslinked electrospun gelatin mats," *Biomaterials*, vol. 34, no. 31, pp. 7754–7765, 2013.

[38] S. Singh, B. M. Wu, and J. C. Y. Dunn, "Delivery of VEGF using collagen-coated polycaprolactone scaffolds stimulates angiogenesis," *Journal of Biomedical Materials Research Part A*, vol. 100, no. 3, pp. 720–727, 2012.

Hindawi Publishing Corporation
BioMed Research International
Volume 2015, Article ID 592523, 6 pages
http://dx.doi.org/10.1155/2015/592523

Research Article

Attenuating Tumour Angiogenesis: A Preventive Role of Metformin against Breast Cancer

Shan Gao, Jingcheng Jiang, Pan Li, Huijuan Song, Weiwei Wang, Chen Li, and Deling Kong

Tianjin Key Laboratory of Biomaterial Research, Institute of Biomedical Engineering, Chinese Academy of Medical Science and Peking Union Medical College, Tianjin 300192, China

Correspondence should be addressed to Chen Li; plumlichen@163.com

Received 3 October 2014; Accepted 9 December 2014

Academic Editor: Gang Niu

Metformin is one of the most widely prescribed antidiabetics for type 2 diabetes. A critical role of metformin against tumorigenesis has recently been implicated, although several studies also reported the lack of anticancer property of the antidiabetics. Given the controversies regarding the potential role of metformin against tumour progression, the effect of metformin against breast, cervical, and ovarian tumour cell lines was examined followed by *in vivo* assessment of metformin on tumour growth using xenograft breast cancer models. Significant inhibitory impact of metformin was observed in MCF-7, HeLa, and SKOV-3 cells, suggesting an antiproliferative property of metformin against breast, cervical, and ovarian tumour cells, respectively, with the breast tumour cells, MCF-7, being the most responsive. *In vivo* assessment was subsequently carried out, where mice with breast tumours were treated with metformin (20 mg/kg body weight) or sterile PBS solution for 15 consecutive days. No inhibition of breast tumour progression was detected. However, tumour necrosis was significantly increased in the metformin-treated group, accompanied by decreased capillary formation within the tumours. Thus, despite the lack of short-term benefit of metformin against tumour progression, a preventive role of metformin against breast cancer was implicated, which is at partially attributable to the attenuation of tumour angiogenesis.

1. Introduction

In recent years, epidemiological analyses have indicated a positive association between long-term diabetes and elevated risk of malignant neoplasms [1]. In particular, patients with preexisting type 2 diabetes (T2D) present a higher risk of cancer development and cancer-related mortality. Moreover, cancer patients with diabetes also showed increased mortality compared to nondiabetic cancer patients. Given the potential causal relationship between T2D and cancer, multiple plasma glucose lowering agents have been selected to be tested for potential anticancer effects, with metformin showing the most promising result.

Metformin is one of the most efficacious and safe front-line antidiabetics for type 2 diabetes (T2D). In addition to its antiglycaemic impact, recent reports also implicated critical role of metformin in tumourigenesis [1, 2]. Indeed, antiproliferative effects of metformin have been reported in multiple tumour cell lines via several molecular pathways, including the adenosine monophosphate kinase (AMPK) pathway, the insulin receptor cascade, and the AMPK-independent RagGTPase-dependent 3mTORC1 signalling network [1, 3]. Evidence also supports an anti-inflammatory role of metformin against cancer progression by inhibiting cancer stem cells [4]. In contrast, some studies observed no association between metformin and cancer-related mortality [5]. Results from a newly published epidemiological analysis also reported no direct association between metformin and cancer outcome [6]. Given the controversies regarding the use of metformin as potential anticancer treatment, we examined the effect of metformin against selective tumour cell lines followed by *in vivo* assessment of metformin on tumour growth.

2. Methods and Materials

2.1. Cell Culture and Viability Assay. Human breast (MCF-7), ovarian (SKOV-3), and cervical (HeLa) cancer cells

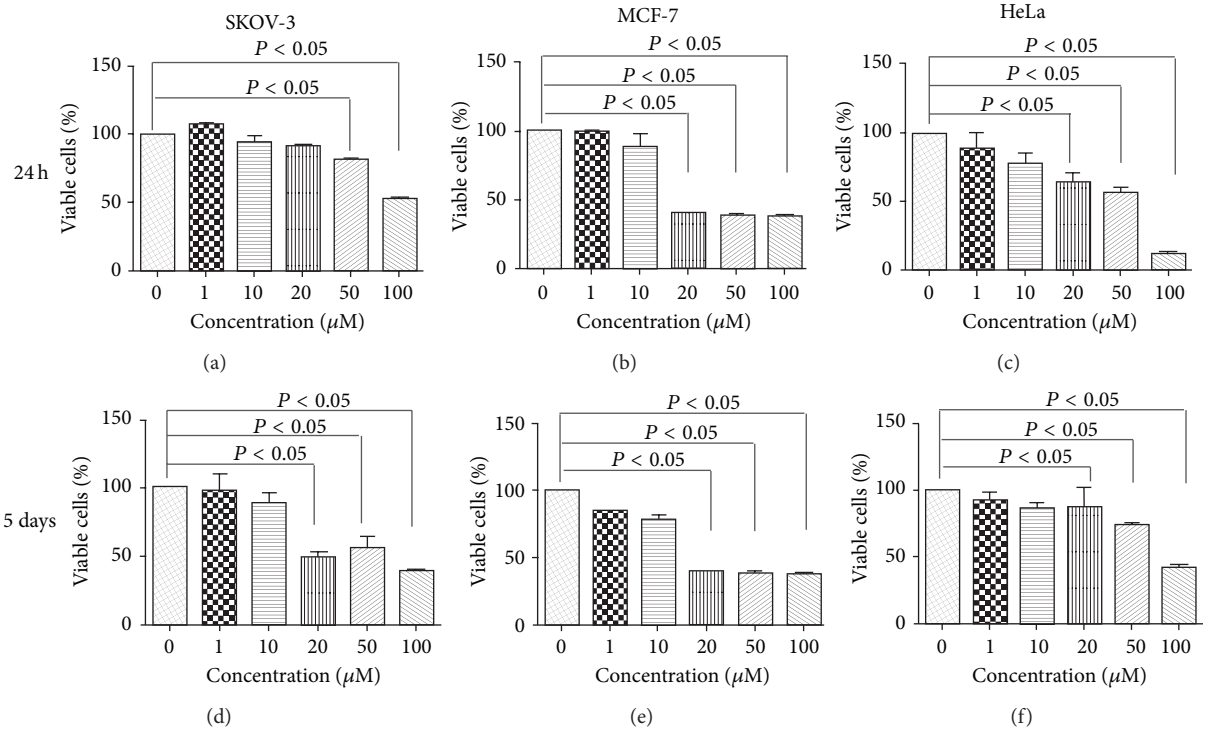

Figure 1: Metformin inhibits tumour cell growth. Human ovarian (SKOV-3), breast (MCF-7), and cervical (HeLa) cells were exposed to a series of concentrations of metformin for 24 h ((a), (b), and (c)) and 5 days ((d), (e), and (f)). Cell viability was assessed using a cell viability (CCK-8) assay. Data are presented as means ± SD, $n = 6$.

were cultured in DMEM media (Hyclone, Beijing, China) supplemented with 10% foetal bovine serum (Gibco, Beijing, China), 100 units/mL penicillin, and 100 μg/mL streptomycin (Sigma-Aldrich, Beijing, China). Cells were seeded at a density of ~5000 cells per well in 96-well plates and maintained at 37°C under standard culturing conditions. Cells were exposed to a series of concentrations of metformin (Sigma-Aldrich, Beijing, China) continuously and cell viability was determined at the end of 24 h and 5 days using a cell counting kit-8 (CCK-8; Dojindo, Japan).

2.2. In Vivo Assessment. Xenograft breast tumour models were established by injecting MCF-7 cells into 6-week-old female BALB/c nude mice (Charles River Laboratories, Beijing, China). Once the tumour size reached ~100–150 mm^3, mice were randomly assigned to either control group or metformin-treated group. Local injection of metformin (20 mg/kg body weight) or sterile PBS was administered for 15 consecutive days. Changes of body weight were monitored and tumour volumes were measured and corrected according to standard formula [7].

2.3. Histomorphological and Immunofluorescence Analysis. 15 days after initial injection, tumours were dissected and fixed in 4% paraformaldehyde before being paraffin embedded. Consecutive sections (thickness, 5 μm) were cut onto microscope slides. Haematoxylin and eosin (H&E) staining was employed to examine tumour morphology and immunofluorescent staining using an antibody raised against von Willebrand factor (vWF; 1 : 200 dilution; Dako, Shanghai, China) was also carried out to evaluate capillary formation. The staining data were analysed with a fluorescent microscope (Leica, Germany) and fluorescent intensity was quantified using ImageJ software (National Institute of Health, USA).

3. Results

3.1. Metformin Inhibits In Vitro Tumour Cell Growth. Given the high prevalence of ovarian, cervical, and, particularly, breast cancers in pre- and postmenopausal women, 3 female tumour cell lines, MCF-7, SKOV-3, and HeLa, were initially selected to investigate the potential anticancer effect of metformin *in vitro*. As shown in Figures 1(b) and 1(c), 24 h exposure to metformin significantly reduced cell viability in all 3 tumour cell lines, with a maximum response of 42 ± 8%, 38 ± 2%, 14 ± 2% for SKOV-3, MCF-7, and HeLa cells, respectively (Figures 1(a)–1(c)). Similar inhibitory responses were also observed from cells treated with metformin for 5 days (Figures 1(d)–1(f)). For both SKOV-3 and HeLa cells, the metformin-exerted attenuation of cell growth appeared to be concentration-dependent, in contrast to MCF-7, of which the inhibitory responses were similar once the administrative dose of metformin was over 20 mM. However, as noted by the National Cancer Institute some years ago, the activity of a pharmacological agent *in vitro* does not necessarily reflect its

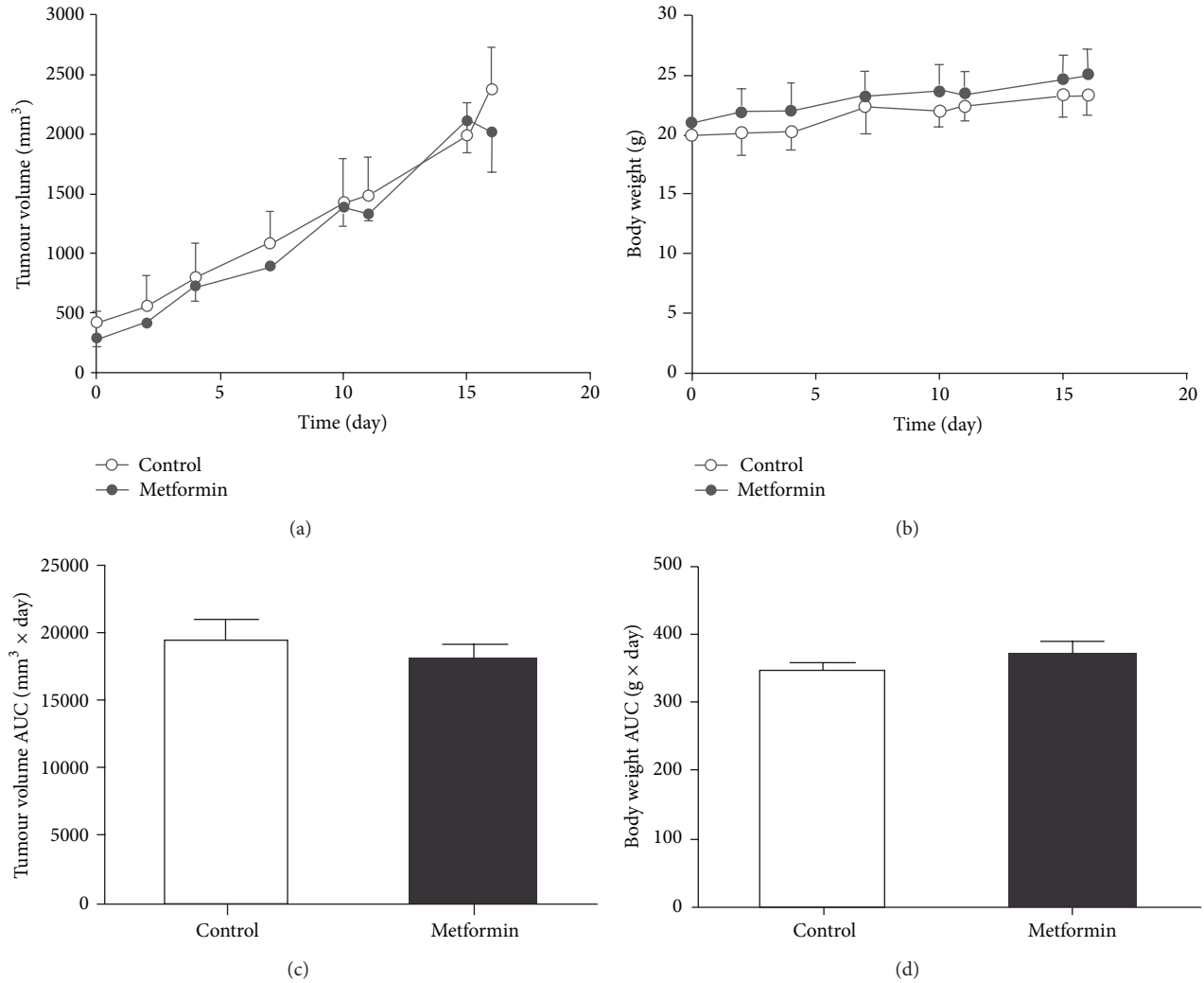

Figure 2: *In vivo* assessment of metformin treatment on tumour growth. Metformin (20 mg/kg body weight; Metformin group) or sterile PBS (Control group) was injected locally to mice with breast carcinoma for 15 consecutive days. (a) Average tumour size and (b) body weight were monitored and plotted against time for Metformin (closed circle) and Control group (open circle). Total changes of tumour volume (c) and body weight (d) were also presented as area under curve (AUC). Data are presented as means ± SD, n = 4-5.

in vivo performance [8], and subsequent *in vivo* assessment was carried out.

3.2. Effect of Metformin on In Vivo Tumour Progression and Tumour Angiogenesis. Our *in vitro* cytotoxicity assay demonstrated marked inhibitory impact of metformin on ovarian, breast, and cervical cancer cell lines, with breast tumour cells, MCF-7, being the most responsive. Indeed, several studies have implicated a positive correlation of short-term use of metformin and breast carcinoma remission [9–11]. A clinical trial study also demonstrated anticancer impact of metformin in nondiabetic postmenopausal women with estrogen receptor positive breast tumours [12]. In contrast, another report observed no inhibitory benefit of metformin on multiple subtypes of breast tumours under euglycaemic condition [13], which was further supported by epidemiological studies also demonstrating a lack of anticancer property of metformin against breast carcinoma [14].

Given the high prevalence of breast cancer and the current controversies concerning the exact impact of metformin use against breast carcinoma, human xenograft breast tumour mouse models were used in the present study for *in vivo* evaluation. Thus, local injection of PBS (Control group) or metformin (20 mg/kg body weight; Metformin group) was administered daily at the tumour site for two weeks. No changes of tumour volume were detectable between the control and metformin-treated groups (Figures 2(a) and 2(b)). No attenuation of tumour progression was observed either as superimposable tumour growth profiles were obtained from both groups (Figure 2(a)). In addition, no significant difference in animal body weight was detected between the two groups (Figure 2(b)).

Despite the lack of inhibitory impact of metformin on tumour growth, subsequent histological analyses revealed marked increase of tumour necrosis in metformin-treated mice (143 ± 11% over control group, $P < 0.01$; Figures

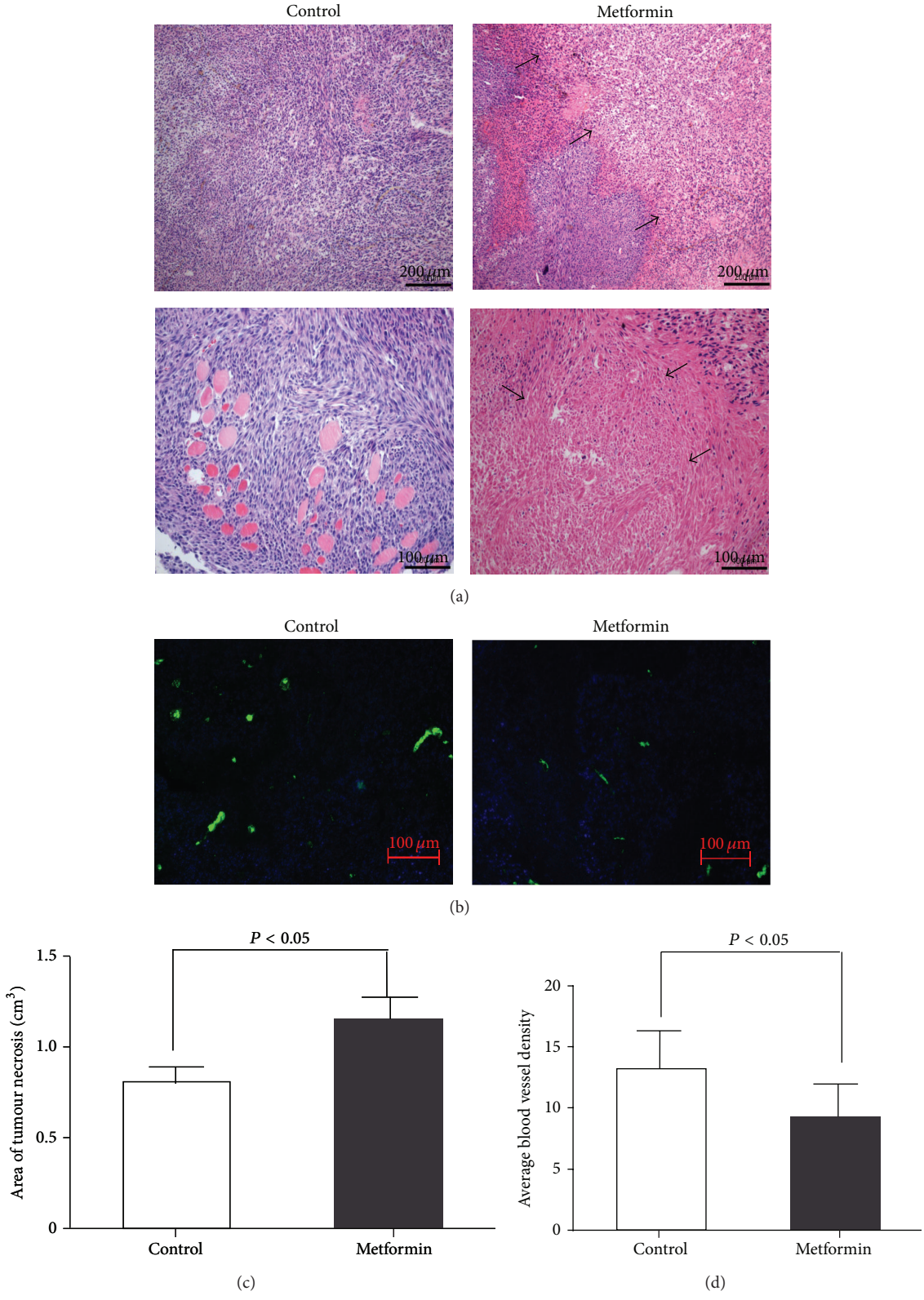

Figure 3: Effect of metformin treatment on tumour necrosis and angiogenesis. H&E staining of tumours obtained from Metformin and Control groups. Scale bar: 200 μm ((a), upper panels) and 100 μm ((a), lower panels). (b) Immunofluorescent staining of vWF (green) in tumours obtained from Metformin and Control groups. Scale bar: 100 μm. Nuclei were counter-stained with DAPI (blue). Area of tumour necrosis (c) and tumour blood vessel density (d) were quantified. Tumour necrosis was indicated by black arrows. Data are presented as means ± SD, n = 4-5. Images are representative of 4-5 animals from 3 separate experiments.

3(a) and 3(c)). Furthermore, immunofluorescence staining of von Willebrand factor (vWF), a microvascular endothelial marker, also revealed reduced average blood vessel density in tumours obtained from the metformin-treated animals (69 ± 29% over control group, $P < 0.02$; Figures 3(b) and 3(d)), implicating an antiangiogenic impact of metformin.

4. Discussion

The cytotoxicity of metformin was observed in all 3 cell types, with breast tumour cells being the most responsive, although cautions need to be exercised when drawing conclusions from *in vitro* results since cultured tumour cells are morphologically and functionally different from native tumours.

Subsequent *in vivo* assessment showed no detectable tumour reduction after local injection of metformin (20 mg/kg body weight) for 15 days. In fact, the effect of metformin against breast cancer has long been extensively investigated albeit contradictory as summarized in a recent review [2]. Most studies have reported decreased incidents and severity of mammary cancer in rodent models after long-term oral or intravenous administration of metformin. Similarly, attenuated tumour progression was observed in humans following treatment with high dosage metformin [2]. In contrast, no inhibition of tumour growth and latency was also recorded, often when low dosage of metformin was applied. Considering the potential implications of different dosage and administrative routes of metformin treatment on cancer outcome, 20 mg per kg body weight metformin was used in the present study and the drug was directly injected to the tumour sites to minimize non-tumour-site distribution caused by different routes of administration [2]. We observed no attenuation of tumour growth after short-term administration of a moderate level of metformin, which suggests limited short-term anticancer ability of metformin treatment *per se*. However, this result may not reflect long-term effect of the drug as the necrosis area was considerably larger in tumours obtained from metformin-treated mice.

In addition, significant attenuation of capillary formation was also evident from the metformin-treated group, consistent with a previous report proposing an AMPK/mTOR-dependent antiangiogenic effect of metformin on ovarian cancer [15]. Thus, despite the lack of short-term benefit of metformin in tumour regression *in vivo*, a preventive role of metformin against breast cancer was implicated, which is at least partially attributable to the attenuation of tumour angiogenesis. Further investigation is required to evaluate whether the antiangiogenic effect of metformin is tumour-specific, particularly since metformin is widely prescribed as an antidiabetic and T2D patients have an elevated risk of vascular disorders. Furthermore, considering the diversity of metformin action, the exact mechanisms underlying the antiangiogenic property of metformin are also required to be elucidated.

Conflict of Interests

The authors declare that there is no conflict of interests.

Acknowledgments

This study was financially supported by the National Natural Science Foundation of China (nos. 31300732 and 81301309) and the Tianjin Research Programme of Application Foundation and Advanced Technology (no. 13JCYBJC39300).

References

[1] C. Li and D. Kong, "Cancer risks from diabetes therapies: evaluating the evidence," *Pharmacology & Therapeutics*, vol. 144, no. 1, pp. 71–81, 2014.

[2] V. N. Anisimov, "Do metformin a real anticarcinogen? A critical reappraisal of experimental data," *Annals of Translational Medicine*, vol. 2, no. 6, p. 60, 2014.

[3] A. Kalender, A. Selvaraj, S. Y. Kim et al., "Metformin, independent of AMPK, inhibits mTORC1 in a rag GTPase-dependent manner," *Cell Metabolism*, vol. 11, no. 5, pp. 390–401, 2010.

[4] H. A. Hirsch, D. Iliopoulos, and K. Struhl, "Metformin inhibits the inflammatory response associated with cellular transformation and cancer stem cell growth," *Proceedings of the National Academy of Sciences of the United States of America*, vol. 110, no. 3, pp. 972–977, 2013.

[5] X. Sui, Y. Xu, J. Yang et al., "Use of metformin alone is not associated with survival outcomes of colorectal cancer cell but AMPK activator AICAR sensitizes anticancer effect of 5-fluorouracil through AMPK activation," *PLoS ONE*, vol. 9, no. 5, Article ID e97781, 2014.

[6] R. J. Stevens, R. Ali, C. R. Bankhead et al., "Cancer outcomes and all-cause mortality in adults allocated to metformin: systematic review and collaborative meta-analysis of randomised clinical trials," *Diabetologia*, vol. 55, no. 10, pp. 2593–2603, 2012.

[7] W. Wang, C. Li, J. Zhang, A. Dong, and D. Kong, "Tailor-made gemcitabine prodrug nanoparticles from well-defined drug-polymer amphiphiles prepared by controlled living radical polymerization for cancer chemotherapy," *Journal of Materials Chemistry B*, vol. 2, no. 13, pp. 1891–1901, 2014.

[8] C. L. Morton and P. J. Houghton, "Establishment of human tumor xenografts in immunodeficient mice," *Nature Protocols*, vol. 2, no. 2, pp. 247–250, 2007.

[9] P. J. Goodwin, V. Stambolic, J. Lemieux et al., "Evaluation of metformin in early breast cancer: a modification of the traditional paradigm for clinical testing of anti-cancer agents," *Breast Cancer Research and Treatment*, vol. 126, no. 1, pp. 215–220, 2011.

[10] S. Niraula, R. J. O. Dowling, M. Ennis et al., "Metformin in early breast cancer: a prospective window of opportunity neoadjuvant study," *Breast Cancer Research and Treatment*, vol. 135, no. 3, pp. 821–830, 2012.

[11] S. Hadad, T. Iwamoto, L. Jordan et al., "Evidence for biological effects of metformin in operable breast cancer: aA pre-operative, window-of-opportunity, randomized trial," *Breast Cancer Research and Treatment*, vol. 128, no. 3, pp. 783–794, 2011.

[12] J. Kim, W. Lim, E.-K. Kim et al., "Phase II randomized trial of neoadjuvant metformin plus letrozole versus placebo plus letrozole for estrogen receptor positive postmenopausal breast cancer (METEOR)," *BMC Cancer*, vol. 14, no. 1, article 170, 2014.

[13] S. Sadighi, S. Amanpour, B. Behrouzi, Z. Khorgami, and S. Muhammadnejad, "Lack of metformin effects on different molecular subtypes of breast cancer under normoglycemic

conditions: an in vitro study," *Asian Pacific Journal of Cancer Prevention*, vol. 15, no. 5, pp. 2287–2290, 2014.

[14] N. Besic, N. Satej, I. Ratosa et al., "Long-term use of metformin and the molecular subtype in invasive breast carcinoma patients—a retrospective study of clinical and tumor characteristics," *BMC Cancer*, vol. 14, no. 1, article 298, 2014.

[15] R. Rattan, R. P. Graham, J. L. Maguire, S. Giri, and V. Shridhar, "Metformin suppresses ovarian cancer growth and metastasis with enhancement of cisplatin cytotoxicity in vivo," *Neoplasia*, vol. 13, no. 5, pp. 483–491, 2011.

Hindawi Publishing Corporation
BioMed Research International
Volume 2015, Article ID 795672, 8 pages
http://dx.doi.org/10.1155/2015/795672

Research Article

Diffuse Calcifications Protect Carotid Plaques regardless of the Amount of Neoangiogenesis and Related Histological Complications

Francesco Vasuri,[1] Silvia Fittipaldi,[1] Rodolfo Pini,[2] Alessio Degiovanni,[1] Raffaella Mauro,[2] Antonia D'Errico-Grigioni,[1] Gianluca Faggioli,[2] Andrea Stella,[2] and Gianandrea Pasquinelli[1]

[1] *Pathology Unit, Department of Experimental, Diagnostic and Specialty Medicine (DIMES), S. Orsola-Malpighi Hospital, Bologna University, Via Massarenti 9, 40138 Bologna, Italy*
[2] *Vascular Surgery Unit, Department of Experimental, Diagnostic and Specialty Medicine, S. Orsola-Malpighi Hospital, Bologna University, Via Massarenti 9, 40138 Bologna, Italy*

Correspondence should be addressed to Francesco Vasuri; vasurifrancesco@libero.it

Received 9 October 2014; Revised 16 December 2014; Accepted 13 January 2015

Academic Editor: Qiang Zhao

Background. Neoangiogenesis is crucial in plaque progression and instability. Previous data from our group showed that Nestin-positive intraplaque neovessels correlated with histological complications. The aim of the present work is to evaluate the relationship between neoangiogenesis, plaque morphology, and clinical instability of the plaque. *Materials and Methods.* Seventy-three patients (53 males and 20 females, mean age 71 years) were consecutively enrolled. Clinical data and 14 histological variables, including intraplaque hemorrhage and calcifications, were collected. Immunohistochemistry for CD34 and Nestin was performed. RT-PCR was performed to evaluate Nestin mRNA (including 5 healthy arteries as controls). *Results.* Diffusely calcified plaques (13/73) were found predominantly in females ($P = 0.017$), with a significantly lower incidence of symptoms (TIA/stroke ($P = 0.019$) than noncalcified plaques but with the same incidence of histological complications ($P = 0.156$)). Accordingly, calcified and noncalcified plaques showed similar mean densities of positivity for CD34 and Nestin. Nestin density, but not CD34, correlated with the occurrence of intraplaque hemorrhage. *Conclusions.* Plaques with massive calcifications show the same incidence of histological complications but without influencing symptomatology, especially in female patients, and regardless of the amount of neoangiogenesis. These results can be applied in a future presurgical identification of patients at major risk of developing symptoms.

1. Introduction

The vulnerable atheromatous plaques have been originally described as characterized by a large lipid core, a thin fibrous cap, a rich infiltrate of macrophages, and little smooth muscle cell component [1]. Neoangiogenesis began to stand out as one of the most important pathological processes involved in the plaque progression only in the recent years [2], when neovessel formation was related to an increased plaque vulnerability and to the onset of clinical symptoms [3, 4]. In particular, the intraplaque hemorrhage and the incidence of symptomatic plaques were directly related to the neovessel density, simply measured by means of immunohistochemistry (IHC) for CD34 [3]. If the density of neovessels is likely to be directly related with plaque growth and progression [5], the morphology of the neoangiogenetic structures plays a key role in the onset of the plaque instability. In fact plaque neovessels are reported to lack extracellular junctions [6]; moreover, symptomatic plaques show larger and more irregular neoangiogenetic structures compared to the neovessels of asymptomatic plaques [7]. Recently we described the IHC and immunofluorescence positivity for Nestin and WT1 in *vasa vasorum* from healthy arteries, hypothesizing that they might represent the starting point of

the neoangiogenesis during atherosclerosis [8]. Afterwards we actually confirmed the expression of Nestin and WT1 in diseased arteries but together with the observation that nearly 36% of the neovessels showed positivity for Nestin and negativity for WT1 (Nestin+/WT1−). As a matter of fact, hemorrhagic plaques showed significantly more Nestin+/WT1− neoangiogenesis than uncomplicated plaques at both IHC and RT-PCR [9].

The aims of the present study were (i) to evaluate the relationship between the intraplaque neoangiogenesis (as quantified by CD34 and Nestin IHC) and the main histopathological plaque characteristics (especially complications and calcifications) and (ii) to evaluate the relationship between the immunohistochemical and histopathological characteristics and the clinical plaque instability.

2. Materials and Methods

2.1. Patients and Clinical Data. This study was carried out in conformity to the ethical guidelines of the 1975 Declaration of Helsinki (and following modifications); informed consent was obtained from all patients before surgery. We evaluated all consecutive cases of carotid endarterectomy specimens that came to our Surgery Unit in 2 years, from January 2011. According to the European Society for Vascular Surgery (ESVS) and the Society of Vascular Surgeons (SVS) recommendations [11, 12], the patients were submitted to carotid endarterectomy (CEA) for either symptomatic carotid plaques ≥50% or asymptomatic carotid stenosis ≥70%. For each patient the following clinical data were collected: occurrence of symptoms related to the carotid disease, that is, transient ischemic attack (TIA) and stroke, association with chronic ischemic cardiopathy, chronic obstructive bronchopneumonia and/or chronic renal failure, smoke, diabetes, dyslipidemia, and therapy with acetylsalicylic acid or statins.

2.2. Histopathological Analysis. Endarterectomy specimens were sent to our Pathology Unit, fixed in formalin, routinely processed, and paraffin embedded. Two μm thick slices were cut from the paraffin blocks for haematoxylin-eosin and trichrome stains. For each case, the following histopathological features were collected as single variables, as previously reported [9]: the occurrence of intraplaque complications (hemorrhage, thrombosis, and/or surface defects) which put the plaque into the AHA type VI [10], maximum and minimum size of the fibrous cap, extension of the lipid core, and extension of the inflammatory infiltrate. For the purposes of the study, the amount of calcifications was assessed and graded from 0 to 4+ in relation to their extension along the vessel circumference; the intraplaque calcification was therefore simplified in low-grade (if 0 to 2+) and high-grade (if 3+ or 4+).

2.3. Immunohistochemistry. The monoclonal antibodies used in this study are listed in Table 1. Immunohistochemistry (IHC) for Nestin was performed manually, as previously described [8, 9]. IHC for CD34 was performed automatically, by means of Benchmark XT (Ventana Medical System), using the XT ultraView DAB v3 program.

Table 1: Technical characteristics of the antibodies used for immunohistochemistry.

Antibody	Clone	Manufacturer
Nestin	*10C2 (mouse IgG)*	Millipore
CD34	*QBEnd/10 (mouse IgG)*	Roche Ventana

The microvessel "density of positivity" [9] for Nestin was evaluated after the identification of specific Regions of Interest (ROI). ROI were defined as areas with CD34-positive neoangiogenesis, and at 20x magnification each ROI was divided into 1 mm^2 fields using an Olympus ocular micrometer (1 length unit = 5 μm, which means that an area of 100 × 100 units is equal to 0.25 mm^2). Firstly, CD34 and Nestin microvessel positivity were counted separately; the Nestin-positive vessels were counted in the same ROI where CD34 was evaluated. Afterwards we calculated the "density of positivity" for CD34 and Nestin by dividing the sum of all the positive vascular structures observed by the number of the counted fields in each section. Finally we calculated the ratio between the densities of positivity of Nestin and CD34 in each case: the Nestin/CD34 ratio represents how many CD34-positive neovessels concomitantly express Nestin in the intraplaque neoangiogenesis.

2.4. RT-PCR. Reverse Transcriptase-Polymerase Chain Reaction (RT-PCR) for the product of the Nestin gene was carried out on 5 type V and on 5 type VI plaques, in order to evaluate the different expression in complicated and uncomplicated carotid plaques. A pool composed of 5 healthy carotid arteries was used as controls. Healthy carotids were kindly provided by the Cardiovascular Tissue Bank of S. Orsola-Malpighi University Hospital of Bologna from 5 multiorgan donors (3 males and 2 females, mean age 33.8 ± 13.2 years, range 18–53 years), without known comorbidities.

Tissues were homogenized with an Ultraturax and incubated with 800 ul of Trizol reagent (TRIzol Life Technologies, Carlsbad, CA, USA) for 5 min at RT. RNA extraction with Trizol was performed following manufacturer instructions. RNA quality and concentration were measured by using an ND-1000 spectrophotometer (NanoDrop, Thermo Fisher Scientific, Wilmington, DE, USA). Reverse transcription assay was performed using 2.0 μg of starting total RNA quantity per 25 μL of mix, following the manufacturer's protocol (High capacity cDNA Archive kit, Life Technologies). The cDNA was stored at −20°C until RT-PCR was performed. RT-PCR was carried out following MasterMix TaqMan Protocol (TaqMan Univ PCR MasterMix, Life Technologies). Four μL of neat cDNA was amplified using specific probes for Nestin (NC_000001.10) and GUSB (NM_000181.3) in the RT-PCR mix (TaqMan Gene Expression Assay, Life Technologies, respective ID assay: Hs04187831_g1, Hs00939627_m1). Reactions were run on ABI PRISM 7900HT Sequence Detection System (Life Technologies). Cycling conditions were as

Table 2: Summary of the baseline clinical characteristics of the 73 patients.

	Number of patients	Percentage
Stroke	11	15.1%
Transient ischemic attack	18	24.6%
Hypertension	65	89.0%
Dyslipidemia	51	69.9%
Diabetes	20	27.4%
Smoke	6	8.5%
Chronic ischemic cardiopathy	25	34.2%
Chronic obstructive pulmonary Disease	4	5.5%
Chronic renal failure	4	5.5%
Acetylsalicylic acid use	64	87.7%
Statins use	42	57.5%

follows: 10 min at 95°C, 50 cycles at 95°C for 15 s, and 60°C for 60 sec. Each assay was carried out in triplicate and the transcription level was normalized using GUSB as a reference gene.

2.5. Statistical Analysis. All statistical analyses were carried out with SPSS software for Windows, version 20. All continuous variables are expressed as means, standard deviations, and ranges; all categorical variables (both nominal and ordinal) are expressed as number of cases and percentages. The Spearman test, the chi-square test, the Mann-Whitney U test, and the Kruskal-Wallis test were used when appropriate. The mRNA expression values for atheromatous type V and type VI plaques are presented as fold expression in relation to healthy arteries; the actual values were calculated using the $2^{-\Delta\Delta CT}$ equation, where $\Delta\Delta CT$ = [CT Target − CT GUSB] (atheromatous sample V or VI) − [CT Target − CT GUSB] (healthy sample). RT-PCR data were analyzed assuming the null hypothesis that the CT differences between target and reference genes will be the same in type V tissue versus type VI tissue. If the null hypothesis is not rejected, then the $\Delta\Delta CT$ would not be significantly different from 0. Analyses of differences between the three groups (healthy, class V, and class VI plaques) were performed with one-way ANOVA test, followed by Tukey's test. All the P values are derived from testing the null hypothesis that $\Delta\Delta CT$ are equal to 0 (at $P = 0.05$). SEM, SD, and the confidence interval (CI) of $2^{-(\Delta\Delta CT)}$ are all derived from the SEM, SD, and CI of $\Delta\Delta CT$ as explained by Yuan et al. [13].

3. Results

3.1. Patients and Histopathological Analysis. Seventy-three patients were finally enrolled, 53 (72.6%) males and 20 (27.4%) females, with a mean age at the time of endarterectomy of 70.8 ± 8.7 years (range 42–86 years). The clinical characteristics of the patients, including ongoing therapy, are summarized in Table 2. Notably, 29 (39.7%) plaques were symptomatic, since 11 (15.1%) patients had a stroke as clinical presentation and 18 (24.6%) had a transient ischemic attack (TIA).

At histopathological analysis, mean maximum cap size was 1132.8 ± 485.6 μm (range 120–2500 μm) and mean minimum cap size was 284.3 ± 199.7 μm (range 40–1125 μm); the lipid core was not evident in 8 (11.0%) cases, 1/4 in 16 (21.9%), 2/4 in 18 (24.7%), 3/4 in 23 (31.4%), and 4/4 in 8 (11.0%); the inflammatory infiltrate was mild/focal or absent in 14 (19.2%) cases, moderate in 20 (27.4%) cases, and severe/diffuse in 39 (53.4%) cases. Fifty-two (71.2%) plaques were classified as AHA type VI [10]: the most common complication observed was intraplaque hemorrhage, present in 41 cases, followed by endothelial erosion in 22 cases and thrombosis in 4 cases. Eight (11.0%) further noncomplicated plaques were classified as type VII due to the prevalently calcified core in 8 (11.0%) cases, while the remaining 13 (17.8%) cases were classified as type VIII (prevalently fibrotic core) or type V (fibroatheroma) [10].

Intraplaque calcifications were graded 0 in 11 (15.1%) cases, 1+ in 21 (28.8%), 2+ in 20 (27.4%), 3+ in 16 (21.9%), and 4+ in 5 (6.8%). According to this semiquantitative assessment of the calcification extent, low-grade calcifications (up to 2+) were recorded in 52 (71.2%) plaques, and high-grade calcification (3+ and 4+) was recorded in 21 (28.8%) plaques (Figure 1).

Finally, according to the occurrence of intraplaque complications and/or calcifications, our cases were sorted in noncalcified complicated plaques (type VI-nc, $N = 39$), calcified and complicated plaques (type VI-c $N = 13$), calcified noncomplicated plaques (type VII, $N = 8$), and noncalcified noncomplicated plaques (types V–VIII, $N = 13$). No correlations were found between plaque morphological criteria used in the present study (i.e., calcifications and histological complications) and the occurrence of chronic ischemic cardiopathy, chronic obstructive bronchopneumonia, chronic renal failure, smoke, diabetes, hypertension, dyslipidemia, or therapy with acetylsalicylic acid or statins (data not shown, chi-square test).

3.2. Nestin-Positive Neoangiogenesis. Two cases had no appreciable intraplaque neoangiogenesis after IHC for CD34. In the remaining 71 cases, the mean density of positivity for CD34 was 10.1 ± 3.9 structures/field (range 3.5–22.1/field). The mean density of positivity for Nestin, evaluated in the same ROI, was 6.8 ± 3.7 structures/field (range 1.4–18.5/field). The mean Nestin/CD34 ratio was 0.7 ± 0.2, which means that 70% of the CD34-positive neovessels examined coexpressed Nestin. This result is in line with what is previously described [9].

The total amount of neoangiogenesis, expressed as CD34-positive vessels, was not significantly different between type VI plaques and uncomplicated plaques ($P = 0.111$, Mann-Whitney U test), while the density of Nestin-positive neovessels was significantly higher in type VI ($P = 0.015$, Table 3).

The calcified plaques (including complicated and uncomplicated) showed overall less neoangiogenesis, measured with both CD34 and Nestin, than noncalcified plaques ($P < 0.001$, Table 3; Figure 2).

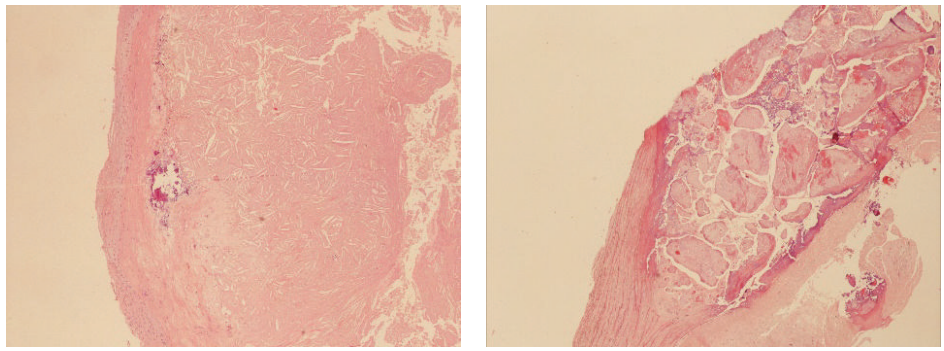

(a) (b)

Figure 1: Details of two cases of carotid plaque with low-grade calcification (a) and high-grade calcification (b), respectively. Haematoxylin-eosin stain, magnification 10x.

Table 3: Densities of positivity of intraplaque neovessels for CD34 and Nestin in our series of plaques, sorted by calcification and by the occurrence of complications.

	Noncalcified plaques	Calcified plaques	Complicated plaques	Uncomplicated plaques
CD34 density	11.19 ± 3.84	7.52 ± 3.09	10.68 ± 3.79	8.99 ± 4.13
Mann-Whitney	$P < 0.001$		$P = 0.111$	
Nestin density	7.69 ± 3.77	4.59 ± 2.31	7.45 ± 3.71	5.31 ± 3.09
Mann-Whitney	$P < 0.001$		$P = 0.015$	

At RT-PCR, the total mean extracted mRNA from healthy tissue and type V and type VI plaques was 8764 ng, 5069.4 ng, and 2172 ng, respectively. The mean CT values of endogenous control GUSB were 36.28 ± 0.21 in healthy tissue, 31.36 ± 0.32 in type V plaques, and 34.20 ± 0.22 in type VI plaques. Mean CT for tested gene Nestin were 33.04 ± 0.06 in healthy tissue, 32.37 ± 0.12 in type V plaques, and 34.21 ± 0.30 in type VI plaques. ΔΔCT Nestin was significantly different from 0 ($P = 0.0001$); thus the null hypothesis was rejected, which indicated a change in Nestin gene expression among healthy, type V and type VI plaques. In type V and type VI plaques, the mean ΔΔCT Nestin was, respectively, 4.25 and 3.25; this corresponds to $2^{-(\Delta\Delta CT)}$ of 0.05 for Nestin gene expression in type V plaques and 0.11 in type VI plaques. The type VI plaques showed a 2-fold expression increase for Nestin gene compared to type V plaques, as a confirmation of the IHC results (Figure 3).

These data confirm that Nestin-positive neoangiogenesis, studied both on the protein (IHC) and the mRNA level (RT-PCR), plays a key role in the development of intraplaque complications and that plaques with massive calcifications generally have a minor density of neoangiogenesis compared to other plaques.

3.3. Intraplaque Calcifications and Clinical Stability. Despite the differences in neoangiogenesis, the incidence of histological complications did not differ significantly between calcified and noncalcified plaques ($P = 0.167$, chi-square test; Figure 4).

As for the clinical presentation, unsurprisingly, 25 out of 29 (86.2%) symptomatic patients (i.e., with stroke or TIA) had a type VI plaque, versus 27 out of 44 (61.4%) asymptomatic patients ($P = 0.026$, chi-square test). Interestingly, among the 21 patients with calcified plaques, only 4 (19.0%) had symptoms at the onset, regardless of the occurrence of histological complications; conversely 25 out of 52 (48.1%) patients with noncalcified plaques were symptomatic ($P = 0.019$, chi-square test).

The patients' gender was correlated with the plaque morphology and instability as well; first of all only 3 (15.0%) of the 20 female patients in our study were symptomatic versus 26 (49.1%) out of 53 males ($P = 0.007$, chi-square test). All three symptomatic female patients had a type VI-nc atheromatous lesion. Notably, a higher incidence of calcified plaques was observed in female patients ($P = 0.017$): 10 (50.0%) females had calcified plaques (5 type VII and 5 type VI-c) versus only 11 (20.8%) males (3 type VII and 8 type VI-c).

4. Discussion

The severity and extent of calcification reflect the atherosclerotic plaque burden and strongly predict cardiovascular morbidity and mortality [14, 15]; in a relatively recent study, no patients were found to have calcifications confined only to the coronary or carotid beds [16]. The extent of calcification is associated with a worse prognosis, albeit the real impact of calcifications within a specific vascular pathological district remains unclear [17]. For example, in the coronary vessels small calcium depositions increase the probability of atherosclerotic plaque rupture, especially on their edges, while massive calcification seems to be associated with a

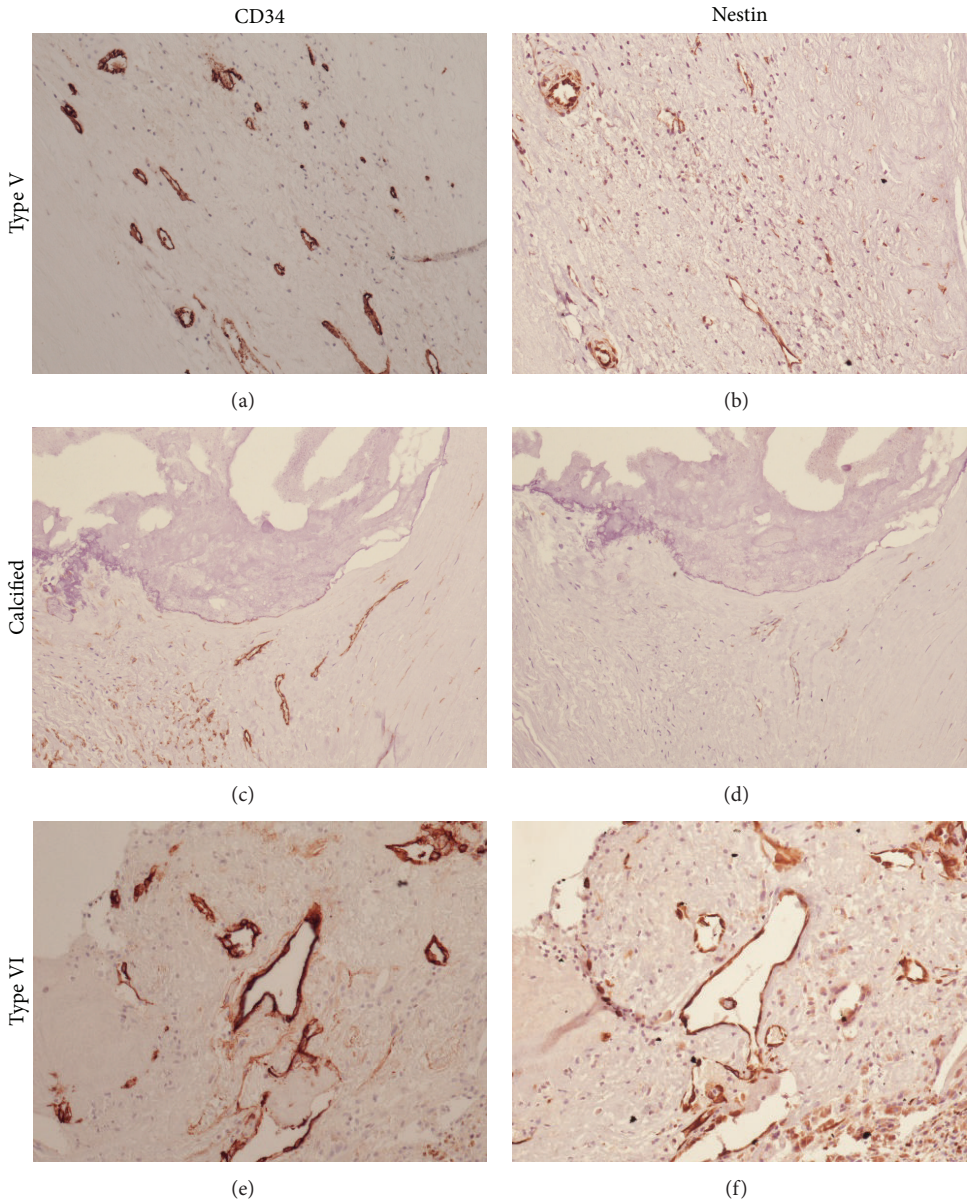

Figure 2: Immunohistochemical staining for CD34 (a), (c), and (e) and Nestin (b), (d), and (f) in an uncomplicated noncalcified plaque (a) and (b), a calcified plaque (c) and (d), and a complicated noncalcified plaque (e) and (f). Neoangiogenesis in uncomplicated plaques is generally Nestin-negative. The overall neoangiogenesis in calcified plaques (complicated or not) is generally lower (both CD34 and Nestin) than in complicated plaques. Magnification 20x.

decreased risk [17, 18]. Anyway, vascular calcification is considered a worsening factor, probably due to its coexistence with the general risk factors; a study by Iribarren et al. [19] found that aortic arch calcification was associated with coronary heart disease risk both in men and in women. Thus aortic arch calcification may reflect the general burden of disease or be a marker of more aggressive disease. At any chance, the clinical impact of a plaque in which both calcification and histological complications coexist is far from being clarified.

Our aims were to evaluate the relationship between the intraplaque neoangiogenesis, the main histopathological characteristics (histological complications and calcifications), and the clinical plaque instability. For these purposes, neoangiogenesis was evaluated and semiquantified by CD34 and Nestin IHC, followed by RT-PCR. The majority of tissue obtained from endarterectomy was used for the routine histological diagnosis of surgical specimens. The remaining tissue had to be fully processed for RT-PCR and Western blot analysis was not included in our protocol. However, in our experience [8, 9] we observed that Nestin staining in IHC is very reliable, allowing us to evaluate its cell location and its expression at a protein level as well, without the need of the more sensible immunoblot techniques. The correlation

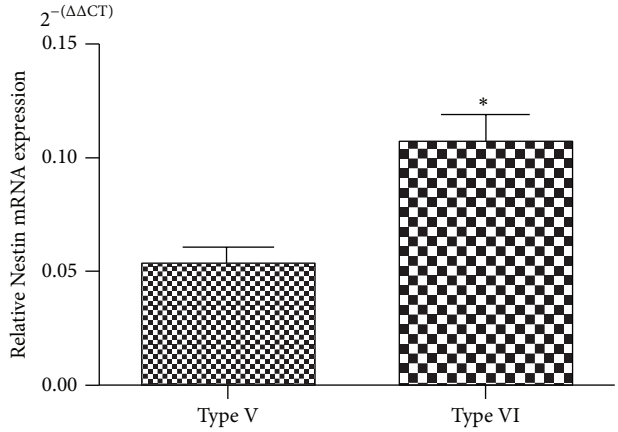

Figure 3: Difference in Nestin mRNA expression between type V (uncomplicated) and type VI (complicated) plaques ($^{*}P < 0.001$).

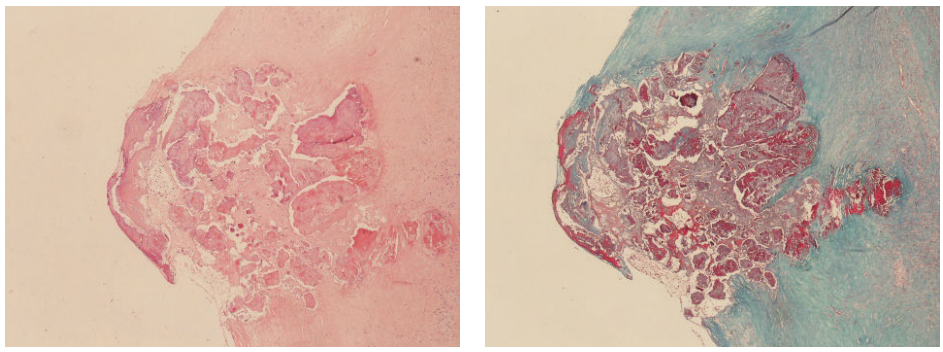

(a) (b)

Figure 4: An example of calcified plaque with histopathological complications (i.e., hemorrhage) with haematoxylin-eosin stain (a). The trichrome stain highlights the hemorrhagic foci (in red (b)). Magnification 10x.

between IHC and RT-PCR confirmed that there is a direct relationship between Nestin protein and mRNA.

According to our data calcified plaques show less inflammatory infiltrate, a smaller lipid core, and less neoangiogenesis than other plaques, but with the same incidence of hemorrhage, thrombosis, and surface defects, which define the plaque as histologically complicated [10]. Yet, interestingly, in these calcified plaques complications are not correlated with clinical plaque instability (evaluated as symptomatology); indeed, the incidence of TIA/stroke in patients with calcified plaques was sensibly lower than patients with noncalcified plaques, despite the same incidence of intraplaque complications. This is noteworthy, since at least in the carotid district the presence of calcifications seems to imply a sort of clinical "protection" to complications, making the histological complications play second fiddle. For these reasons, in our opinion, these plaques can be classified among the type VII plaques, instead of type VI, at least on clinical grounds. Alternatively, they can be classified as type VI, but the extension of the calcifications should be stated in the pathological report, to highlight their protective nature.

The reason why in the massively calcified plaques the neoangiogenesis and the histological complications do not affect symptomatology remains unclear, but it is possible that the hemorrhages and erosions found in these plaques might have a different pathogenesis. For example, it is possible that they can be due directly by the mechanical stresses of the calcified mass and not by immature neoangiogenesis and endothelial damage. Another possible explanation is that the "calcified type VI" plaques can represent an early stage of type VII plaques, in which the regressive process is more recent, and the complications have not disappeared yet (Figure 5).

The last result that emerged from our data is that 50% of the female patients had calcified plaques, showing a significantly lower incidence of symptoms and type VI plaques than the male patients. Ten years ago, Allison et al. have found 53% and 30% prevalence of "zero calcification" in female and male patients, respectively, before age of 50; after that age the prevalence of a diffuse vessel calcification increases, in a linear fashion in males and exponentially in females [16]. Actually, female sex hormones play an important role in bone tissue metabolism, increasing bone density and inhibiting osteoclast activity [20–22]. Nevertheless, it should be kept in mind that most women in our series were postmenopausal and their age at the moment of surgery did not differ from males (70.2 ± 9.5 versus 71.0 ± 8.5 years), so the question

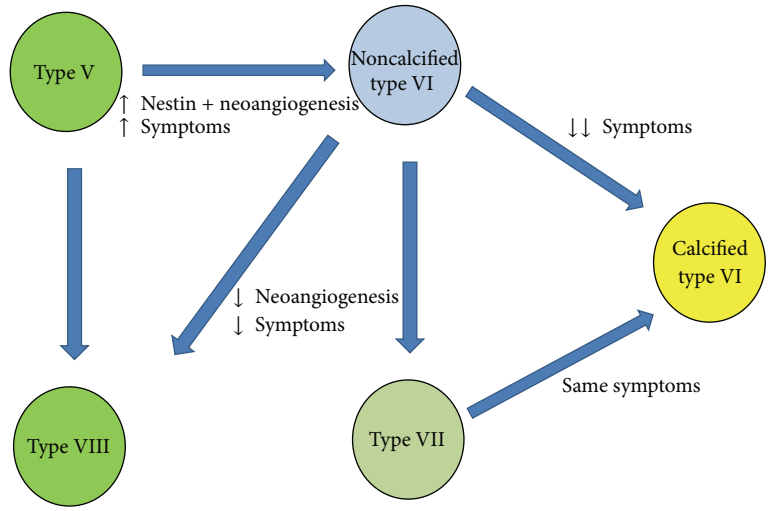

Figure 5: Flowchart illustrating the hypothetical plaque progression in relation to the Nestin-positive neoangiogenesis and calcification features. According to AHA classification [10], type V plaque is the uncomplicated fibroatheroma, type VI is the complicated plaque, type VII is the calcified plaque, and type VIII is the fibrotic plaque.

whether the postmenopausal hormone therapy might play a role in the pathophysiology of the atherosclerosis is still open.

Study Limitations. A limitation of our study is represented by heterogeneity in the sample size of each plaque group (e.g., 8 cases of type VII plaques were available). However, this is a monocentric perspective study, and our series reflects the incidence of the different plaque types in the general population. Moreover, the patients submitted to surgery generally have advanced plaques, and complicated type VI plaques are the most represented. Furthermore, there is a discrepancy between the age of the patients with plaques and the controls, due to obvious differences in the populations of multiorgan donors and atheromatous patients.

5. Conclusions

In conclusion, this study confirms that the Nestin+/WT1− phenotype characterizes the plaques with morphological features of instability, regardless of the actual amount of the neoangiogenesis (expressed as CD34-positive vessels). The plaques with massive calcifications show the same incidence of histological complications but with a lower incidence of neurological symptoms. Female patients show a much higher incidence of noncomplicated or calcified plaques, receiving *de facto* a sort of protection compared to male patients.

A possible indication emerging from these findings could be a comparison between the plaque dynamic imaging and the histological assessment of calcification, to evaluate the possibility of a presurgical risk stratification of patients, based on their sex, risk factors, and intraplaque calcification. The presurgical identification of those patients at major risk of developing stroke or brain lesions is likely to make the priority for endarterectomy more rational.

Conflict of Interests

The authors declare that there is no conflict of interests regarding the publication of this paper.

References

[1] I. J. Kullo, W. D. Edwards, and R. S. Schwartz, "Vulnerable plaque: pathobiology and clinical implications," *Annals of Internal Medicine*, vol. 129, no. 12, pp. 1050–1060, 1998.

[2] L. Hermus, I. F. J. Tielliu, B. M. de Wallis Vries, J. J. A. M. van den Dungen, and C. J. Zeebregts, "Imaging the vulnerable carotid artery plaque," *Acta Chirurgica Belgica*, vol. 110, no. 2, pp. 159–164, 2010.

[3] R. Mofidi, T. B. Crotty, P. McCarthy, S. J. Sheehan, D. Mehigan, and T. V. Keaveny, "Association between plaque instability, angiogenesis and symptomatic carotid occlusive disease," *British Journal of Surgery*, vol. 88, no. 7, pp. 945–950, 2001.

[4] G. L. Faggioli, R. Pini, R. Mauro et al., "Identification of carotid 'Vulnerable Plaque' by contrast-enhanced ultrasonography: correlation with plaque histology, symptoms and cerebral computed tomography," *European Journal of Vascular and Endovascular Surgery*, vol. 41, no. 2, pp. 238–248, 2011.

[5] P. R. Moreno, K.-R. Purushothaman, M. Sirol, A. P. Levy, and V. Fuster, "Neovascularization in human atherosclerosis," *Circulation*, vol. 113, no. 18, pp. 2245–2252, 2006.

[6] J. C. Sluimer, F. D. Kolodgie, A. P. J. J. Bijnens et al., "Thin-walled microvessels in human coronary atherosclerotic plaques show incomplete endothelial junctions relevance of compromised structural integrity for intraplaque microvascular leakage," *Journal of the American College of Cardiology*, vol. 53, no. 17, pp. 1517–1527, 2009.

[7] M. J. McCarthy, I. M. Loftus, M. M. Thompson et al., "Angiogenesis and the atherosclerotic carotid plaque: an association between symptomatology and plaque morphology," *Journal of Vascular Surgery*, vol. 30, no. 2, pp. 261–268, 1999.

[8] F. Vasuri, S. Fittipaldi, M. Buzzi et al., "Nestin and WT1 expression in small-sized vasa vasorum from human normal arteries," *Histology & Histopathology*, vol. 27, no. 9, pp. 1195–1202, 2012.

[9] S. Fittipaldi, F. Vasuri, A. Degiovanni et al., "Nestin and WT1 expression in atheromatous plaque neovessels: association with vulnerability," *Histology and Histopathology*, vol. 29, pp. 1565–1573, 2014.

[10] H. C. Stary, "Natural history and histological classification of atherosclerotic lesions an update," *Arteriosclerosis, Thrombosis, and Vascular Biology*, vol. 20, no. 5, pp. 1177–1178, 2000.

[11] R. W. Hobson II, W. C. Mackey, E. Ascher et al., "Management of atherosclerotic carotid artery disease: clinical practice guidelines of the Society for Vascular Surgery," *Journal of Vascular Surgery*, vol. 48, no. 2, pp. 480–486, 2008.

[12] C. D. Liapis, P. R. Bell, D. Mikhailidis et al., "ESVS guidelines. Invasive treatment for carotid stenosis: indications, techniques," *European Journal of Vascular and Endovascular Surgery*, vol. 37, no. 4, supplement, pp. 1–19, 2009.

[13] J. S. Yuan, A. Reed, F. Chen, and C. N. Stewart Jr., "Statistical analysis of real-time PCR data," *BMC Bioinformatics*, vol. 7, article 85, 2006.

[14] G. Sangiorgi, J. A. Rumberger, A. Severson et al., "Arterial calcification and not lumen stenosis is highly correlated with atherosclerotic plaque burden in humans: a histologic study of 723 coronary artery segments using nondecalcifying methodology," *Journal of the American College of Cardiology*, vol. 31, no. 1, pp. 126–133, 1998.

[15] R. Vliegenthart, M. Oudkerk, A. Hofman et al., "Coronary calcification improves cardiovascular risk prediction in the elderly," *Circulation*, vol. 112, no. 4, pp. 572–577, 2005.

[16] M. A. Allison, M. H. Criqui, and C. M. Wright, "Patterns and risk factors for systemic calcified atherosclerosis," *Arteriosclerosis, Thrombosis, and Vascular Biology*, vol. 24, no. 2, pp. 331–336, 2004.

[17] H. Huang, R. Virmani, H. Younis, A. P. Burke, R. D. Kamm, and R. T. Lee, "The impact of calcification on the biomechanical stability of atherosclerotic plaques," *Circulation*, vol. 103, no. 8, pp. 1051–1056, 2001.

[18] Y. Vengrenyuk, S. Carlier, S. Xanthos et al., "A hypothesis for vulnerable plaque rupture due to stress-induced debonding around cellular microcalcifications in thin fibrous caps," *Proceedings of the National Academy of Sciences of the United States of America*, vol. 103, no. 40, pp. 14678–14683, 2006.

[19] C. Iribarren, S. Sidney, B. Sternfeld, and W. S. Browner, "Calcification of the aortic arch: risk factors and association with coronary heart disease, stroke, and peripheral vascular disease," *The Journal of the American Medical Association*, vol. 283, no. 21, pp. 2810–2815, 2000.

[20] R. H. Mackey, L. H. Kuller, K. Sutton-Tyrrell, R. W. Evans, R. Holubkov, and K. A. Matthews, "Hormone therapy, lipoprotein subclasses, and coronary calcification: the healthy women study," *Archives of Internal Medicine*, vol. 165, no. 5, pp. 510–515, 2005.

[21] J. E. Manson, M. A. Allison, J. E. Rossouw et al., "Estrogen therapy and coronary-artery calcification," *The New England Journal of Medicine*, vol. 356, no. 25, pp. 2591–2602, 2007.

[22] G.-H. Jeon, S. H. Kim, S.-C. Yun, H. D. Chae, C.-H. Kim, and B. M. Kang, "Association between serum estradiol level and coronary artery calcification in postmenopausal women," *Menopause*, vol. 17, no. 5, pp. 902–907, 2010.

Hindawi Publishing Corporation
BioMed Research International
Volume 2014, Article ID 453972, 10 pages
http://dx.doi.org/10.1155/2014/453972

Review Article

Anticancer Activities of Citrus Peel Polymethoxyflavones Related to Angiogenesis and Others

Liwen Wang,[1] Jinhan Wang,[1,2] Lianying Fang,[1] Zuliang Zheng,[1] Dexian Zhi,[1] Suying Wang,[1] Shiming Li,[3,4] Chi-Tang Ho,[4] and Hui Zhao[1,5]

[1] *Tianjin Key Laboratory of Food and Biotechnology, School of Biotechnology and Food Science, Tianjin University of Commerce, Tianjin 300134, China*
[2] *Institute of Radiation Medicine, Chinese Academy of Medical Sciences and Peking Union Medical College, Tianjin 300192, China*
[3] *Hubei Key Laboratory of Economic Forest Germplasm Improvement and Resources Comprehensive Utilization, Huanggang Normal University, Huanggang, Hubei 438000, China*
[4] *Department of Food Science, Rutgers University, New Brunswick, NJ 08901-8502, USA*
[5] *Department of Hematology and Translation Medicine Centre, Hebei Union University Affiliated Hospital, Tangshan, Hebei 063000, China*

Correspondence should be addressed to Hui Zhao; zhaohui@tjcu.edu.cn

Received 5 July 2014; Accepted 28 July 2014; Published 28 August 2014

Academic Editor: Zongjin Li

Citrus is a kind of common fruit and contains multiple beneficial nutrients for human beings. Flavonoids, as a class of plant secondary metabolites, exist in citrus fruits abundantly. Due to their broad range of pharmacological properties, citrus flavonoids have gained increased attention. Accumulative in vitro and in vivo studies indicate protective effects of polymethoxyflavones (PMFs) against the occurrence of cancer. PMFs inhibit carcinogenesis by mechanisms like blocking the metastasis cascade, inhibition of cancer cell mobility in circulatory systems, proapoptosis, and antiangiogenesis. This review systematically summarized anticarcinogenic effect of citrus flavonoids in cancer therapy, together with the underlying important molecular mechanisms, in purpose of further exploring more effective use of citrus peel flavonoids.

1. Introduction

In our daily diet, the average intake of flavonoids of every day ranges from 150 mg to 300 mg [1]. As the primary source, flavonoids from citrus fruit or juice take up to 10%, of which juices and fruits offer 8 mg and 3 mg, respectively [2]. The main components in citrus possess phenols, amino acids, essential oils, pectin, carotenoids, flavonoids, and vitamin C. Although flavonoids are generally considered to be non-nutritive agents, interest in flavonoids has arisen because of their potential role in the prevention of major chronic diseases. Flavonoids are polyphenolic compounds and include a phenyl benzopyrone structure, representing as two benzene rings (C6) joined by a linear three-carbon chain (C3), with a carbonyl group at the C_4 position. The citrus flavonoids include a class of glycosides, namely, hesperidin and naringin, and another class of O-methylated aglycones of flavones such as nobiletin and tangeretin, which are relatively common two polymethoxylated flavones (PMFs) [3]. PMFs exist almost ubiquitously in citrus plants. Six PMFs and three major 5-demethoxyflavones can be extracted from a variety of citrus peels. The wide biochemical functions of flavonoids in orange peel have been studied extensively recently. They increased serum antioxidant capacity against lipid peroxidation [4] and reduced the elderly oxidative stress. These compounds also performed beneficial effects of anti-inflammation, antitumor [5, 6], and antiatherosclerosis [7]. Meanwhile, they serve as supplementary of drug chemotherapy [8], diabetes health food [9], and neuroprotective drug [10].

In recent years, epidemiological studies have shown that there is a connection that flavonoid intake may reduce the risk of developing colon cancer [11, 12]. Moreover, it may prevent

men against Parkinson's disease (PD) after identifying 805 participants (438 men and 367 women) who developed PD during 20–22 years of follow-up [13], help women get out of the risk of gastric cancer and breast cancer with 10% reduction in risk of breast cancer associated with high intake of citrus fruits [14], and reduce the possibility of ischemic stroke during 14 years of follow-up, confirmed with 1803 incident strokes. After adjusting for potential confounders, women in the highest compared with the lowest quintile of flavanone intake had a relative risk of ischemic stroke of 0.81 [15].

Cancer is the life threatening and dreadful disease characterized by the abnormal proliferation of cells that invade the adjacent tissues and cause the destruction of these tissues. It is the second leading cause of death all over the world. More than six million deaths each year occurring in the world are due to cancer. Several lines of evidence indicated that tumorigenesis in humans is a multistep process and these steps reflect genetic alterations that drive the progressive transformation of normal human cells into highly malignant derivatives [16]. Conventional treatment chemotherapy could cause adverse and toxic side effects on normal cells while curing cancer and therefore fails to control the disease. The alternative solution for the harmful effects of synthetic agents is the use of natural plants, which provide outstanding contribution to modern therapeutics [17]. It has been shown by clinical studies and phytochemical investigation currently that many herbs exhibit antitumor potential. In this review, we center on the latest research progress on the antitumor activities of citrus peel compounds.

2. Anticarcinogenic Properties

In the tumor microenvironment, from cancer cells initiation to promotion and eventually progression, compelling evidence indicates the potential activities of flavonoids in citrus peel cover inhibiting oncogenesis, proliferation, neovascularization, and metastasis and inducing apoptosis. Figure 1 schematizes the main anticarcinogenic pathways of citrus peels flavonoids and different bioactivity aspects of specific compounds stated in this review are summarized in Table 1.

2.1. Cell Cycle Arrest. Cell cycle abnormalities are closely associated with cancer, and citrus peel flavonoids substantially influence on cell cycle arrest. Cell cycle is an important regulatory mechanism of cell growth, development, and differentiation. In mammals, the cell cycle comprises the G1, S, G2, and M phases. Cell cycle checkpoints keep the maintenance of genomic integrity by inhibiting damaged or incomplete DNA. G2/M checkpoint ensures that the cells do not initiate mitosis before repairing damaged DNA after replication. The cell cycle progression depends on a cascade of enzymes by sequential activation and inactivation of cyclin, cyclin-dependent kinases (CDKs), and cyclin-dependent kinase inhibitors (CDKIs) [18]. Cdc2 interacts with cyclin B1 and forms a cdc2-cyclin complex. The G2/M transition is regulated by the sequential activation and inactivation of the cdc2/cyclin B complex [19]. Non-small-cell lung cancer (NSCLC) A549 cells arrest and apoptosis can be induced by flavonoids extracted from Korean *Citrus aurantium* L. [20]. Downregulation of cdc2, cdc25c, and cyclin B1 and the upregulation of p21 resulted in G2/M arrest in A549 cell line. Actually, the mechanisms of parts of flavonoids components are being further explained. As one of the most prevalent flavonoids extracted from orange, hesperetin repressed CDK2, CDK4, and cyclin D and simultaneously enhanced p21 and p27 expression to block cell cycle in G1 phase [21]. It is also reported that hesperetin and naringenin exhibited the same results in cervical cancer cell SiHa and liver cancer cell HepG2, respectively [22, 23]. In human breast and colon cancer cells, both tangeretin and nobiletin inhibited the proliferation and led to accumulation of cells in the G1/S cell cycle compartment and did not involve induction of cell death or apoptosis. This finding may provide advantageous theory basis in treating tumors as it would restrict proliferation in a manner less likely to induce cytotoxicity and death in normal tissues [24]. More recently, the study on derivatives of citrus peel flavonoids causes widely concern as well. For instance, in all three NSCLC cells A549, H460, and H1299, 5-demethyltangeretin mediated G2/M cell cycle arrest by upregulating p53 and $p21^{Cip1/Waf1}$ and downregulating cdc2 and cyclin B1 [25]. Among three 5-hydroxy polymethoxyflavones (5OH-PMFs), 5-hydroxy-3,6,7,8,3′,4′-hexamethoxyflavone (5HHMF), 5-hydroxy-6,7,8,3′,4′-pentamethoxyflavone (5HPMF), and 5-hydroxy-6,7,8,3′,4′-pentamethoxyflavone (5HTMF), the data showed that the 5HTMF-induced G0/G1 arrest was the most responsive to the change of the p21 and p53 status of the colon cancer cells, indicating the essential role of the 4′-methoxyl group on B ring of 5HTMF in inducing cell cycle arrest [26]. The chemical structures of flavonoids in citrus peel can be found in Figure 2. Results above inevitably support the idea that specific structural elements of the flavonoids are the key determinants of pharmacological activities.

2.2. Suppression of Proliferation and Proapoptosis. One of the most basic features of cancer cells is their ability to proliferate chronically. Apart from blocking cell cycle, flavonoids in citrus peel can also inhibit cell proliferation and promote apoptosis, especially in triple-negative (ER-/PR-/HER2-) breast cancer (TNBC). PMFs triggered influx of Ca^{2+} and mobilization of intracellular Ca^{2+} store, accompanied by activation of calpain and caspase-12 [27]. There are further researches on mechanisms of these functions. Crude methanol extracts of the peels of *Citrus aurantium* L. induced caspase-dependent apoptosis through Akt pathway by inhibiting expression of XIAP and Bcl-2 which are antiapoptotic proteins, providing the fact that they have anticarcinogenic activity on human leukemia cells U937 [28]. In another leukemia cell line NALM-6, hesperidin, as the glycoside of hesperetin, promoted apoptosis via conducting the expression of p53 and peroxisome proliferator-activated receptor gamma (PPAR γ) and suppressing the activation of NF-κB [29]. Tangeretin-induced caspase-3 activation and elevated surface phosphatidylserine exposure demonstrated tangeretin apoptosis-inducing activity in LoVo/Dx cells, which might also enhance

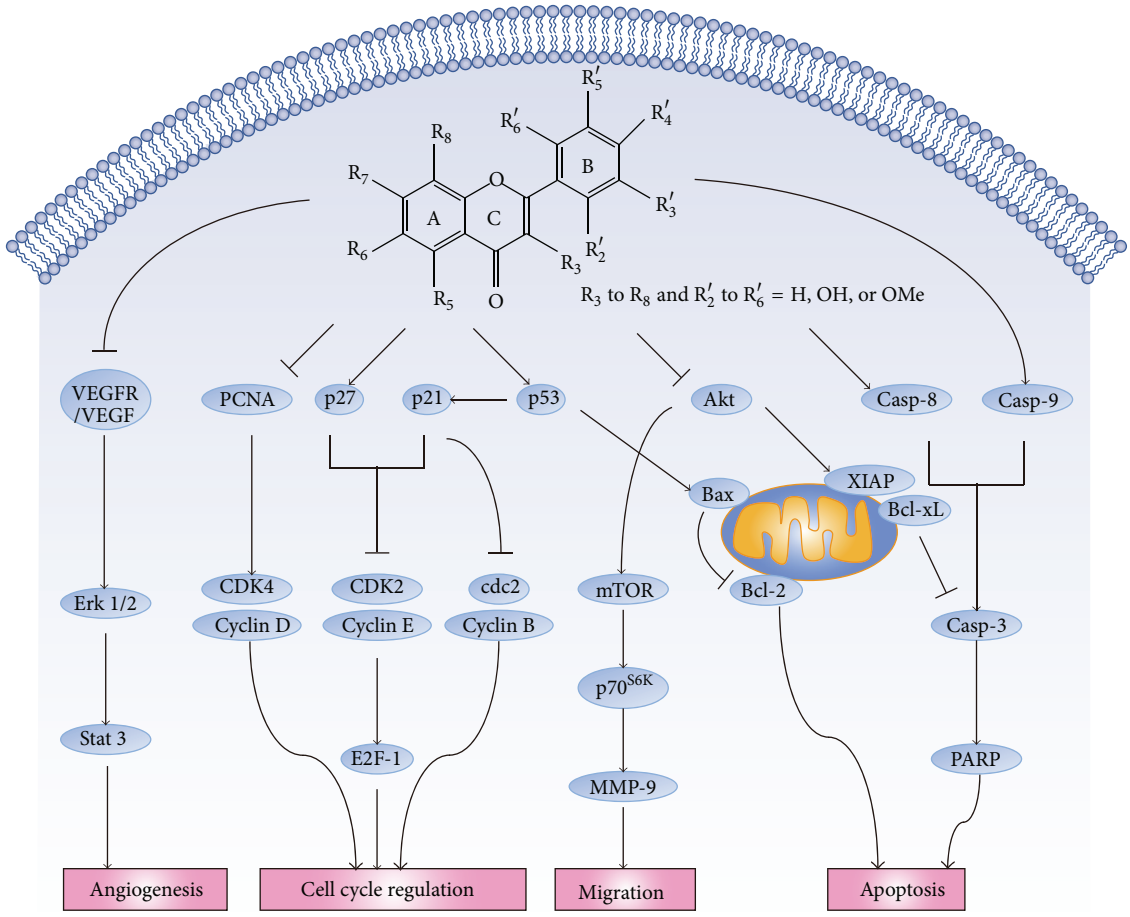

Figure 1: Polymethoxyflavones exert beneficial effects through antigrowth, antiangiogenesis and cell cycle arrest commands or mediate signals to live or die by apoptosis. At one level, this depiction is simplistic, as different cancer cells are exposed to a specific complex microenvironment, each of these pathways regulated by PMFs is connected with signals originating from other cells in the tumor microenvironment. Schematic representation of the main molecular mechanisms of flavonoids in citrus peel on anticancer.

multidrug-resistance [30]. In HCT116 human colon cancer cells, 5-hydroxy polymethoxyflavones (5OH-PMFs), especially 5HHMF and 5HTMF, induce cellular apoptosis in human colon cancer cells by p53- and Bax-dependent mechanisms [26]. Noteworthy, by looking for relationships between chemical profiles and cell viability profiles, cytotoxic effects as indicated by a decrease of IC_{50} values with increasing concentration of OH-PMFs were observed in different orange peel extracts [31]. Subsequent data showed that when MCF-7 breast cancer cells were treated with PMF and hydroxylated PMF separately, effective concentrations of hydroxylated PMFs in inhibiting growth, inducing apoptosis, and increasing intracellular Ca^{2+} were lower than those of nonhydroxylated PMFs [32]. These already available results may offer a conclusion that OH-PMFs have better potential cytotoxic effect.

In the research of mice, oral feeding of gold lotion (GL), a formulated product made from the peels of six citrus fruits, decreased the number of aberrant crypt foci (ACF) in mice colonic tissues [33]. This compound is rich in flavonoids with a total measured content of at least 450 ppm or 0.45 mg/mL; its PMFs content is as high as 106 ppm or 0.1 mg/mL. Due to its high content of flavonoids, it has also been proven to inhibit the nuclear translocation of NF-κB into the nucleus [34]. Similarly, hesperetin has potential effect on proliferation of cancer cell in vivo. For 1,2-dimethylhydrazine- (DMH-) induced colon cancer model in rats, it exerted significant inhibitory effect on proliferating cell nuclear antigen in ACF [35]. Moreover, hesperetin inhibited growth of aromatase-expressing MCF-7 tumor in ovariectomized athymic mice by reducing cyclin D1, CDK4, and Bcl-x(L), while upregulating the level of $p57^{Kip2}$ [36]. Data above provided supporting evidence that flavonoids from citrus peel could suppress carcinogenesis in vivo.

Our latest research showed that, in MCF-7 human breast cancer cells, 5-acetyl-6,7,8,4′-tetramethylnortangeretin (5-ATAN), which replaces the methyl groups of tangeretin with acetyl groups at the C5 position of tangeretin, showed more powerful abilities than its parent compound. Then, we looked for evidence of 5-ATAN on apoptosis. Translocation of apoptosis-inducing factor (AIF) and phosphorylation of H2AX are commonly used for evaluating the impact of

Table 1: Anticarcinogenic activity of citrus polymethoxyflavonoids and their derivatives.

Polymethoxyflavone	Functions	Mechanisms	References
Naringin	Cell cycle arrest	G1 cycle arrest by increasing p21 and decreasing survivin in MDA-MB-231 xenograft mice	[25]
	Anticancer metastasis	Suppressed the upregulation of metallopeptidase-9 (MMP-9) and repressed the PI3K/AKT/mTOR/p70S6K signaling pathway	[36]
Hesperetin	Cell cycle arrest	G1-phase cell cycle arrest in human breast cancer MCF-7 cells by downregulating CDK2 and CDK4 together with cyclin D and upregulating $p21^{Cip1}$ and $p27^{Kip1}$	[19]
		Induced the G2/M phase and increased expression of caspase-3, caspase-8, caspase-9, p53, Bax, and Fas death receptor and its adaptor protein Fas-associated death domain-containing protein (FADD) in human cervical cancer SiHa cells	[20]
	Suppress proliferation	Exerted significant inhibitory effect on proliferating cell nuclear antigen in ACF in 1,2-dimethylhydrazine induced colon cancer model in rats	[33]
		Inhibited growth of aromatase-expressing MCF-7 tumor in ovariectomized athymic mice by reducing cyclin D1, CDK4, and Bcl-x(L), while upregulating the level of $p57^{Kip2}$	[34]
Nobiletin	Cell cycle arrest	Blocked cell cycle progression at G1 breast cancer cell lines MDA-MB-435 and MCF-7 and human colon cancer line HT-29	[22]
	Antiangiogenesis	Inhibited angiogenic differentiation induced by VEGF and FGF by downregulation of ERK1/2 and c-JNK and activation of the caspase pathway	[42, 44]
Tangeretin	Cell cycle arrest	Blocked cell cycle progression at G1 breast cancer cell lines MDA-MB-435 and MCF-7 and human colon cancer line HT-29	[22]
	Suppress proliferation	Led to caspase-3 activation and elevated surface phosphatidylserine in human cocon LoVo/Dx cells	[28]
	Anticancer metastasis	Inhibited PGDF-BB-induced proliferation and migration of aortic smooth muscle cells by blocking AKT activation	[38]
	Scavenging of ROS	Inhibited cancer cell proliferation by SOD, CAT, GPx, and nonenzymatic antioxidants and phase II detoxification in 7,12-dimethyl benz(a)anthracene induced mammary carcinoma in rats	[45]
5-Demethyltangeretin (5DT)	Cell cycle arrest	Upregulated p53 and $p21^{Cip1/Waf1}$ and downregulated cdc-2 and cyclin B1 leading to G2/M cell cycle arrest	[23]
Sinensetin	Antiangiogenesis	Inhibited angiogenesis by inducing cell cycle arrest in the G0/G1 phase in HUVEC culture; in zebrafish embryos, it downregulated the mRNA expressions of angiogenesis genes *flt1*, *kdrl*, and *hras*	[43]
5HTMF	Suppress proliferation	Induced cellular apoptosis in human colon cancer cells by p53- and Bax-dependent mechanisms in HCT116 colon cancer cells	[24]
	Cell cycle arrest	Induced cell cycle arrest at G0/G1 phase through a p53- and $p21^{Cip1/Waf}$-dependent mechanism in HCT116 colon cancer cells	[24]
5HPMF	Suppress proliferation	Induced cellular apoptosis in human colon cancer cells by p53- and Bax-dependent mechanisms in HCT116 colon cancer cells	[24]
5HHMF	Cell cycle arrest	Induced G2/M arrest through p53- and p21-independent mechanisms in HCT116 colon cancer cells	[24]
	Suppress proliferation	Induced cellular apoptosis in human colon cancer cells by p53- and Bax-dependent mechanisms in HCT116 colon cancer cells	[24]
Naringenin	Cell cycle arrest	Partly formed an accumulation of cells in the G0/G1 and G2/M phases of the cell cycle in human hepatocellular carcinoma HepG2 cells	[21]
	Anticancer metastasis	Induced heme oxygenase-1(HO-1) expression and subsequently decreased ROS generation and VSMC activation induced by TNF-α	[37]
Hesperidin	Suppress proliferation	Promoted apoptosis via conducting the expression of p53 and PPAR γ and suppressing the activation of NF-κB in leukemia cell NALM-6	[27]
Flavonoids extracted from Korean *Citrus aurantium* L.	Cell cycle arrest	Induced non-small-cell lung cancer (NSCLC) A549 cells arrest at the G2/M checkpoint	[18]
	Suppress proliferation	Induced caspase-dependent apoptosis through AKT pathway by inhibiting expression of XIAP and Bcl-2 in human leukemia cells U937	[26]

Table 1: Continued.

Polymethoxyflavone	Functions	Mechanisms	References
Gold lotion	Suppress proliferation	In azoxymethane-induced aberrant crypt foci formation, it downregulated the protein levels of iNOS, COX-2, ornithine decarboxylase, VEGF, and matrix metallopeptidase 9 in colonic tissues of mice	[31]
	Anticancer metastasis	Downregulated MMP-2 and MMP-9 protein expression levels and reduced tumor volumes and weights in human prostate tumor xenograft mouse model	[39]
	Antiangiogenesis	Significantly suppressed the protein expression level of VEGF	[39]
		Reduced the protein levels of VEGF in AOM-induced colonic tissues	[31]

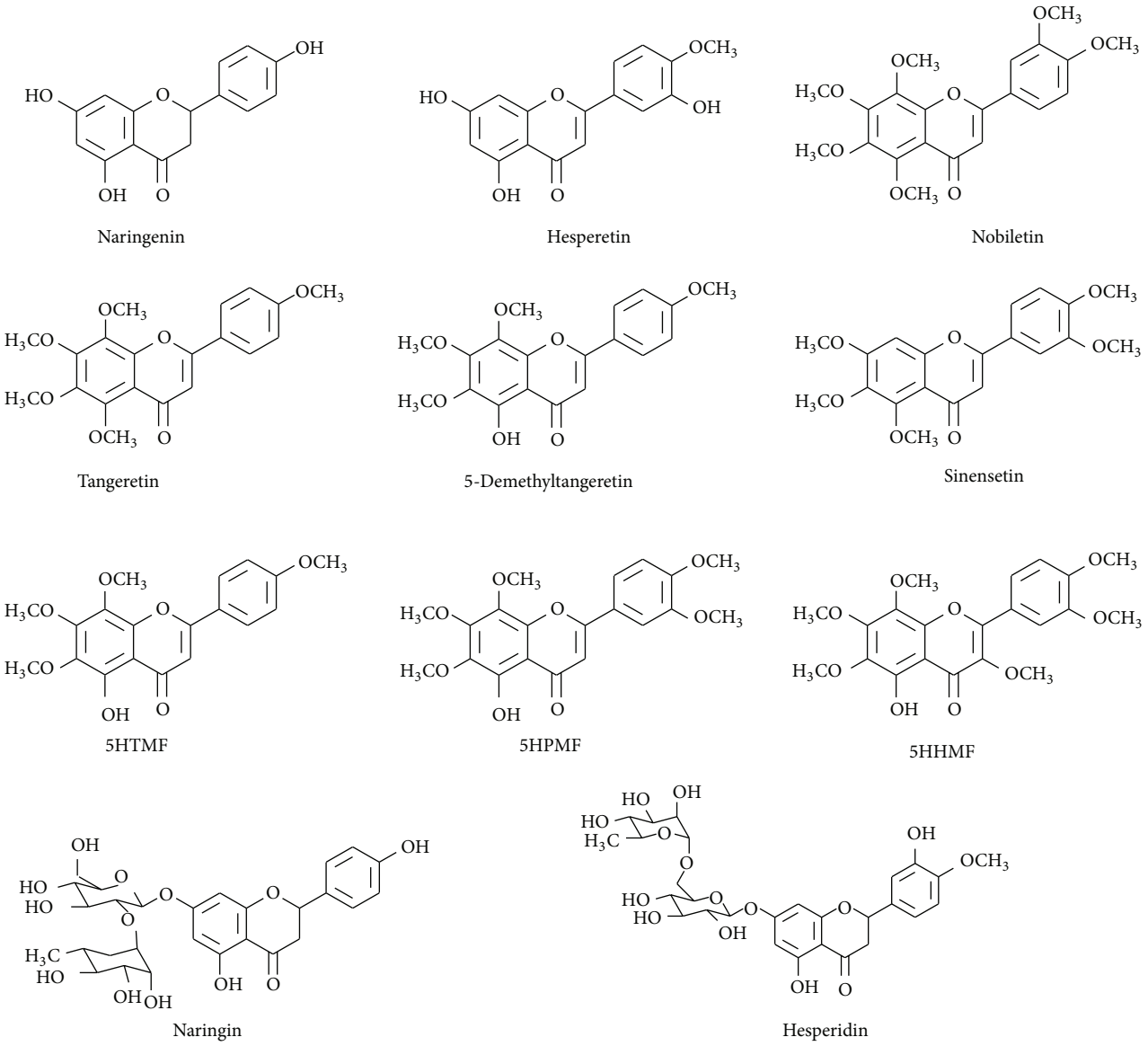

Figure 2: The chemical structures of citrus peel flavonoids molecules that are discussed in this paper.

natural compounds-induced caspase-independent apoptosis pathway [37, 38]. Our results clearly supported the notion that proapoptosis of 5-ATAN acted through caspase-independent mechanisms in case AIF translocation and H2AX phosphorylation took place in MCF-7 cells when 5-ATAN was added. Allowing for apoptotic extrinsic pathway, no clear evidence had been found about activation of caspase-8, cleavage of BID, and regulation of FADD, indicating extrinsic pathway was not required under this circumstance. Strikingly, we also found that increase of Bax/Bcl-2 ratio, $\Delta\psi$m dissipation, release of cytochrome C, and cleavage of caspase-9 after exposure to 5-ATAN in a time-dependent manner which indicated caspase-dependent intrinsic pathway were also required in the MCF-7 cells [39]. All these researches together point to a possible protective effect of citrus flavonoids and their derivatives against sustained proliferation of cancer cells.

2.3. Combined Chemotherapy. Traditional treatment of cancer has been facing a huge number of problems, in view of its complex molecular pathophysiology that varies according to each type. Several ways in the treatment of breast cancer have been developed that are surgery, chemotherapy, hormonal therapy, and radiation. Doxorubicin, a chemotherapeutic agent commonly used in breast cancer treatment, showed low effectivity, rendering its resistance and toxicity on normal tissues [40]. An approach in overcoming such problem is the development of agents used in combination with chemotherapeutic agents to lead to better result. Cochemotherapy may increase chemotherapeutic agents' efficacy, allowing the use of lower dosage of chemotherapeutic agent, resulting in the decrease of toxicity on normal tissues compared to chemotherapeutic agent alone [41]. In terms of medicine, hesperidin, tangeretin, and nobiletin could all improve doxorubicin cytotoxic chemotherapy [8]. When combining concentration of 200 nM doxorubicin and 100 μM hesperidin together in treating with MCF-7 cells, they increased cytotoxic effect, modulated cell cycle, and induced apoptosis of MCF-7 cells [42]. Meanwhile, tangeretin synergistically increased the cytotoxic effect of doxorubicin by inducing cells death and arresting cell cycle's phase both in MCF-7 and T47D breast cancer cells. Different from tangeretin, nobiletin increased doxorubicin's cytotoxic activity in MCF-7 cells, but not in T47D cells [8]. Cyclophosphamide is a cytotoxic alkylating drug with a high therapeutic index and is effective against a variety of cancers. Despite its effectiveness for the treatment of cancer, it induces a wide range of adverse side effects and toxicity, such as nausea, vomiting, and hematopoietic toxicity, which limit the use of this drug in clinic. In animal experiments, hesperetin can decrease the genotoxic effect of mice bone marrow cells when synergistically functioned with cyclophosphamide [43].

2.4. Anticancer Metastasis. Invasion and metastasis are a multistep process and are described as a series of discrete steps, usually called invasion—the metastatic cascade [44]. It describes a process of continuous change of cell biology, local invasion from the beginning, followed by intravasation into surrounding blood and lymphatic vessels, and transit and extravasation of cancer cells through the lymph or blood transport system and lumina vessels, then cancer nodules formation, and finally into the solid tumor growth. Metastasis of malignant tumors and proliferation of vascular smooth muscle (VSMC) are greatly related to inflammatory cell adhesion. As for matrix metallopeptidase-2 (MMP-2) and metallopeptidase-9 (MMP-9), they contribute greatly to tumor metastasis and invasion and are considered to be predictive markers for cancer. Naringin, a major flavonoid extracted from grapefruit and other citrus fruits, suppressed the upregulation of MMP-9 and repressed the PI3K/AKT/mTOR signaling pathway. Furthermore, naringin suppressed TNF-a-mediated release of interleukin-6 and interleukin-8 (IL-6 and IL-8) [45]. AKT, a serine/threonine protein kinase, is a downstream target of PI3K and it plays a pivotal role in cell migration, growth, and antiapoptotic events in various types of cells [46]. Tangeretin inhibited platelet-derived growth factor- (PGDF-) BB-induced proliferation and migration of aortic smooth muscle cells by blocking AKT activation in a dose-dependent manner [47]. As the aglycone moiety of naringin chemical structure, naringenin, induced heme oxygenase-1 (HO-1) expression and subsequently decreased ROS generation and VSMC activation induced by TNF-α [48]. Besides, in human prostate tumor xenograft mouse model, intraperitoneal injection or oral administration GL can downregulate MMP-2 and MMP-9 protein expression levels and dramatically reduce both the weights (57%–100% inhibition) and volumes (78%–94% inhibition) of the tumors without any observed toxicity in the meantime [49].

2.5. Antiangiogenesis. Angiogenesis is a physiological process of forming new blood vessels from preexisting vessels, which involves the induction of new sprouts, coordinated and directed endothelial cell migration, proliferation, sprout fusion, and lumen formation [50]. Similar to normal tissue, tumors need supplies like nutrients and oxygen. They also need to remove metabolic waste. Tumor-associated neovasculature delivers these needs. In fact, angiogenesis is essentially required at almost every step of tumor progression and metastasis. In some physiological processes such as wound repair, angiogenesis starts only in the adult temporarily. Oppositely, in tumor growth, angiogenic switch is almost always activated and continuing to generate new blood vessels, which in turn support the tumor growth [51]. Tumor angiogenesis is a complex process and involves the crosstalk of tumor cells, endothelial cells, phagocytes, and their secreted factors, which may act as promoters or inhibitors of angiogenesis [52]. So, a balance between proangiogenic and antiangiogenic growth factors and cytokines tightly controls angiogenesis.

As one of the angiogenesis inducers, vascular endothelial growth factor-A (VEGF) can be used as a marker of angiogenesis. *VEGF-A* gene encodes the ligand involved in neovascularization during the embryonic and neonatal development, homeostasis, and survival of endothelial cells, as well as physiological and pathological state of adult [50].

When mice with human prostate tumor xenograft were intraperitoneally injected with GL, the protein expression level of VEGF was suppressed significantly [49]. In addition, oral administration of GL strongly and dose dependently reduced the protein levels of VEGF in AOM-induced colonic tissues. GL suppressing the ACF formation might be through inhibiting the colonic mucosa cellular proliferation and angiogenesis [33].

Through combined inhibition of multiple angiogenesis-related endothelial cells (EC) functions, nobiletin had been demonstrated to have concentration-dependent inhibitory effects on angiogenic differentiation induced by VEGF and FGF (fibroblast growth factors). In a chick embryo chorioallantoic membrane assay, nobiletin showed an antiangiogenic activity with the ID_{50} value being 10 lg (24.9 nmol) per egg [53].

With human umbilical vein endothelial cells (HUVECs) in vitro and zebrafish in vivo models, PMFs showed different degrees of potency of antiangiogenesis activity. Sinensetin, which showed the most potent antiangiogenesis activity and the lowest toxicity, inhibited angiogenesis by inducing cell cycle arrest in the G0/G1 phase in HUVEC culture and downregulating the mRNA expressions of angiogenesis genes *flt1*, *kdrl*, and *hras* in zebrafish [54]. Nobiletin differs from sinensetin by having methylation at the C8 position. Together with previous research of nobiletin [55], structure-activity relationship analysis indicated that the absence of a methoxylated group at the C8 position offers lower lethal toxicity in addition to enhancing the antiangiogenesis activity via observing intersegmental vessel development in zebrafish embryos [54].

2.6. Scavenging of ROS. Flavonoids also exert their chemopreventative effect via inhibition of certain phase I metabolizing enzymes, such as cytochrome P450 which metabolically activates a large number of procarcinogens triggering carcinogenesis. The chemopreventative effects of flavonoids are closely linked to their anticancer properties that involve the scavenging of reactive oxygen species (ROS) and growth promoting oxidants which are the major catalysts for tumor promotion. Tangeretin, a polymethoxylated flavone, can inhibit cancer cell proliferation by improving antioxidant properties such as decreasing the levels of lipid peroxide, enzymatic antioxidants SOD, CAT, and GPx, and nonenzymatic antioxidants such as GSH, vitamin C, and vitamin E in 7,12-dimethyl benz(a)anthracene (DMBA) induced mammary carcinoma in rats [56]. Otherwise, the propensity of a flavonoid to inhibit free radical mediated events is governed by its chemical structure. Specific structural elements of the flavonoids determinate antioxidation activity of these compounds. Free radical scavenging capacity is primarily attributed to the high reactivity of hydroxyl substituents. Flavonols and flavanols with a 3-OH group both have planarity, which increased flavonoid phenoxyl radical stability correspondingly [57]. Furthermore, methoxy groups introduce unfavorable steric effects and increase lipophilicity and membrane partitioning. A double bond and carbonyl function in the heterocycle or polymerization of the nuclear structure increased activity by affording a more stable flavonoid radical through conjugation and electron delocalization [58]. Remarkably, glycosylation of flavonoids reduced their in vitro antioxidantive activity compared to the corresponding aglycones [59]. The same results were observed in O-methylated flavonoids, which showed weaker antioxidation than their respective aglycones [60]. As an example, 5,3-didemethylnobiletin showed much stronger inhibitory effect on human colon cancer cell growth than 5-demethylnobiletin by cell viability assay [61]. These correlations between the flavonoid structure and their free radical scavenging activity need to be further investigated for better understanding and clinical application.

3. Pharmacokinetics of PMFs and Cancer Therapy

Pharmacokinetics describes how the body affects a specific drug after administration through mechanisms of absorption and distribution, as well as the chemical changes of the substance in the body. At a practical level, a drug's bioavailability can be defined as the proportion of the drug that reaches its site of action. Poor absorption and extensive conjugative metabolisms greatly limit bioavailability of dietary flavonoids.

3.1. PMF's Bioavailability. The bioavailability is an overall effect of absorption, distribution, metabolism, and excretion and plays an important role in dictating cancer preventive efficacy of dietary components in humans. Bioavailability testing can be divided into in vitro and in vivo bioavailability. In vitro bioavailability test can be a good predictor of the latter one.

Currently, human colon adenocarcinoma cell line caco-2 cell model is established to simulate the human intestinal absorption so as to test permeability and study absorption mechanism. The caco-2 data of 3′-hydroxy-5,6,7,4′-tetramethoxyflavone, 3,5,6,7,8,3′,4′-heptamethoxyflavone, and 3-hydroxy-5,6,7,8,3′,4′-hexamethoxyflavone showed superb permeability [62]. Meanwhile, the lyophilisation solubility assay (LYSA), a rapid method to test drugs and active nutrients compounds, was adapted to measure the solubility of PMFs. The solubility data showed that hydroxylated PMFs were better than their fully methoxylated counterparts. Considering the solubility and permeability together, the overall high absorption of PMFs contributes to their good bioavailability.

Also, in NSCLC A549 cell line, 5-hydroxylated PMFs had much stronger inhibitory effects on cancer cells in comparison with their permethoxylated counterparts, for IC_{50} value of 5-demethyltangeretin (5DT) was 78.9-fold lower than that of tangeretin. Since cancer cells can pump the cytotoxic agents out via overexpression of multidrug resistant efflux proteins, cells were treated with 5DT or tangeretin at the same concentration. HPLC analysis revealed that the intracellular levels of 5DT in NSCLC cells were 2.7–4.9-fold higher than those of TAN. This suggested that NSCLC cells may have better uptake efflux of 5DT compared with TAN. Additionally, molecular structure showed that 5DT had higher lipophilicity than tangeretin [63]. High lipophilicity

could enhance 5DT binding to the plasma membrane, which in turn could promote the uptake of 5DT into cytosol of the cancer cells.

3.2. PMFs and Metabolites in Cancer Therapy. Biotransformation of dietary components is crucial for their in vivo biological activities after oral ingestion because the process of drug metabolism notably influences drugs effects and toxicity. In the research of nobiletin metabolites, by comparing supercritical fluid chromatography (SFC) profiles of metabolite mixtures with the synthesized standard compounds, three major metabolites were proved to be 4′-demethylnobiletin, 3′-demethylnobiletin, and 3′,4′-didemethylnobilietin in mouse urine [64]. Further research had demonstrated that 3′,4′-didemethylnobilietin exhibited greater bioactivities than nobiletin. As another example, it has been confirmed that 5-demethylnobiletin had strong antiproliferative effects on cancer cells. Thus, urine samples were collected from mice fed with 5-demethylnobiletin and processed for HPLC-ESI-MS analysis. Three major metabolites were characterized as 5,3′-didemethylnobiletin, 5,4′-didemethylnobiletin, and 5,3′,4′-tridemethylnobiletin. Cell viability assay in human colon cancer cells demonstrated that these three metabolites showed IC_{50} of 0.12, 5.5, and 4.2 μM in SW620 cells, while 5-demethylnobiletin at 10 μM only caused 37% inhibition [61]. Hence, it can be concluded that PMFs in citrus peels may produce much stronger active anticancer compounds through biotransformation.

4. Conclusions

Taken all together, a considerable number of well-established lines of evidence have confirmed that flavonoids in citrus peel exhibit a remarkable spectrum of efficacious biological activities, particularly in antitumorigenesis. Excellent permeability through membrane allows citrus flavonoids to possess great bioavailability which consequently attracts researchers to perform scientific studies for effective disease prevention and treatment. There are more modified flavonoids in citrus peel being investigated, which could offer help to improve dose-effect relationship greatly and advance the security and stability of compounds.

Conflict of Interests

The authors declare that there is no conflict of interests regarding the publication of this paper.

Acknowledgments

This study was supported by the National Natural Science Foundation of China (Grant nos. 81172837 and 31270050), the Tianjin Research Program of Application Foundation and Advanced Technology (Grant no. 13JCQNJC12200), and the Tianjin Innovative Research Team Grant of Agriculture Storage and Procession (TD-12-5049).

References

[1] M. Danihelová and E. Šturdík, "Flavonoid natural sources and their importance in the human diet," *Potravinarstvo*, vol. 5, no. 4, pp. 12–24, 2011.

[2] K. C. Ock, J. C. Sang, and W. O. Song, "Estimated dietary flavonoid intake and major food sources of U.S. adults," *Journal of Nutrition*, vol. 137, no. 5, pp. 1244–1252, 2007.

[3] S. Li, H. Wang, L. Guo, H. Zhao, and C.-T. Ho, "Chemistry and bioactivity of nobiletin and its metabolites," *Journal of Functional Foods*, vol. 6, pp. 2–10, 2014.

[4] J. M. Assini, E. E. Mulvihill, B. G. Sutherland et al., "Naringenin prevents cholesterol-induced systemic inflammation, metabolic dysregulation, and atherosclerosis in Ldlr/mice," *Journal of Lipid Research*, vol. 54, no. 3, pp. 711–724, 2013.

[5] D. F. Romagnolo and O. I. Selmin, "Flavonoids and cancer prevention: a review of the evidence," *Journal of Nutrition in Gerontology and Geriatrics*, vol. 31, no. 3, pp. 206–238, 2012.

[6] E. Park and J. M. Pezzuto, "Flavonoids in cancer prevention," *Anti-Cancer Agents in Medicinal Chemistry*, vol. 12, no. 8, pp. 836–851, 2012.

[7] E. E. Mulvihill and M. W. Huff, "Citrus flavonoids and the prevention of atherosclerosis," *Cardiovascular & Hematological Disorders-Drug Targets*, vol. 12, no. 2, pp. 84–91, 2012.

[8] E. Meiyanto and A. Hermawan, "Natural products for cancer-targeted therapy: citrus flavonoids as potent chemopreventive agents," *Asian Pacific Journal of Cancer Prevention*, vol. 13, no. 2, pp. 427–436, 2012.

[9] O. I. Aruoma, B. Landes, D. Ramful-Baboolall et al., "Functional benefits of citrus fruits in the management of diabetes," *Preventive Medicine*, vol. 54, pp. S12–S16, 2012.

[10] S. Hwang, P. Shih, and G. Yen, "Neuroprotective effects of citrus flavonoids," *Journal of Agricultural and Food Chemistry*, vol. 60, no. 4, pp. 877–885, 2012.

[11] L. Andrews, "Dietary flavonoids for the prevention of colorectal cancer," *Clinical Journal of Oncology Nursing*, vol. 17, no. 6, pp. 671–672, 2013.

[12] C. La Vecchia, A. Decarli, M. Serafini et al., "Dietary total antioxidant capacity and colorectal cancer: a large case-control study in Italy," *International Journal of Cancer*, vol. 133, no. 6, pp. 1447–1451, 2013.

[13] X. Gao, A. Cassidy, M. A. Schwarzschild, E. B. Rimm, and A. Ascherio, "Habitual intake of dietary flavonoids and risk of Parkinson disease," *Neurology*, vol. 78, no. 15, pp. 1138–1145, 2012.

[14] J. K. Song and J. M. Bae, "Citrus fruit intake and breast cancer risk: a quantitative systematic review," *Journal of Breast Cancer*, vol. 16, no. 1, pp. 72–76, 2013.

[15] A. Cassidy, E. B. Rimm, É. J. O'Reilly et al., "Dietary flavonoids and risk of stroke in women," *Stroke*, vol. 43, no. 4, pp. 946–951, 2012.

[16] D. Hanahan and R. A. Weinberg, "The hallmarks of cancer," *Cell*, vol. 100, no. 1, pp. 57–70, 2000.

[17] S. Sultana, H. M. Asif, H. M. Nazar, N. Akhtar, J. U. Rehman, and R. U. Rehman, "Medicinal plants combating against cancer—a green anticancer approach," *Asian Pacific Journal of Cancer Prevention*, vol. 15, no. 11, pp. 4385–4394, 2014.

[18] X. Grana and E. P. Reddy, "Cell cycle control in mammalian cells: Role of cyclins, cyclin dependent kinases (CDKs), growth suppressor genes and cyclin-dependent kinase inhibitors (CKIs)," *Oncogene*, vol. 11, no. 2, pp. 211–219, 1995.

[19] K. Vermeulen, D. R. van Bockstaele, and Z. N. Berneman, "The cell cycle: a review of regulation, deregulation and therapeutic targets in cancer," *Cell Proliferation*, vol. 36, no. 3, pp. 131–149, 2003.

[20] K. I. Park, H. S. Park, A. Nagappan et al., "Induction of the cell cycle arrest and apoptosis by flavonoids isolated from Korean *Citrus aurantium* L. in non-small-cell lung cancer cells," *Food Chemistry*, vol. 135, no. 4, pp. 2728–2735, 2012.

[21] E. J. Choi, "Hesperetin induced G1-phase cell cycle arrest in human breast cancer MCF-7 cells: involvement of CDK4 and p21," *Nutrition and Cancer*, vol. 59, no. 1, pp. 115–119, 2007.

[22] A. A. Alshatwi, E. Ramesh, V. S. Periasamy, and P. Subash-Babu, "The apoptotic effect of hesperetin on human cervical cancer cells is mediated through cell cycle arrest, death receptor, and mitochondrial pathways," *Fundamental and Clinical Pharmacology*, vol. 27, no. 6, pp. 581–592, 2013.

[23] D. Arul and P. Subramanian, "Naringenin (citrus flavonone) induces growth inhibition, cell cycle arrest and apoptosis in human hepatocellular carcinoma cells," *Pathology and Oncology Research*, vol. 19, no. 4, pp. 763–770, 2013.

[24] K. L. Morley, P. J. Ferguson, and J. Koropatnick, "Tangeretin and nobiletin induce G1 cell cycle arrest but not apoptosis in human breast and colon cancer cells," *Cancer Letters*, vol. 251, no. 1, pp. 168–178, 2007.

[25] N. Charoensinphon, P. Qiu, P. Dong et al., "5-demethyltangeretin inhibits human nonsmall cell lung cancer cell growth by inducing G2/M cell cycle arrest and apoptosis," *Molecular Nutrition & Food Research*, vol. 57, no. 12, pp. 2103–2111, 2013.

[26] P. Qiu, H. Guan, P. Dong et al., "The p53-, Bax- and p21-dependent inhibition of colon cancer cell growth by 5-hydroxy polymethoxyflavones," *Molecular Nutrition and Food Research*, vol. 55, no. 4, pp. 613–622, 2011.

[27] H. Li, B. Yang, J. Huang et al., "Naringin inhibits growth potential of human triple-negative breast cancer cells by targeting β-catenin signaling pathway," *Toxicology Letters*, vol. 220, no. 3, pp. 219–228, 2013.

[28] M. H. Han, W. S. Lee, J. N. Lu et al., "*Citrus aurantium* L. exhibits apoptotic effects on U937 human leukemia cells partly through inhibition of Akt," *International Journal of Oncology*, vol. 40, no. 6, pp. 2090–2096, 2012.

[29] A. Ghorbani, M. Nazari, M. Jeddi-Tehrani, and H. Zand, "The citrus flavonoid hesperidin induces p53 and inhibits NF-κB activation in order to trigger apoptosis in NALM-6 cells: involvement of PPARγ-dependent mechanism," *European Journal of Nutrition*, vol. 51, no. 1, pp. 39–46, 2012.

[30] O. Wesołowska, J. Wiśniewski, K. Środa-Pomianek et al., "Multidrug resistance reversal and apoptosis induction in human colon cancer cells by some flavonoids present in citrus plants," *Journal of Natural Products*, vol. 75, no. 11, pp. 1896–1902, 2012.

[31] A. Gosslau, K. Y. Chen, C.-T. Ho, and S. Li, "Anti-inflammatory effects of characterized orange peel extracts enriched with bioactive polymethoxyflavones," *Food Science and Human Wellness*, vol. 3, no. 1, pp. 26–35, 2014.

[32] I. N. Sergeev, C. T. Ho, S. Li, J. Colby, and S. Dushenkov, "Apoptosis-inducing activity of hydroxylated polymethoxyf lavones and polymethoxyflavones from orange peel in human breast cancer cells," *Molecular Nutrition and Food Research*, vol. 51, no. 12, pp. 1478–1484, 2007.

[33] C. S. Lai, S. Li, C. B. Liu et al., "Effective suppression of azoxymethane-induced aberrant crypt foci formation in mice with citrus peel flavonoids," *Molecular Nutrition and Food Research*, vol. 57, no. 3, pp. 551–555, 2013.

[34] S. Li, Y. C. Lin, C. T. Ho et al., "Formulated extract from multiple citrus peels impairs dendritic cell functions and attenuates allergic contact hypersensitivity," *International Immunopharmacology*, vol. 20, no. 1, pp. 12–23, 2014.

[35] N. Nalini, S. Aranganathan, and J. Kabalimurthy, "Chemopreventive efficacy of hesperetin (citrus flavonone) against 1,2-dimethylhydrazine-induced rat colon carcinogenesis," *Toxicology Mechanisms and Methods*, vol. 22, no. 5, pp. 397–408, 2012.

[36] L. Ye, F. L. Chan, S. Chen, and L. K. Leung, "The citrus flavonone hesperetin inhibits growth of aromatase-expressing MCF-7 tumor in ovariectomized athymic mice," *Journal of Nutritional Biochemistry*, vol. 23, no. 10, pp. 1230–1237, 2012.

[37] C. Candé, N. Vahsen, C. Garrido, and G. Kroemer, "Apoptosis-inducing factor (AIF): caspase-independent after all," *Cell Death and Differentiation*, vol. 11, no. 6, pp. 591–595, 2004.

[38] C. Lu, F. Zhu, Y. Cho et al., "Cell apoptosis: requirement of H2AX in DNA ladder formation, but not for the activation of caspase-3," *Molecular Cell*, vol. 23, no. 1, pp. 121–132, 2006.

[39] J. Wang, Y. Duan, D. Zhi et al., "Pro-apoptotic effects of the novel tangeretin derivate 5-acetyl-6,7,8,4′-tetramethylnortangeretin on MCF-7 breast cancer cells," *Cell Biochemistry and Biophysics*, 2014.

[40] C. Fimognari, M. Nüsse, M. Lenzi, D. Sciuscio, G. Cantelli-Forti, and P. Hrelia, "Sulforaphane increases the efficacy of doxorubicin in mouse fibroblasts characterized by p53 mutations," *Mutation Research: Fundamental and Molecular Mechanisms of Mutagenesis*, vol. 601, no. 1-2, pp. 92–101, 2006.

[41] A. Bast, H. Kaiserová, G. J. den Hartog, G. R. Haenen, and W. J. F. van der Vijgh, "Protectors against doxorubicin-induced cardiotoxicity: flavonoids," *Cell Biology and Toxicology*, vol. 23, no. 1, pp. 39–47, 2007.

[42] A. Hermawan, "Hesperidin increase cytotoxic effect of doxorubicin in MCF-7 cells," *Indonesian Journal of Pharmacy*, vol. 21, no. 1, pp. 8–16, 2010.

[43] A. Ahmadi, S. J. Hosseinimehr, F. Naghshvar, E. Hajir, and M. Ghahremani, "Chemoprotective effects of hesperidin against genotoxicity induced by cyclophosphamide in mice bone marrow cells," *Archives of Pharmacal Research*, vol. 31, no. 6, pp. 794–797, 2008.

[44] J. E. Talmadge and I. J. Fidler, "AACR centennial series: the biology of cancer metastasis: historical perspective," *Cancer Research*, vol. 70, no. 14, pp. 5649–5669, 2010.

[45] E. Lee, D. Kim, W. Kim, and S. Moon, "Naringin inhibits matrix metalloproteinase-9 expression and AKT phosphorylation in tumor necrosis factor-α-induced vascular smooth muscle cells," *Molecular Nutrition and Food Research*, vol. 53, no. 12, pp. 1582–1591, 2009.

[46] E. A. Goncharova, A. J. Ammit, C. Irani et al., "PI3K is required for proliferation and migration of human pulmonary vascular smooth muscle cells," *American Journal of Physiology—Lung Cellular and Molecular Physiology*, vol. 283, no. 2, pp. L354–L363, 2002.

[47] J. Seo, H. S. Lee, S. Ryoo, J. H. Seo, B. Min, and J. H. Lee, "Tangeretin, a citrus flavonoid, inhibits PGDF-BB-induced proliferation and migration of aortic smooth muscle cells by blocking AKT activation," *European Journal of Pharmacology*, vol. 673, no. 1–3, pp. 56–64, 2011.

[48] S. Chen, Y. Ding, W. Tao, W. Zhang, T. Liang, and C. Liu, "Naringenin inhibits TNF-α induced VSMC proliferation and migration via induction of HO-1," *Food and Chemical Toxicology*, vol. 50, no. 9, pp. 3025–3031, 2012.

[49] C. Lai, S. Li, Y. Miyauchi, M. Suzawa, C. Ho, and M. Pan, "Potent anti-cancer effects of citrus peel flavonoids in human prostate xenograft tumors," *Food and Function*, vol. 4, no. 6, pp. 944–949, 2013.

[50] N. M. Pandya, N. S. Dhalla, and D. D. Santani, "Angiogenesis—a new target for future therapy," *Vascular Pharmacology*, vol. 44, no. 5, pp. 265–274, 2006.

[51] D. Hanahan and R. A. Weinberg, "Hallmarks of cancer: the next generation," *Cell*, vol. 144, no. 5, pp. 646–674, 2011.

[52] T. A. Bhat and R. P. Singh, "Tumor angiogenesis: a potential target in cancer chemoprevention," *Food and Chemical Toxicology*, vol. 46, no. 4, pp. 1334–1345, 2008.

[53] K. Kunimasa, M. Ikekita, M. Sato et al., "Nobiletin, a citrus polymethoxyflavonoid, suppresses multiple angiogenesis-related endothelial cell functions and angiogenesis in vivo," *Cancer Science*, vol. 101, no. 11, pp. 2462–2469, 2010.

[54] I. K. Lam, D. Alex, Y. H. Wang et al., "In vitro and in vivo structure and activity relationship analysis of polymethoxylated flavonoids: identifying sinensetin as a novel antiangiogenesis agent," *Molecular Nutrition and Food Research*, vol. 56, no. 6, pp. 945–956, 2012.

[55] K. H. Lam, D. Alex, I. K. Lam, S. K. W. Tsui, Z. F. Yang, and S. M. Y. Lee, "Nobiletin, a polymethoxylated flavonoid from citrus, shows anti-angiogenic activity in a zebrafish in vivo model and HUVEC in vitro model," *Journal of Cellular Biochemistry*, vol. 112, no. 11, pp. 3313–3321, 2011.

[56] A. Lakshmi and S. Subramanian, "Chemotherapeutic effect of tangeretin, a polymethoxylated flavone studied in 7, 12-dimethylbenz(a)anthracene induced mammary carcinoma in experimental rats," *Biochimie*, vol. 99, pp. 96–109, 2014.

[57] S. A. B. E. van Acker, M. J. de Groot, D. D. van Berg et al., "A quantum chemical explanation of the antioxidant activity of flavonoids," *Chemical Research in Toxicology*, vol. 9, no. 8, pp. 1305–1312, 1996.

[58] K. E. Heim, A. R. Tagliaferro, and D. J. Bobilya, "Flavonoid antioxidants: chemistry, metabolism and structure-activity relationships," *Journal of Nutritional Biochemistry*, vol. 13, no. 10, pp. 572–584, 2002.

[59] B. Mishra, K. I. Priyadarsini, M. S. Kumar, M. K. Unnikrishnan, and H. Mohan, "Effect of *O*-glycosilation on the antioxidant activity and free radical reactions of a plant flavonoid, chrysoeriol," *Bioorganic and Medicinal Chemistry*, vol. 11, no. 13, pp. 2677–2685, 2003.

[60] D. Amić and B. Lučić, "Reliability of bond dissociation enthalpy calculated by the PM6 method and experimental TEAC values in antiradical QSAR of flavonoids," *Bioorganic and Medicinal Chemistry*, vol. 18, no. 1, pp. 28–35, 2010.

[61] J. Zheng, M. Song, P. Dong et al., "Identification of novel bioactive metabolites of 5-demethylnobiletin in mice," *Molecular Nutrition & Food Research*, vol. 57, no. 11, pp. 1999–2007, 2013.

[62] S. Li, M.-H. Pan, C.-Y. Lo et al., "Chemistry and health effects of polymethoxyflavones and hydroxylated polymethoxyflavones," *Journal of Functional Foods*, vol. 1, no. 1, pp. 2–12, 2009.

[63] P. Dong, P. Qiu, Y. Zhu et al., "Simultaneous determination of four 5-hydroxy polymethoxyflavones by reversed-phase high performance liquid chromatography with electrochemical detection," *Journal of Chromatography A*, vol. 1217, no. 5, pp. 642–647, 2010.

[64] S. Li, Z. Wang, S. Sang, M. T. Huang, and C. T. Ho, "Identification of nobiletin metabolites in mouse urine," *Molecular Nutrition and Food Research*, vol. 50, no. 3, pp. 291–299, 2006.

Hindawi Publishing Corporation
BioMed Research International
Volume 2014, Article ID 783459, 12 pages
http://dx.doi.org/10.1155/2014/783459

Research Article

SIRT1 Inhibition Affects Angiogenic Properties of Human MSCs

Botti Chiara,[1,2] Caiafa Ilaria,[1] Coppola Antonietta,[1] Cuomo Francesca,[1] Miceli Marco,[3] Altucci Lucia,[1,3] and Cobellis Gilda[1,2]

[1] *Department of Biochemistry, Biophysics and General Pathology, Second University of Napoli, Via L. De Crecchio 7, 80138 Napoli, Italy*
[2] *Istituto Nazionale Tumori, Struttura Complessa Oncologia Medica Melanoma Immunoterapia Oncologica e Terapia Innovativa, Via Mariano Semmola, 80131 Napoli, Italy*
[3] *Institute of Genetics and Biophysics "A. Buzzati-Traverso", CNR, Via P. Castellino 111, 80131 Napoli, Italy*

Correspondence should be addressed to Botti Chiara; chiara_botti@yahoo.it and Cobellis Gilda; g.cobellis@unina2.it

Received 18 July 2014; Revised 7 August 2014; Accepted 8 August 2014; Published 27 August 2014

Academic Editor: Zongjin Li

Human mesenchymal stem cells (hMSCs) are attractive for clinical and experimental purposes due to their capability of self-renewal and of differentiating into several cell types. Autologous hMSCs transplantation has been proven to induce therapeutic angiogenesis in ischemic disorders. However, the molecular mechanisms underlying these effects remain unclear. A recent report has connected MSCs multipotency to sirtuin families, showing that SIRT1 can regulate MSCs function. Furthermore, SIRT1 is a critical modulator of endothelial angiogenic functions. Here, we described the generation of an immortalized human mesenchymal bone marrow-derived cell line and we investigated the angiogenic phenotype of our cellular model by inhibiting SIRT1 by both the genetic and pharmacological level. We first assessed the expression of SIRT1 in hMSCs under basal and hypoxic conditions at both RNA and protein level. Inhibition of SIRT1 by sirtinol, a cell-permeable inhibitor, or by specific sh-RNA resulted in an increase of premature-senescence phenotype, a reduction of proliferation rate with increased apoptosis. Furthermore, we observed a consistent reduction of tubule-like formation and migration and we found that SIRT1 inhibition reduced the hypoxia induced accumulation of HIF-1α protein and its transcriptional activity in hMSCs. Our findings identify SIRT1 as regulator of hypoxia-induced response in hMSCs and may contribute to the development of new therapeutic strategies to improve regenerative properties of mesenchymal stem cells in ischemic disorders through SIRT1 modulation.

1. Introduction

Human mesenchymal stem cells (hMSCs) have become an important tool for cell-based strategies. They can differentiate into a variety of cell types such as muscle, neural precursors, cardiomyocytes, and perivascular cells and are currently being tested in several approved clinical trials [1]. hMSCs can improve myocardial remodeling in infarcted heart [2] or promote angiogenesis in critical limb ischemia [3], due to their capacity to stimulate endothelial progenitor cells. Furthermore, hMSCs support neoangiogenesis also by releasing soluble factors that stimulate angiogenesis [4–9]. However, the molecular mechanisms of beneficial effects from hMSCs-based therapy remain unclear.

A recent report showed that SIRT1 might regulate MSCs function, providing a connection between sirtuin families and MSCs multipotency [10].

Sirtuins are classified as class III histone deacetylases (HDACs) [11], originally identified in yeast. They modulate a wide range of biological processes, spanning from DNA repair and oxidative stress responses to energy metabolism. Sirtuins activity is controlled by the cellular [NAD+]/[NADH] ratio, where NAD+ works as an activator, whereas nicotinamide and NADH act as inhibitors.

In mammals, the sirtuin family comprises seven members (SIRT1–SIRT7) with different biological functions and subcellular localizations [12–14]. SIRT1, SIRT6, and SIRT7 are mainly nuclear, whereas SIRT2 is found primarily in the

cytosol. SIRT3, SIRT4, and SIRT5 are mitochondrial proteins [12]. Sirtuins are generally known to regulate the acetylation levels and the activity of histone and nonhistone regulatory proteins.

To date, sirtuins have emerged as potential therapeutic targets for treatment of human pathologies such as cardiovascular disease, inflammation, and cancer [15]. SIRT1 is the most studied member of sirtuins. It acts in various cellular processes and exerts its action activating and deactivating factors such as NF-κB, p53, p73, SOD, and hypoxia-inducible transcription factors (HIFs) [16–19].

Since SIRT1 targets several proteins in distinct signaling pathways, modulation of SIRT1 activity alters the biological activity of entire signaling networks modifying disease progression, such as pathological angiogenesis or atherosclerosis.

An important component of pathological angiogenesis is represented by hypoxia that alters the cellular redox state and activates SIRT1. In addition, hypoxia works through multiple pathways to regulate angiogenesis, for instance, through the modulation of secreted angiogenic proteins, such as vascular endothelial growth factor (VEGF), stimulated by increased expression of transcription factors such as HIF-1α [20].

Furthermore, a "protective" role of SIRT1 in endothelial cells was described [21, 22]. A recent report has investigated the function of SIRT1 in regulating the differentiation of mesenchymal stem cells by deacetylating β-catenin in mice [10]. Several studies demonstrated that inhibition of SIRT1 impairs cell growth in cancer cells [23, 24]. Gorenne et al. [25] reported that SIRT1 expression was reduced in human atherosclerotic plaques and in vascular smooth muscle cells. However, to the best of our knowledge, the effects of SIRT1 modulation on angiogenesis in hMSCs have not been studied yet.

In this study, we described the generation of an immortalized human mesenchymal bone marrow-derived cell line (MeBM) and we investigated whether SIRT1 has an effect on angiogenic capability of hMSCs by inhibiting SIRT1 through pharmacological and genetic approaches.

Since recent studies have identified SIRT1 as a critical modulator of angiogenesis [18, 26], we tested whether the inhibition of SIRT1 activity is associated with the reduction of angiogenic ability of hMSCs and impaired hypoxic response in these settings. We found that the inhibition of SIRT1 activity resulted in reduced capacity to proliferate, to migrate, and to form three-dimensional networks of vessel-like structures. In addition, SIRT1 inhibition reduced the hypoxia-induced accumulation of HIF-1α and its transcriptional activity in hMSCs.

Our results suggested that SIRT1 is involved in angiogenic response of hMSCs in vitro and modulates the hypoxic response through inhibiting HIF-1α activity.

Our findings may help to understand the role of SIRT1 in hMSCs in promoting angiogenesis and may contribute to the development of new strategies to improve the hMSCs-based regenerative effects by modulating SIRT1 activity.

2. Methods

2.1. Reagents. Sirtinol was purchased from Selleck Chemicals LLC (Houston, TX, USA). Culture medium and its supplements including antibiotics and fetal bovine serum (FBS) were purchased from Euroclone (Italy). Primary antibodies against SIRT1 (Abcam, Cambridge, UK), HIF-1α (Santa Cruz Biotechnology, Santa Cruz, CA, USA), and tubulin (Sigma-Aldrich, Milan, Italy) were used. Sirtinol was dissolved in dimethyl sulfoxide (DMSO, Sigma-Aldrich) to the appropriate concentrations according to reported procedures. DMSO was also present in the corresponding control.

2.2. Cell Lines and Culture Medium. Human mesenchymal stem cells (hMSCs) were obtained from bone marrow as described by Cobellis et al. [8]. Cells were plated in RPMI 1640 growth medium (Euroclone SPA, Italy), containing 10% heat-inactivated FBS, 1% Pen-strep, and 1% L-Glutamine.

Cells were maintained as monolayers in a humidified atmosphere containing 5% CO_2 at 37°C and the culture medium was replaced every two days.

Hypoxic culture conditions were achieved in a BD GasPak EZ Anaerobe Gas Generating Pouch System (BD Biosciences, San Diego). As certified by the manufacturer, the Anaerobe Gas Generating Pouch System produces an atmosphere containing 10% carbon dioxide and 1% oxygen.

Starvation conditions were obtained incubating cells in RPMI 1640 containing 0.2% FBS.

2.3. Infection. After plating, bone marrow cells were grown to confluence and coinfected with HPV16 E6/E7 and hTERT lentiviral vectors (infection number 1). After a week the cells were split and infected again only with hTERT (infection number 2) and cultured until stabilization. Samples were observed and photographed with DMI 6000 inverted microscope (Leica Microsystems) using Leica LAS Image Analysis software (Leica Microsystems). The protocol was also reported in Miceli et al. [27].

2.4. hPV16 E6/E7 and hTERT Lentiviral Production. HIV-1based SIN lentiviral vectors were derived from SINF-MU3-W-S vector backbone. hPV16 E6/E7 was inserted upstream of an encephalomyocarditis virus internal ribosome entry site- (IRES-) yellow fluorescent protein (YFP) gene cassette into SINF-MU3-W-S to generate SINF-MU3-E6E7-IRES-YFPW-S. SINF-MU3-hTERT-IRES-GFPW-S was generated by inserting hTERT cDNA upstream of an IRES-green fluorescent protein (GFP) gene cassette into SINF-MU3-W-S. VSV-G-pseudotyped lentiviral vectors were generated in 150 mm tissue culture dishes by transient cotransfection with (1) VSV-G-expressing construct pCMV-VSV-G (Invitrogen, USA) (66 μg), (2) packaging construct pCMVΔR8.2 (addgene) (48 μg), and (3) lentiviral vector plasmids (pSin hTERT or Psin E6-E7) (66 μg) into subconfluent HEK 293FT cells (Invitrogen) by calcium phosphate precipitation (Clontech, Calphos Mammalian Transfection Kit). The supernatant containing the virus was produced in HEK-293FT, collected, filtered, and used to infect bone marrow cells.

2.5. Gene Knockdown Using Lentiviral Vector. Cells (10^5) were grown in RPMI 1640 medium 4.5 g/L glucose (Euroclone SPA, Italy) supplemented with 20% FBS (Euroclone SPA, Italy), 100 U/mL Pen-strep (Lonza Group Ltd), and 2 mM L-Glutamine (Lonza Group Ltd) at 37°C, in 5% CO_2 fully humidified atmosphere. Cells were first grown for 24 h and then infected with the rLV.H1.sh2Sirt1.EF1.GFP Lentivirus, with a 2.5 MOI, overnight as described by Miceli et al. [27].

2.6. RNA Extraction and qPCR. Total RNA was isolated from hMSCs by miRNeasy Mini kit (QIAGEN GE). 500 ng was converted to cDNA using the Quantitect Reverse Transcription kit (QIAGEN GE).

qPCR assays were performed using an iCycler (BioRad Laboratories, USA) and the Sybergreen Super mix (BioRad Laboratories, USA). The primer sequences and qPCR conditions are available on request.

2.7. Protein Extraction and Western Blot Analysis. hMSCs were incubated with 100 μM sirtinol for 24 h and then we collected lysates from cells exposed to 1% O_2 for 6 h.

Cells were lysed in buffer containing 20 mM Tris HCl, 100 mM NaCl, 10 mM $MgCl_2$, 1% NP40, 10% glycerol, 0.1 M NaF, 100 μM sodium vanadate, and protease inhibitors mixture (Roche LTD, GE). Equal amounts of supernatant were separated by SDS-polyacrylamide gels. Proteins were transferred to nitrocellulose membranes (WhatmanProtran, GE Healthcare) and membranes were blocked with blocking buffer (TBS-Tween buffer containing 5% milk). Subsequently, the membranes were incubated with primary antibodies at 4°C overnight. After three washes for 10′ with TTBS buffer (50 mM Tris HCl, pH 8, 150 mM NaCl, and 0.5% Tween-20), the membranes were incubated with horseradish peroxidase-conjugated anti-mouse or anti-rabbit antibody (1 : 10.000, Santa Cruz Biotechnology, Santa Cruz, CA, USA) for 1 h at room temperature and then washed for 30 min with TTBS buffer. The resulting immunoblots were detected using Amersham ECL Plus (GE Healthcare).

2.8. Senescence Associated Beta-Galactosidase (SA-Beta-Gal) Staining. Cells were cultured on 6-well plates at a density allowing reaching 20–30% confluence and exposed for 24 h to 50 and 100 μM sirtinol. After exposure, the cells were washed three times with inhibitor-free medium and cultured for up to additional 8 days. On the ninth day, the cells were fixed with 2% (v/v) formaldehyde/0.2% (v/v) glutaraldehyde for 10 min. The cells were then washed twice with PBS and incubated with staining solution (30 mM citric acid/phosphate buffer (pH 6), 5 mM $K_4Fe(CN)_6$, 5 mM $K_3Fe(CN)_6$, 150 mMNaCl, 2 mM $MgCl_2$, and 1 mg/mL X-Gal solution (all reagents were purchased from Sigma, Milan, Italy)) at 37°C for 24 h. The cells were photographed and quantified with an inverted microscope (Leica, Heidelberg, Germany).

2.9. Cell Proliferation. Cells were plated (5×10^3 cells/well in 96 well plates) in RPMI 1640 (Euroclone SPA, Italy) and allowed to attach overnight. The day after, hMSCs were treated with 100 μM sirtinol for 24, 48, and 72 h. The number of living cells was measured by determination of ATP cellular levels using ViaLight Plus Kit (Lonza Group Ltd). The kit is based upon the bioluminescent measurement of ATP that is present in all metabolically active cells. The bioluminescent method utilizes an enzyme, luciferase, which catalyzes the formation of light from ATP and luciferin. The emitted light intensity is linearly related to the ATP concentration and is measured using a luminometer. RLUs (relative light units) are internal unit of the kit, proportional to the amount of light produced for ATP unit.

All experiments were performed in triplicates.

2.10. Flow Cytometry Analysis. Cells were treated with 100 μM sirtinol for 24, 48, and 72 h. Cells were resuspended in the staining solution containing RNAseA, propidium iodide (50 μg/mL), sodium citrate (0.1%), and NP40 (0.1%) in PBS 1X for 30 min in the dark. Cell cycle distribution was assessed with a FACScalibur flow cytometer (Becton Dickinson, San Jose, CA, USA), and 10.000 cells were analyzed by ModFit version 3 Technology (Verity Software House, Topsham, ME, USA) and Cell Quest (Becton Dickinson, San Jose, CA, USA) [27].

2.11. Migration Assay. Cells were plated on 24-well plates at a density allowing reaching 50–75% confluence and hMSCs were treated for 24, 48, and 72 h with 100 μM sirtinol. A total of 1.5×10^4 cells were resuspended in 250 μL of RPMI 1640 containing 0.2% FBS and pipetted in the upper chamber of a modified Boyden chamber (Costar Transwell assay, 8 μm pore size, Corning, NY). The chamber was placed in a 24-well culture dish containing 750 μL complete RPMI 1640 with 10% FBS and growth factors. After 24 h incubation at 37°C, transmigrated cells were counted by independent investigators at the inverted microscope.

2.12. Capillary Tube Formation Assay in Matrigel. Cells were plated on 6-well plates at a density allowing reaching 50–75% confluence and hMSCs were treated for 24 h with 50 and 100 μM sirtinol. For analysis of capillary tube formation, 150 μL Matrigel (Becton Dickinson, San Jose, CA, USA) was laid into a 96-well plates (BD Falcon, Heidelberg, Germany) and incubated at 37°C for 30 minutes. Cells were trypsinized and 3×10^4 cells were suspended in 150 μL of medium and plated onto Matrigel. Cells were incubated at 37°C and capillary tube formation in Matrigel was observed under an inverted microscope (Leica, Heidelberg, Germany) after 4 and 24 h of incubation.

2.13. Statistical Analysis. All data are represented as mean ± S.D. Statistical significance was evaluated by performing Student's t-test and significance was accepted if P value was <0.05.

3. Results

3.1. Immortalization of hMSCs. The ectopic expression of hTERT has been reported to extend the life span of cells [28].

However, the use of hTERT alone is not sufficient to immortalize hMSCs, requiring the combinatorial expression of human papillomavirus type 16 genes (HPV16) E6 and E7 [29].

Therefore, primary hMSCs were infected with HPV16 E6-E7 and hTERT lentiviral vectors expressing pSin hTERT and pSin E6-E7 [30] using a multi-infection program, as reported in Methods section. Two clones were obtained and tested for the presence of hTERT and E6-E7 transcripts. Based on RT-PCR data, both clones (MeBM1E1, MeBM1E2) showed similar levels of hTERT and E6-E7 transcripts. No hTERT and E6-E7 expression were detected in untransduced hMSCs (Supplementary Figure 1(a); see the Supplementary Material available online at http://dx.doi.org/10.1155/2014/783459). The resulting cell lines maintained a fibroblast-like phenotype comparable to primary hMSCs and showed no differences in hMSCs markers expression, such as CD73, CD90, and CD105 (Supplementary Figure 1(b)). Thus, these immortalized mesenchymal cells (MeBM1E1, MeBM1E2) represent a valuable model that can be used for basic studies of mesenchymal biology.

3.2. Differential Sirtuin Expression in hMSCs. Using the MeBM1E1 clone, we assessed the expression profile of the Sirt1–Sirt7 genes. We collected RNAs from cells exposed to either 21% O_2 or 1% O_2 for 24 h and we performed RT-qPCR analysis to quantify their expression. As shown in Figure 1(a), a significant induction of Sirt1 and Sirt7 (P value ≤ 0.05) was detected at mRNA levels in hMSCs under hypoxic conditions compared to normoxia. No significant differences in other sirtuin transcripts were observed under the same conditions.

Next, we evaluated the contribution of hypoxia on SIRT1 protein expression and we collected lysates from cells exposed to 1% O_2 for 24 h in the presence or absence of growth factors (i.e., serum).

As shown in Figure 1(b), Western blot analysis showed that there was no change in SIRT1 protein levels in hMSCs exposed to 1% O_2 for 24 h grown in presence of serum, whereas hypoxia increased SIRT1 levels when hMSCs were cultured in low serum conditions. These data showed that hypoxia alone did not stimulate SIRT1 protein accumulation, whereas depletion of growth factors in combination with hypoxia resulted in an increase of SIRT1 protein expression.

3.3. Inhibition of SIRT1 Induces Premature Senescence-Like Phenotype in hMSCs. To evaluate the effects of targeting SIRT1, we decided to use pharmacological and genetic approaches to inhibit SIRT1. Genetic inhibition was obtained by silencing SIRT1 with lentiviral vector expressing sh-Sirt1-GFP. In order to determine the infection efficiency, green fluorescent protein (GFP) was monitored using fluorescence microscopy after 10 days from infection. As shown in Supplementary Figure 2(a), high levels of GFP in sh-Sirt1-hMSCs were observed with a concomitant reduction of SIRT1 protein (Supplementary Figure 2(b)). In addition, pharmacological inhibition was obtained by sirtinol, a cell permeable specific inhibitor of SIRT deacetylase activity [19].

To investigate whether SIRT1 modulates premature senescence-like phenotype in hMSCs, we examined the effect of SIRT1 inhibition in our cells. hMSCs were treated with sirtinol at 50 and 100 μM for 24 h. After exposure, the cells were washed with inhibitor-free medium and cultured for additional 8 days. As shown in Figure 1(c), sirtinol induced senescence-like morphological changes in hMSCs that showed enlarged and flattened shapes with a concomitant cell number reduction. Then, we evaluated SA-β-gal activity, a characteristic feature of senescence phenotype. Sirtinol increased SA-β-gal activity in hMSCs compared to control. Importantly, sirtinol increased SA-β-gal activity in a dose-dependent manner (Figures 1(d)-1(e)). To confirm the prosenescence role of SIRT1 inhibition, we examined SA-β-gal activity in sh-Sirt1 infected cells. As expected, similar results were obtained in sh-Sirt1 cells (data not shown). These results demonstrated that inhibition of SIRT1 induced a senescence phenotype in hMSCs.

3.4. Effects of SIRT1 Inhibition on Proliferation. We then examined the effects of SIRT1 inhibition on the proliferation of hMSCs. Cells were treated as previously described and proliferation was measured by intracellular levels of ATP at different times (24, 48, and 72 h). Sirtinol significantly inhibited the proliferation of hMSCs in a time-dependent manner compared to control. Similar results were obtained in sh-Sirt1 hMSCs (Figures 2(a)-2(b)).

To investigate whether inhibition of SIRT1 induced growth arrest or cell death, a cell cycle analysis was performed on hMSCs treated with sirtinol for 24, 48, and 72 h by fluorescence activated cell sorting (FACS). By this analysis, we observed a significant cell accumulation in pre-G1 phase, corresponding to apoptotic cells after 24, 48, and 72 h of treatment compared to untreated cells. No significant effect was observed in G1, G2, and S phase (Figure 2(c)), compared to control. Similar results were obtained in sh-Sirt1 cells (data not shown). These data suggested that inhibition of SIRT1, obtained by both pharmacological and genetic approaches, induced apoptosis in hMSCs, without altering the cell cycle distribution of the cells.

3.5. SIRT1 Inhibition Impairs Migration and Capillary Tube Network Formation. Then, we examined whether inhibition of SIRT1 impinged on the migration ability of hMSCs. Cells were exposed for 24, 48, and 72 h to 100 μM sirtinol and we examined the migratory ability of hMSCs in presence of growth factors. The number of migrated cells was significantly reduced in cells treated with SIRT1 inhibitor in a time-dependent manner (Figure 3(a)), compared to control. Consistent with these findings, silenced SIRT1 resulted in a significant reduction of migration compared to control (Figure 3(b)).

These results suggested that inhibition of SIRT1 reduces the capability of hMSCs to migrate. To further assess whether inhibition of SIRT1 might play a role in the ability to form capillary-like networks, we performed a tubule formation assay. We used Matrigel as the basement matrix to induce tubule formation. Cells were exposed to sirtinol (50 and 100 μM) for 24 h; then sirtinol was removed from the culture media. The cells were plated on Matrigel and allowed to form

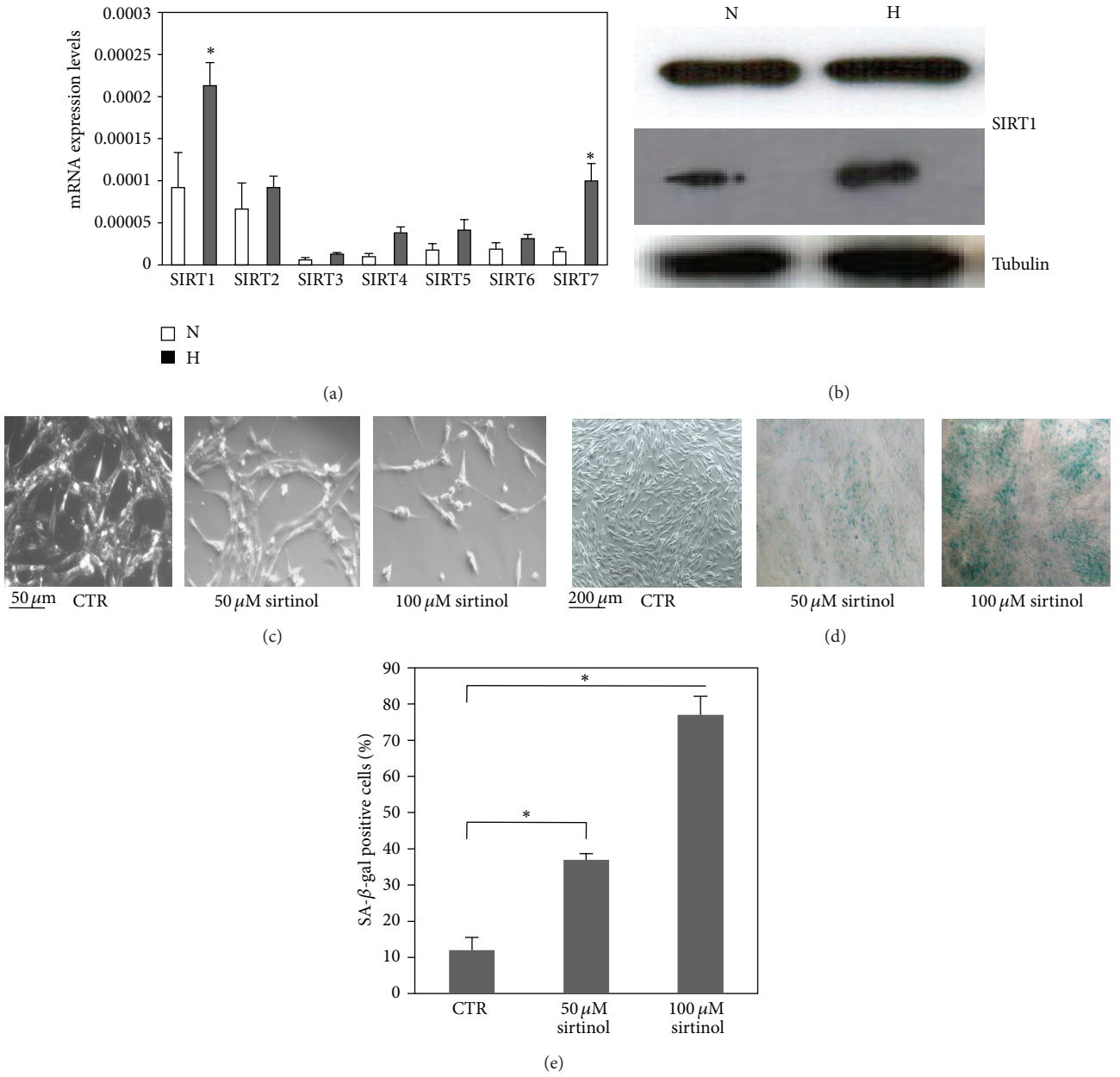

Figure 1: SIRT1–SIRT7 expression in hMSCs and effects of SIRT1 inhibition on phenotype. (a) SIRT1–SIRT7 mRNA levels were measured by real-time PCR (RT-PCR) analyses of total RNAs obtained from hMSCs exposed to either 21% O_2 (N) or 1% O_2 (H) for 24 h and relative expression (±SD) were shown. (b) Western blot analysis of hMSCs grown at either 21% O_2 (N) or 1% O_2 (H) for 24 h under normal conditions (upper panel) and serum-starved (lower panel). Antibodies against SIRT1 and tubulin were used. (c) Morphological changes in hMSCs were examined 8 days after treatment with sirtinol (50 and 100 μM) for 24 h (40x magnification, scale bars = 50 μm). (d) Representative photographs of blue-stained cells for SA-β-Gal activity are shown (10x magnification, scale bars = 200 μm) at 8 days after sirtinol (50 and 100 μM) treatment compared to control (CTR). (e) SA-β-Gal-positive cells were quantified by counting in at least 3 random fields for each condition. Results show the mean of three independent experiments. Graph represents means ± SD, $n = 3$. $*$ indicates statistical significance from control, $P \leq 0.05$.

tubule networks in vitro. As shown in Figure 3(c), we found that hMSCs exposed to 50 μM sirtinol formed less developed tubule structures than untreated cells within a 4-hour period and the number of branch points significantly diminished (Figure 3(d)). Additionally, cell treatment at a concentration of 100 μM sirtinol resulted in the complete suppression of tubule-like structure formation, in contrast to stable tubular networks present in the control (Figure 3(c), upper panel-3D). A reduced ability to form tubule-like formation was also observed in sh-Sirt1 cells compared to control (Figure 3(c) lower panel-3D). These data indicated that SIRT1 activity is involved in tubule-like formation of hMSCs.

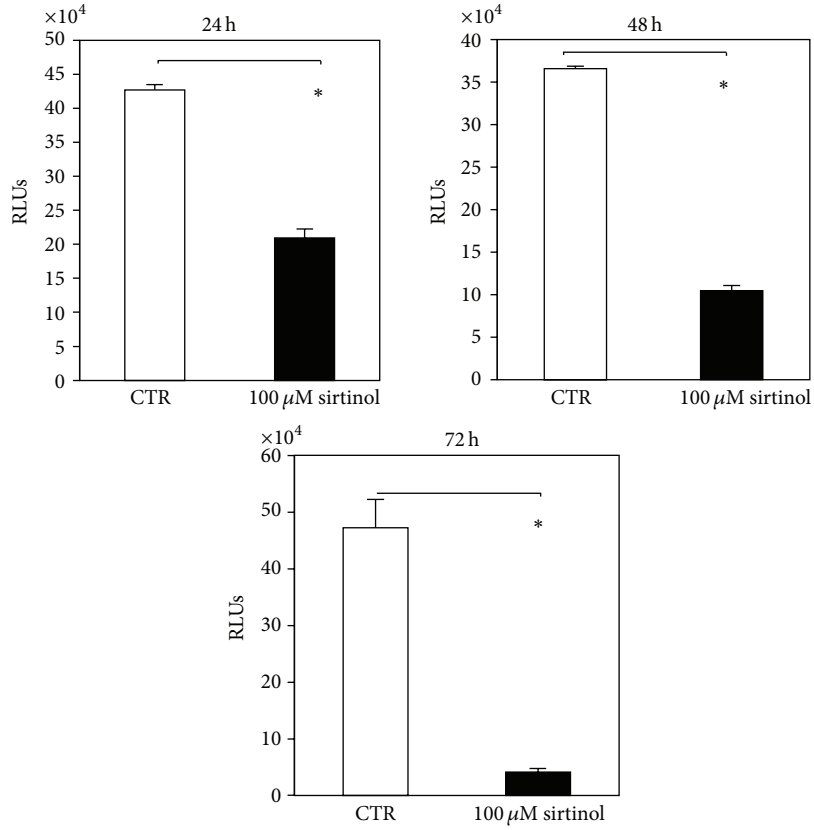

(a)

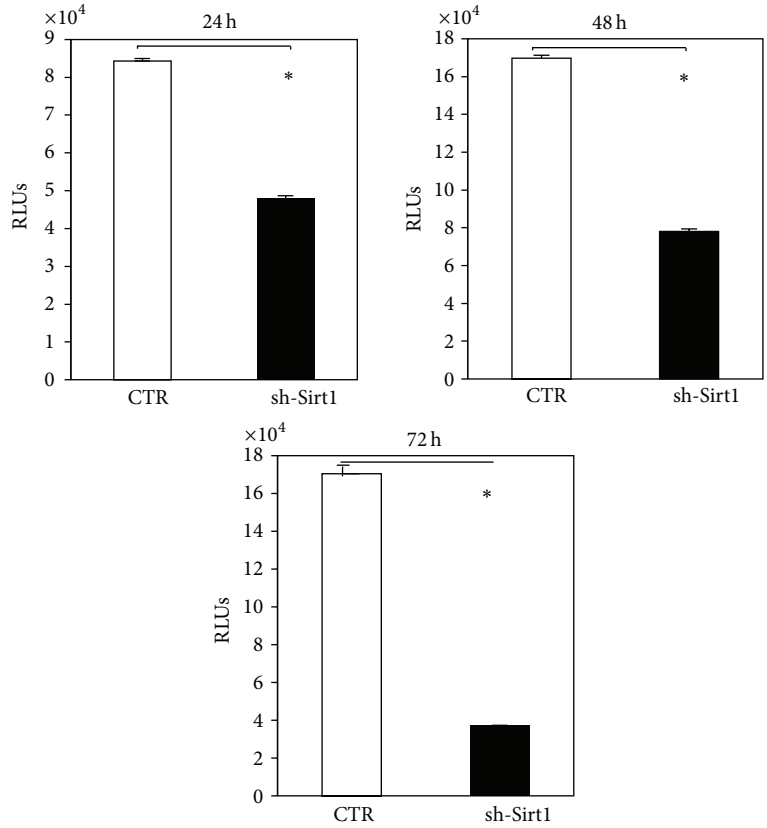

(b)

Figure 2: Continued.

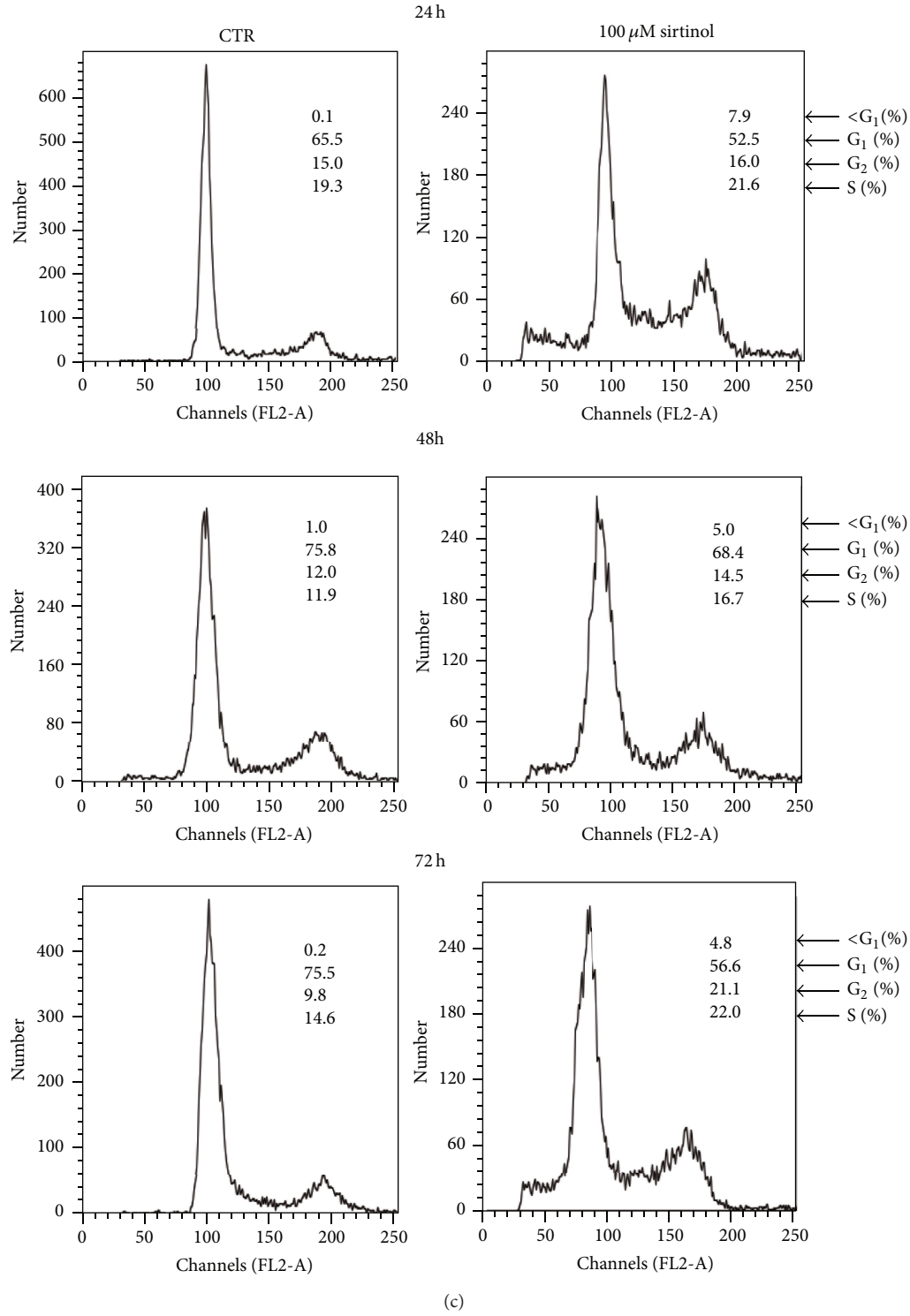

Figure 2: Effects of SIRT1 inhibition on proliferation, cell cycle, and apoptosis. (a) hMSCs were treated with sirtinol 100 μM (black bars) or equivalent concentration of DMSO (white bars) for 24, 48, and 72 h. (b) sh-Sirt1 infected hMSCs were plated and proliferation was measured for 24, 48, and 72 h. Each histogram indicates the RLUs[#] related to cell growth measured at different times. Error bars represent SD of $n = 3$. $*$ denotes statistical differences when $P \leq 0.05$ is compared to control. (c) hMSCs were treated with sirtinol 100 μM or equivalent concentration of DMSO for 24, 48, and 72 h. The cells stained with propidium iodide (PI) were subjected to flow cytometric analysis to determine the cell distributions at each phase of the cell cycle. [#]RLUs are relative light units (RLUs) related to ATP cellular level.

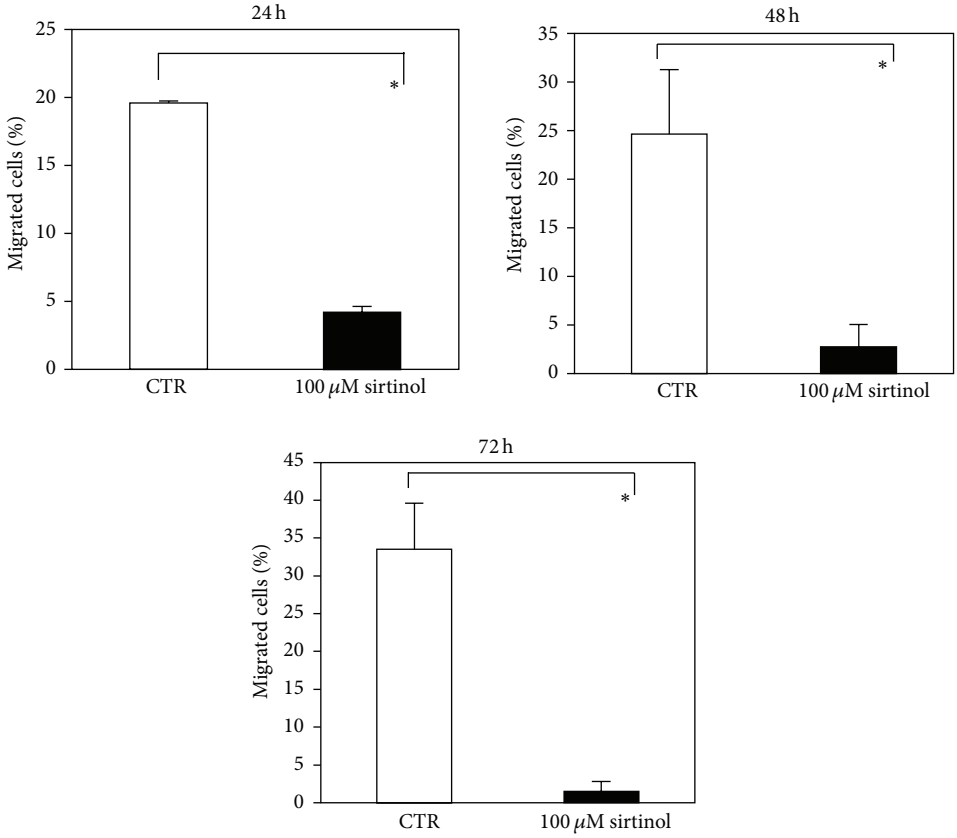

(a)

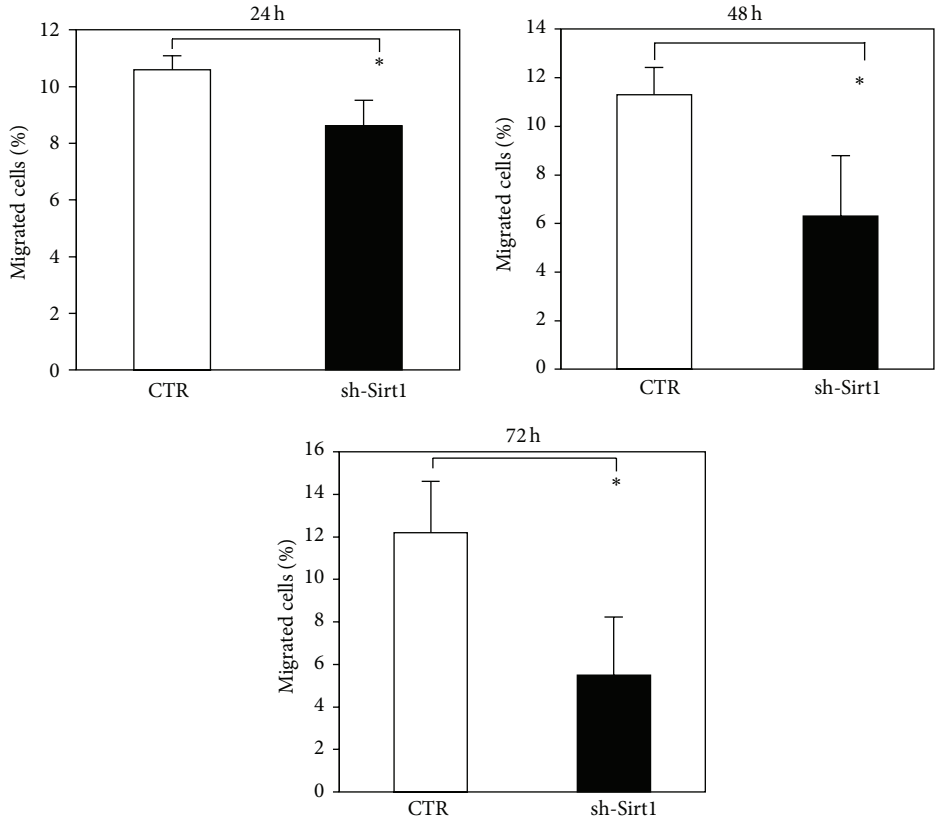

(b)

Figure 3: Continued.

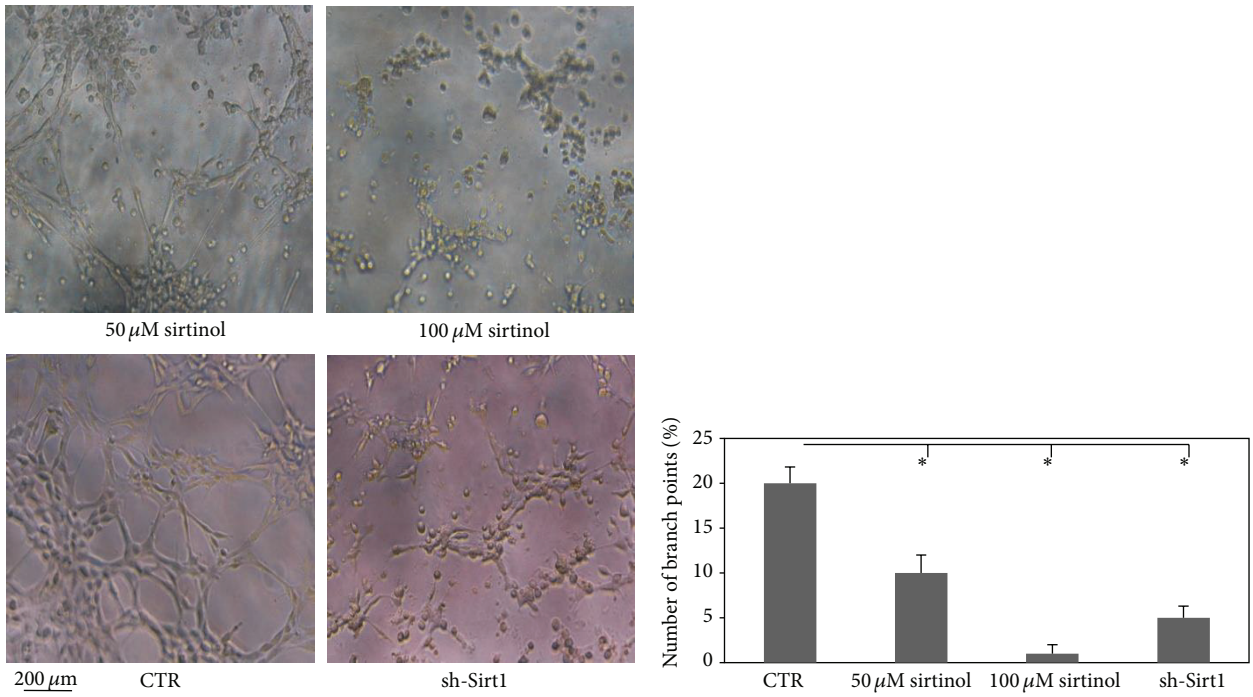

Figure 3: Effects of SIRT1 inhibition on migration and capillary tube network formation. (a) hMSCs were treated with sirtinol 100 μM (black bars) or equivalent concentration of DMSO (white bars) for 24, 48, and 72 h. (b) sh-Sirt1-hMSCs migration (black bars) compared to control (white bars) at 24, 48, and 72 h. Each histogram indicates the % of migrated cells measured at different times. Statistical differences were denoted with $*$ when $P \leq 0.05$ is compared to control. (c) Tubule formation promoted by hMSCs treated with sirtinol (50 and 100 μM) (upper panel) and tubular structures of sh-Sirt1 infected hMSCs plated on Matrigel compared to control (lower panel). Magnification 10x. Scale bar = 200 μm. (d) Tubule formation was quantified by counting the number of branch points of the capillary network. Data are expressed as mean ± SD. $*$ denotes statistical differences when $P \leq 0.05$ is compared to control.

3.6. Impaired Angiogenic Properties of hMSCs Resulting from SIRT1 Inhibition Are Mediated by HIF-1α Protein. To investigate whether SIRT1 activity could regulate HIF-1α accumulation, we analyzed the effects of SIRT1 inhibition on HIF-1α.

Cells were incubated with 100 μM sirtinol for 24 h and then exposed to 1% O_2 for 6 h, known to induce HIF-1α. We then collected cell lysates and Western blotting analysis was performed. Interestingly, as shown in Figure 4(a), inhibition of SIRT1 led to a reduction of SIRT1 protein, as expected, and a strong repression of HIF-1α protein accumulation in hypoxic conditions, compared to control.

To determine if reduction in HIF-1α levels, conferred by SIRT1 inhibition, could affect HIF-1α transcriptional activity, we looked at the expression of known HIF-1α target genes. Cells were treated with 100 μM sirtinol for 24 h and exposed to either 21% O_2 or 1% O_2 for 6 h. Then, we collected RNAs from cells and RT-qPCR analysis was performed. As shown in Figure 4(b), the treatment with sirtinol in combination with hypoxia significantly reduced the hypoxic induction of SIRT1 expression and HIF-1α target genes: Glut1 and VEGF. These data indicated that inhibition of SIRT1 decreased HIF-1α protein accumulation and its transcriptional activity under hypoxic conditions.

4. Discussion

In the present study, we have generated an immortalized human bone marrow-derived mesenchymal cell line (MeBM) that represent a valuable tool to study mesenchymal biology and we investigated whether SIRT1 can influence angiogenic capacity of these cells.

Cell therapy with hMSCs is a promising and safe modality with the potential for vascular regeneration in the treatment of several diseases, especially critical limb ischemia. Pilot human studies have shown that autologous transplantation of bone marrow cells induced therapeutic angiogenesis in patients with critical limb ischemia [3]. hMSCs are pluripotent progenitors that can differentiate into a variety of cell types and have been shown to promote angiogenesis both in vivo and in vitro. It is widely accepted that hMSCs present in bone marrow are therapeutic cells. Emerging evidence suggests that most of the beneficial effects of hMSCs can be explained by the secretion of soluble factors that induce endogenous reparatory processes. However, the mechanisms by which hMSCs promote angiogenesis are not clear.

The present investigation was undertaken to identify the function, if any, of SIRT1 in hMSCs and clarify the molecular

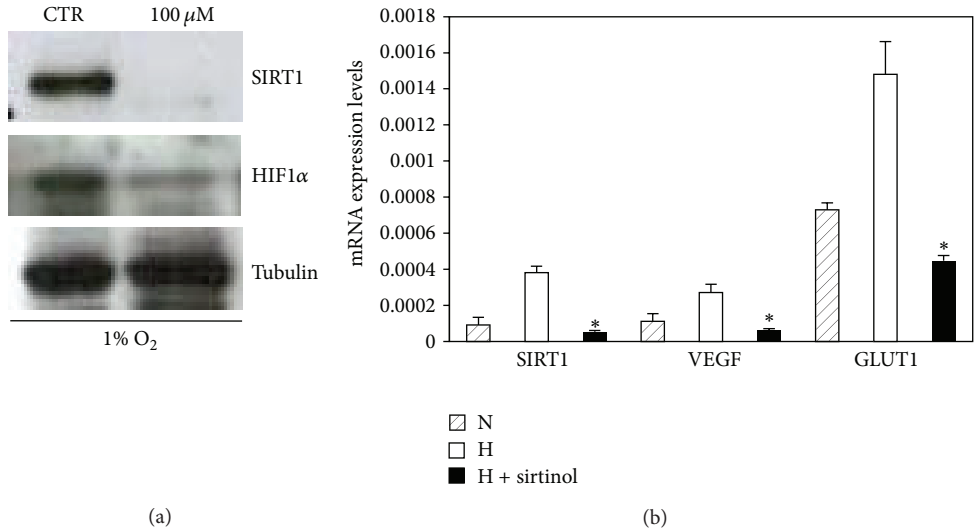

Figure 4: Effects of sirtinol on SIRT1 expression and HIF-1α. (a) hMSCs were treated with sirtinol (100 μM) or equivalent concentration of DMSO (CTR) for 24 h and then exposed to 1% O_2 for 6 h. All cells lysates were analyzed for SIRT1, HIF-1α, and tubulin by Western blot. (b) The amounts of SIRT1, VEGF, and GLUT1 mRNA of hMSCs treated with sirtinol at concentration of 100 μM (black bars) or equivalent concentration of DMSO (white bars) for 24 h and exposed to 1% O_2 (H) for 6 h were quantified with real-time PCR. The levels of SIRT1, VEGF, and GLUT1 mRNA of hMSCs exposed to 21% O_2 (N) for 24 h were measured. $*$ indicates statistical significance from control, $P \leq 0.05$.

mechanism by which SIRT1 regulate angiogenesis in hypoxic conditions.

Sirtuins represent a family of NAD+-dependent protein deacetylases involved in several pathologies. In mammals, SIRT1 is the most closely related homologue of yeast Sir2 and belongs to class III histone deacetylases. It regulates a wide variety of biological functions including gene expression, cell survival, proliferation, differentiation, metabolism, immune response, carcinogenesis, and angiogenic response through multiple targets [15].

Investigation of sirtuin expression was an important preliminary step to study the selective role of class III HDACs. Since sirtuins have been shown to respond to perturbations in the ratio of oxidized NAD+/reduced NADH and, therefore, to modulate the response to hypoxic stress [31], we first looked at sirtuin expression of the family members, both in normoxic and hypoxic conditions.

Therefore, we assessed the expression profile of the Sirt1–7 genes in our cells. We found that SIRT1 and SIRT7 were significantly upregulated in hypoxic conditions compared to normoxia.

SIRT1 activation improves endothelial function and suppresses vascular inflammation, two central pathophysiological processes involved in the initiation and progression of cardiovascular disease [32]. In particular, SIRT1 has been shown to protect endothelial cells from premature senescence and to regulate angiogenesis and vascular tone [26]; thus we decided to focus our study on SIRT1.

In our study, we evaluated the contribution of hypoxia on SIRT1 protein, showing that no change in SIRT1 was detected in hMSCs grown in presence of growth factors, whereas SIRT1 protein expression increased in hMSCs grown in absence of growth factors under hypoxic conditions. Other experiments will be necessary to clarify this; however, our findings might indicate that SIRT1 may act as a sensor of the metabolic state of MSCs in stress conditions (i.e., hypoxia and absence of growth factors).

Several studies have demonstrated that SIRT1 prevents the onset of senescence in multiple cell types, which exhibit alterations in morphology and gene expression that extinguish essential cellular functions [31].

It is known that primary cells underwent senescence when cultured in vitro, showing increased activity of β-galactosidase (β-gal) when assayed at pH 6 [22]. Therefore, we decided to evaluate whether inhibition of SIRT1 might play a role in undertaking a senescent phenotype in our cells. We found that sirtinol, a cell-permeable 2-hydroxy-1-napthaldehyde derivative that acts as a specific and direct inhibitor of all NAD+-dependent protein deacetylases of sirtuin family, significantly increased SA-β-gal activity in a concentration-dependent manner and sustained enlarged and flattened cell morphology.

Our results are consistent with previous studies in human endothelial cells [22, 33], mouse fibroblasts [34], and human cancer cells [35], concluding that sirtuins are implicated in cellular senescence.

It has been demonstrated that senescence alters mesenchymal stem cell properties, such as proliferation and migration [36] and activity of SIRT1 has been linked to this condition [37]. In fact, when cells undergo senescence, their proliferation declines significantly.

Our findings showed that SIRT1 inhibition significantly inhibited the proliferation rate of hMSCs in a time-dependent manner and significantly induced apoptosis in hMSCs.

Going through our data, we also noticed that the effect of genetic inhibition of SIRT1 on angiogenesis response of

hMSCs was less pronounced than pharmacological modulation of SIRT1. A possible explanation for this observation is that sirtinol can inhibit other NAD+-dependent protein deacetylases of sirtuin family, especially SIRT2 [22]. In conclusion, we suggested that inhibition of SIRT1 both by pharmacological and genetic approaches reduces significantly angiogenic properties in cultured hMSCs.

The connection between sirtuin and HIF proteins is complex and the current literature is in part contradictory [19]. Recent reports have linked HIF to sirtuin families by demonstrating that SIRT1, SIRT3, SIRT6, and SIRT7 can regulate the activity of HIF proteins [19, 38]. Lim et al. [18] demonstrated that SIRT1 binds to and deacetylates HIF-1α at lysine 674. This interaction blocks p300 recruitment to the promoter of HIF-1α target genes and thereby represses HIF-1α transcriptional activity, whereas Laemmle et al. reported that SIRT1 increased HIF-1α protein levels [19].

In contrast, Dioum et al. [17] have reported that SIRT1 does not target HIF-1α; it rather deacetylates HIF-2α and their interaction promotes HIF-2α transcriptional activity. In addition, because SIRT1 is a redox cellular sensor and dependent on metabolic status of the cell, its regulation by hypoxia has been a point of interest. In one report, SIRT1 is downregulated in hypoxic conditions due to decreased NAD+ levels [18], while in another study it is upregulated in a HIF-dependent manner [39].

Thus, the interaction between SIRT1 and HIF factors and the resulting outcome of their interactions are still unclear. In this study we found that HIF-1α transcriptional activity is impaired by SIRT1 inhibition under hypoxic conditions, as reported in [19].

5. Conclusions

Our results suggest that SIRT1 exert a role in angiogenic properties of hMSCs. Thus, our study might have important implications in the field of angiogenesis, possibly leading to the identification of chemical compounds that can positively regulate SIRT1, improving regenerative processes exerted by hMSCs.

Conflict of Interests

The authors have stated that they have no conflict of interests.

Acknowledgments

The authors are grateful to Dr. Antonio Barbieri, Dr. Giosue' Scognamiglio, and Dr. Giuseppina Liguori for microscope assistance. Special thanks are due to Dr. Gabriella Malzone and Dr. Monica Cantile for important suggestions. The authors are grateful to PON01_01227 (Botti Chiara) which gave them the support needed to perform the research.

References

[1] G. Ren, X. Chen, F. Dong et al., "Concise review: mesenchymal stem cells and translational medicine: emerging issues," *Stem Cells Translational Medicine*, vol. 1, no. 1, pp. 51–58, 2012.

[2] C. Stamm, B. Westphal, H. D. Kleine et al., "Autologous bone-marrow stem-cell transplantation for myocardial regeneration," *The Lancet*, vol. 361, no. 9351, pp. 45–46, 2003.

[3] A. Schiavetta, C. Maione, C. Botti et al., "A phase II trial of autologous transplantation of bone marrow stem cells for critical limb ischemia: results of the Naples and Pietra Ligure evaluation of stem cells study," *Stem Cells Translational Medicine*, vol. 1, no. 7, pp. 572–578, 2012.

[4] T. Kinnaird, E. Stabile, M. S. Burnett et al., "Marrow-derived stromal cells express genes encoding a broad spectrum of arteriogenic cytokines and promote *in vitro* and *in vivo* arteriogenesis through paracrine mechanisms," *Circulation Research*, vol. 94, no. 5, pp. 678–685, 2004.

[5] J. Rehman, D. Traktuev, J. Li et al., "Secretion of angiogenic and antiapoptotic factors by human adipose stromal cells," *Circulation*, vol. 109, no. 10, pp. 1292–1298, 2004.

[6] H. M. Mi, Y. K. Sun, J. K. Yeon et al., "Human adipose tissue-derived mesenchymal stem cells improve postnatal neovascularization in a mouse model of hindlimb ischemia," *Cellular Physiology and Biochemistry*, vol. 17, no. 5-6, pp. 279–290, 2006.

[7] R. Estrada, N. Li, H. Sarojini, J. An, M. Lee, and E. Wang, "Secretome from mesenchymal stem cells induces angiogenesis via Cyr61," *Journal of Cellular Physiology*, vol. 219, no. 3, pp. 563–571, 2009.

[8] G. Cobellis, C. Maione, C. Botti et al., "Beneficial effects of VEGF secreted from stromal cells in supporting endothelial cell functions: therapeutic implications for critical limb ischemia," *Cell Transplantation*, vol. 19, no. 11, pp. 1425–1437, 2010.

[9] R. H. Lee, J. Y. Oh, H. Choi, and N. Bazhanov, "Therapeutic factors secreted by mesenchymal stromal cells and tissue repair," *Journal of Cellular Biochemistry*, vol. 112, no. 11, pp. 3073–3078, 2011.

[10] P. Simic, K. Zainabadi, E. Bell et al., "SIRT1 regulates differentiation of mesenchymal stem cells by deacetylating β-catenin," *EMBO Molecular Medicine*, vol. 5, no. 3, pp. 430–440, 2013.

[11] A. Z. Herskovits and L. Guarente, "Sirtuin deacetylases in neurodegenerative diseases of aging," *Cell Research*, vol. 23, no. 6, pp. 746–758, 2013.

[12] M. C. Haigis and D. A. Sinclair, "Mammalian sirtuins: Biological insights and disease relevance," *Annual Review of Pathology: Mechanisms of Disease*, vol. 5, pp. 253–295, 2010.

[13] T. Finkel, C. Deng, and R. Mostoslavsky, "Recent progress in the biology and physiology of sirtuins," *Nature*, vol. 460, no. 7255, pp. 587–591, 2009.

[14] L. Guarente, "Sirtuins, aging, and medicine," *The New England Journal of Medicine*, vol. 364, no. 23, pp. 2235–2244, 2011.

[15] V. Carafa, A. Nebbioso, and L. Altucci, "Sirtuins and disease: the road ahead," *Frontiers in Pharmacology*, vol. 3, article 4, Article ID Article 4, 2012.

[16] G. Corbi, A. Bianco, V. Turchiarelli et al., "Potential mechanisms linking atherosclerosis and increased cardiovascular risk in COPD: focus on sirtuins," *International Journal of Molecular Sciences*, vol. 14, no. 6, pp. 12696–12713, 2013.

[17] E. M. Dioum, R. Chen, M. S. Alexander et al., "Regulation of hypoxia-inducible factor 2alpha signaling by the stress-responsive deacetylase sirtuin 1," *Science*, vol. 324, no. 5932, pp. 1289–1293, 2009.

[18] J. H. Lim, Y. M. Lee, Y. S. Chun, J. Chen, J. Kim, and J. Park, "Sirtuin 1 modulates cellular responses to hypoxia by deacetylating hypoxia-inducible factor 1alpha," *Molecular Cell*, vol. 38, no. 6, pp. 864–878, 2010.

[19] A. Laemmle, A. Lechleiter, V. Roh et al., "Inhibition of SIRT1 impairs the accumulation and transcriptional activity of HIF-1α protein under hypoxic conditions," *PLoS ONE*, vol. 7, no. 3, Article ID e33433, 2012.

[20] C. W. Pugh and P. J. Ratcliffe, "Regulation of angiogenesis by hypoxia: role of the HIF system," *Nature Medicine*, vol. 9, no. 6, pp. 677–684, 2003.

[21] M. Potente, L. Ghaeni, D. Baldessari et al., "SIRT1 controls endothelial angiogenic functions during vascular growth," *Genes and Development*, vol. 21, no. 20, pp. 2644–2658, 2007.

[22] H. Ota, M. Akishita, M. Eto, K. Iijima, M. Kaneki, and Y. Ouchi, "Sirt1 modulates premature senescence-like phenotype in human endothelial cells," *Journal of Molecular and Cellular Cardiology*, vol. 43, no. 5, pp. 571–579, 2007.

[23] S. Portmann, R. Fahrner, A. Lechleiter et al., "Antitumor effect of SIRT1 inhibition in human HCC tumor models in vitro and in vivo," *Molecular Cancer Therapeutics*, vol. 12, no. 4, pp. 499–508, 2013.

[24] D. Rotili, D. Tarantino, A. Nebbioso et al., "Discovery of salermide-related sirtuin inhibitors: binding mode studies and antiproliferative effects in cancer cells including cancer stem cells," *Journal of Medicinal Chemistry*, vol. 55, no. 24, pp. 10937–10947, 2012.

[25] I. Gorenne, S. Kumar, K. Gray et al., "Vascular smooth muscle cell sirtuin 1 protects against dna damage and inhibits atherosclerosis," *Circulation*, vol. 127, no. 3, pp. 386–396, 2013.

[26] M. Potente, "An energy-sensor network takes center stage during endothelial aging," *Circulation Research*, vol. 106, no. 8, pp. 1316–1318, 2010.

[27] M. Miceli, G. Franci, C. Dell'Aversana et al., "MePR: a novel human mesenchymal progenitor model with characteristics of pluripotency," *Stem Cells and Development*, vol. 22, no. 17, pp. 2368–2383, 2013.

[28] A. G. Bodnar, M. Ouellette, M. Frolkis et al., "Extension of lifespan by introduction of telomerase into normal human cells," *Science*, vol. 279, no. 5349, pp. 349–352, 1998.

[29] T. Okamoto, T. Aoyama, T. Nakayama et al., "Clonal heterogeneity in differentiation potential of immortalized human mesenchymal stem cells," *Biochemical and Biophysical Research Communications*, vol. 295, no. 2, pp. 354–361, 2002.

[30] S. S. Akimov, A. Ramezani, T. S. Hawley, and R. G. Hawley, "Bypass of senescence, immortalization, and transformation of human hematopoietic progenitor cells," *Stem Cells*, vol. 23, no. 9, pp. 1423–1433, 2005.

[31] M. F. Oellerich and M. Potente, "FOXOs and sirtuins in vascular growth, maintenance, and aging," *Circulation Research*, vol. 110, no. 9, pp. 1238–1251, 2012.

[32] J. Gracia-Sancho, G. Villarreal, Y. Zhang, and G. García-Cardeña, "Activation of SIRT1 by resveratrol induces KLF2 expression conferring an endothelial vasoprotective phenotype," *Cardiovascular Research*, vol. 85, no. 3, pp. 514–519, 2010.

[33] A. Cardus, A. K. Uryga, G. Walters, and J. D. Erusalimsky, "SIRT6 protects human endothelial cells from DNA damage, telomere dysfunction, and senescence," *Cardiovascular Research*, vol. 97, no. 3, pp. 571–579, 2013.

[34] E. Langley, M. Pearson, M. Faretta et al., "Human SIR2 deacetylates p53 and antagonizes PML/p53-induced cellular senescence," *EMBO Journal*, vol. 21, no. 10, pp. 2383–2396, 2002.

[35] H. Ota, E. Tokunaga, K. Chang et al., "Sirt1 inhibitor, Sirtinol, induces senescence-like growth arrest with attenuated Ras-MAPK signaling in human cancer cells," *Oncogene*, vol. 25, no. 2, pp. 176–185, 2006.

[36] S. D. Barros, S. Dehez, E. Arnaud et al., "Aging-related decrease of human ASC angiogenic potential is reversed by hypoxia preconditioning through ROS production," *Molecular Therapy*, vol. 21, no. 2, pp. 399–408, 2013.

[37] N. Engel and U. Mahlknecht, "Aging and anti-aging: unexpected side effects of everyday medication through sirtuin 1 modulation," *International Journal of Molecular Medicine*, vol. 21, no. 2, pp. 223–232, 2008.

[38] M. E. Hubbi, H. Hu, D. M. Gilkes, and G. L. Semenza, "Sirtuin-7 inhibits the activity of hypoxia-inducible factors," *Journal of Biological Chemistry*, vol. 288, no. 29, pp. 20768–20775, 2013.

[39] R. Chen, M. Xu, R. T. Hogg et al., "The acetylase/deacetylase couple CREB-binding protein/sirtuin 1 controls hypoxia-inducible factor 2 signaling," *The Journal of Biological Chemistry*, vol. 287, no. 36, pp. 30800–30811, 2012.